THE UNIVERSITY OF MICHIGAN

INDUSTRY PROGRAM OF THE COLLEGE OF ENGINEERING

BUBBLE GROWTH ON A GLASS SURFACE DURING BOILING OF ETHYL ALCOHOL AND TOLUENE

Thomas I. McSweeney

A dissertation submitted in partial fulfillment
of the requirements for the degree of
Doctor of Philosophy in the
University of Michigan
Department of Chemical and Metallurgical Engineering
1967

December, 1967

IP-797

To My Father John W. McSweeney

ACKNOWLEDGEMENTS

Without the patience and understanding of my wife and family this study could not have been accomplished.

The author wishes to acknowledge the assistance of Professors J.A. Clark, H.H. Merte, and F. Hammitt for their service on my doctoral committee. Special thanks are due Professors R.E. Balzhiser and J.O. Wilkes who have served as co-chairmen. The stimulating discussions with Professors E.E. Hucke, P.S. Larsen, E.H. Young, R.E. Barry and R.S. Curl have greatly aided in the development of this experimental and theoretical program.

The thin vapor-deposited resistors have been designed and manufactured, according to specifications, by Lear Siegler Inc. of Grand Rapids, Michigan. Without their assistance this study would not have been possible.

Thanks also to the Dow Chemical Company and Cities Service Company for providing scholarships which permitted the author to devote full time to this work.

CONTENTS

LIST OF TABLES

LIST OF FIGURES

LIST OF FIGURES (continued)

LIST OF APPENDICES

NOMENCLATURE

a	Constant in equation (16)
A	Area
At	Constant in equation (8)
b	Constant in equation (8)
B	Constant in equation (8)
C	Constant in equation (16)
Cp	Specific heat
C1	Constant in equation (1)
C2	Constant in equation (22)
C3	Constant in equation (23)
C4	Constant in equation (24)
C5	Constant in equation (25)
C6	Constant in equation (21)
d	Thermal layer thickness
D_d	Departure diameter
f	Frequency
g	Acceleration due to gravity
h	Heat transfer coefficient
H_b	Height of bubble base above the solid surface
H_c	Height of point on a bubble where the bubble radius equals the maximum radial bubble radius
H_{t-c}	Height of bubble cap above H_c
i	Current
ie	Element current
I	Integer
J	Mechanical equivalent of heat

JA	Jakob number
k	Thermal conductivity
k_δ	Constant in equation (18)
k_ε	Eddy diffusivity
K	Constant in equation (3)
Kw	Constant defined by equation (8)
ℓ	Length
L	Latent heat of vaporization
n	Number of active sites
P	Pressure
Pr	Prandtl number
q	Average heat flux
q_r	Initial gradient of the heat flux before nucleation based on the observed experimental surface temperature recovery
Q	Rate of heat transfer
r	Radial distance
R	Bubble radius
R_b	Visual bubble contact radius
$R_{b\ max}$	Maximum base contact radius
R_{cm}	Optimum cavity size
Re	Element resistance
R_m	Maximum radial bubble radius
Rn	Input resistance of Null detector
Rnull	Resistance of the Null point
Ro	Element resistance at 0°C
Rs	Resistance of standard
Rw	Resistance when wet
ΔR	Change in resistance

Se	Potentiometer setting for element
Ss	Potentiometer setting for standard
t	Time
te	Time for complete vaporization
tp	Time of second break in temperature curve after primary fluctuation
tw	Waiting time between bubbles
t_{wm}	Minimum waiting time
t_m	Time of the occurrence of $R_{b\ max}$
T	Temperature
Tcu	Copper temperature
Te	Heating element temperature
$\bar{T}$	Average temperature
ΔT	Temperature difference
u	Radial velocity
U	Free stream radial velocity
v	Vertical velocity
ΔV	Voltage drop
Vs	Voltage across standard
Ve	Voltage across a surface element
x	Dimensionless radial distance or dummy variable of integration
y	Vertical distance from the wall
y_b	Distance into solid below which the influence of the microlayer vaporization is not observed
Z	Dimensionless vertical dimension

Greek Letters

α Thermal diffusivity

β Volumetric coefficient of thermal expansion

βt Temperature coefficient of resistance

δ Dimensionless microlayer thickness

Δ_1 Evaporating microlayer thickness calculated from equation (20) using liquid thermal properties

Δ_s Evaporating microlayer thickness calculated from equation (35) using solid thermal properties

Δ^*_s Evaporating microlayer thickness calculated from equation (35) using solid thermal properties and an initial temperature gradient before nucleation based on q_r

Δ Microlayer thickness

ε Constant defined by equation (8)

ε_1 Liquid eddy diffusivity

η Initial bubble growth parameter defined by equation (26)

θ $T-T_{sat}$ / (T_n-T_{sat})

μ Viscosity

ν Kinematic viscosity

ρ Density

σ Surface tension

τ Dimensionless time

ψ_s Constant in equation (4)

ψ_b Constant in equation (4)

ψ_n Constant in equation (4)

ψ_c Constant in equation (4)

Subscripts

avg	Average
b	Bulk or base
c	Critical
d	Departure
e	Evaporating
l	Liquid
m	Maximum
o	Initial or zero order
s	Solid
sat	Saturation
v	Vapor
w	Wall

ABSTRACT

A study of boiling heat transfer on a glass surface was undertaken to determine the boiling characteristics of ethyl alcohol and toluene and to estimate the contribution of microlayer vaporization to both the overall heat transfer rate and the amount of energy in a departing bubble.

An experimental procedure was developed utilizing thin-film circuity on the boiling surface, a single site heater, an electronic synchronization between photographs of the boiling process and temperature traces displayed on an oscilloscope. The use of the single nucleating site is an excellent method for the study of the boiling process. For instance, the base contact radius, which has been previously neglected and yet was found to be an important parameter, is easily observed.

A theory of microlayer formation, based on experimentally determined bubble growth rate, was developed in the course of this investigation which successfully explains the phenomena associated with the boiling of ethyl alcohol and toluene. This theory predicts surface temperature fluctuations and nucleation characteristics which agree reasonably well with those experimentally observed. Bubble formation in toluene was irregular over the pressure range studied whereas ethyl alcohol exhibited a change from regular to uneven bubble formation. This change in the boiling characteristics was explained by microlayer vaporization theory. The bubble growth rates, which were higher than predicted by previously published theories, were also explained using this theory.

With the microlayer theory, and the experimentally determined variation in the base contact radius, the contribution of microlayer vaporation to heat transfer processes was determined. It was found that about 30% of the energy in a departing bubble arose from microlayer vaporization. The latent heat transport was found to account for 10 percent of the total heat transfer; ninety percent was due to bubble induced boundary layer agitation. Thus, microlayer vaporization accounts for only 3% of the total heat transfer. However, small as it may be, it controls nucleation and since boundary layer agitation is caused by nucleation, growth, and departure, it can be stated that under the conditions studied in this investigation, microlayer vaporization processes govern boiling heat transfer.

INTRODUCTION

Boiling is a very efficient process for transferring heat. This fact has been realized for a long time and many studies have been carried out to investigate the variables governing boiling heat transfer.

Recently, a novel heat transfer mechanism has been suggested as a partial explanation of boiling efficiency. It is called microlayer vaporization. This liquid layer has been shown to exist in a region which was long thought to play no active role in boiling heat transfer. A normal photograph of a bubble boiling on a solid surface shows an apparent contact region between the bubble and the solid. This region, which until recently was assumed to be dry, actually is coated by a thin liquid layer. At the present time, the heat transfer resulting from the evaporation of the microlayer has not been adequately defined. The obvious variables are the amount of the surface covered by bubbles, the thickness of the film under the bubble, and the time interval that the bubble is on the surface. The way these variables control microlayer vaporization has not been investigated in sufficient detail to validate the hypothesis.

The influence of the thermal properties of the solid is another factor which has not been clarified. In fact, it is not included in any presently available theory of bubble growth, departure, or nucleation. Except for one very general correlation, the effect of the solid's thermal properties on the overall rate of heat transfer has not been defined.

In the present investigation, the boiling of ethyl alcohol and toluene from a glass surface is studied. On the surface of the glass plate, vapor-deposited resistors serve as temperature sensors. Several such resistors, located at radial distances from a central resistor, are used to study heat transfer around a single active site. A single-site heater, located under the glass boiling plate, serves as a power source. Electronic synchronization between an oscilloscope, which displays the surface temperature, and two electronic flash units provide a way of relating boiling photographs to the temperature traces.

The goals of this study are to investigate the way boiling occurs on a glass surface, and to develop a theoretical method for estimating the contribution of microlayer vaporization to the amount of energy associated with a departing bubble.

LITERATURE REVIEW

1. Introduction

The studies of boiling heat transfer can be broken down into three distinct areas. First, a general boiling study, termed quantitative study, determines the amount of vapor generated at the boiling surface. Then secondly, from this information, a theoretician can study areas which seem important. The detailed explanation of the boiling process requires a knowledge of bubble nucleation, growth, and departure, and also the number of active boiling sites. The temperature distributions in the solid and liquid as well as the velocity distribution in the liquid can affect bubble parameters. The importance of these variables must also be estimated. Finally, general correlations tie the bubble parameters back to the quantitative studies. Only the variables which have been shown to be important need be included in these general correlations.

2. Quantitative Studies

The investigations of Jakob and his co-workers, summarized in his books "Heat Transfer" (29), were the first quantitative studies of how heat is transferred during boiling. Several terms, first defined by Jakob, are still used. He stated that the amount of energy associated with the vapor in the bubble at departure is removed by latent heat transport; the remaining energy is transferred by a bubble agitation mechanism.

In an effort to discover the relative importance of latent heat transport, Jakob performed three experiments. These experiments were conducted at a low heat flux, just above the flux level where boiling began. By using high speed motion picture photography, he followed a single bubble as it nucleated, grew, departed from the surface, and rose through the liquid. He found that less than 10% of the total bubble growth occurred before bubble departure from the surface. Next, Jakob looked at the region close to the surface and counted the number of active nucleation sites. At each site, he determined the frequency of nucleation and the bubble size at departure. Once again, less than 10% of the energy was transported from the surface as latent heat. Finally, using a movable temperature probe, Jakob observed that the liquid above the boiling plate was superheated a few tenths of a degree. These three studies showed the latent heat transport was not important at low heat fluxes. Since the liquid was found to be superheated slightly, there was the possibility of bubble growth after the bubble left the surface. Since so much of the bubble growth occurred after departure, he concluded that agitation of the thermal boundary layer was important since it provided a mechanism for transferring heat into the liquid.

The experimental techniques developed by Jakob were applied to subcooled boiling by Rohsenow and Clark (41). Their results indicated that only 1-2% of the heat was transferred as latent heat. This figure assumed no condensation of vapor until after the bubble left the surface.

Rallis and Jawurek (38) experimentally determined the contribution of latent heat transfer in saturated boiling as a function of the total heat transfer rate through the surface. At low fluxes, in the region studied by Jakob, they also found that latent heat transport accounted for only a small percentage of the total heat flux. They measured the latent heat contribution as the heat flux was increased until they were no longer able to discern individual bubble departure due to the large number of bubbles existing on the surface. At this highest heat flux the amount of energy removed by latent heat transfer reached 80% of the total amount of heat transferred.

These results show that bubble-induced agitation controls heat transfer at low heat fluxes and that latent heat transport becomes important at high heat fluxes.

The understanding of the interaction between bubble parameters and heat transfer comes from the experimental and theoretical analysis of bubble growth rates, bubble departure criteria, the nature of an active boiling site, and the temperature and velocity profiles around an active site.

3. Bubble Size and the Rate of Bubble Growth

The growth of a vapor bubble in a uniformly superheated liquid of infinite extent was analyzed theoretically by Plesset and Zwick (37), and by Forster and Zuber (12). Both these investigations assumed that the rate of bubble growth was limited by the rate at which heat can be transferred to the liquid vapor interface. The final equation obtained by both sets of investigators was:

$$R = 2C_1 \sqrt{\alpha_1 t} \cdot \qquad (1)$$

The value of C_1 was: $(\sqrt{\pi}/2)$ JA (Forster and Zuber), and $\sqrt{3/\pi}$ JA (Plesset and Zwick). JA is the Jakob number defined by $\rho_1 Cp_1 \Delta T/\rho_v L$. The difference in C_1 for the two investigations was explained by the approximations used to get the final result. Forster and Zuber included a liquid inertia term which Plesset and Zwick neglected. Scriven (44) and Birkhoff(2) solved exactly the same equations used by Plesset and Zwick. In the exact solution the value of C_1 must be obtained from the following expression:

$$JA = 2C_1^2 \exp\left[C_1^2(3+\rho_v/\rho_1)\right] \int_{C_1}^{\infty} \frac{1}{x} \exp\left[\frac{-x^3-2(1-\rho_v/\rho_1)C_1^3}{x}\right] dx \quad . \tag{2}$$

For large values of JA, equation (2) yields the same coefficient reported by Plesset and Zwick.

The more difficult problem of bubble growth on a solid surface with non-uniform temperature field surrounding the bubble has also been studied. Griffith (18) analyzed the problem of a bubble nucleating in the superheated layer close to the surface and then growing into the bulk liquid with the base of the bubble still in the superheated layer. He showed by dimensional analysis that the bubble radius at any time can be expressed in the following form:

$$\frac{R}{d} = K \, JA \, f\left(\frac{t\alpha_1}{d^2}, \frac{T_b - T_{sat}}{T_w - T_b}\right) \tag{3}$$

The dimensionless bubble size (R/d), expressed in equation (3) was calculated on a digital computer. The functional relationship was not specified in Griffith's report. As the dimensionless group $(T_b-T_{sat})/(T_w-T_b)$

becomes more negative the bubble size shows an effect of the bulk liquid temperature. The effect is one of slowing the growth rate because a greater percentage of the bubble is in the liquid bulk, which is subcooled.

Zuber (52) analyzed the problem of bubble growth when all the heat is transferred at the base of the bubble according to the error function relationship, $(\partial T/\partial y)_{y=0} = (T_w - T_{sat})/\sqrt{\pi \alpha_1 t}$. Assuming also that the bubble grows as a hemisphere, the solution is the same as equation (1) with $C_1 = 1/\sqrt{\pi}$ JA.

The validity of using the error function relationship over the whole solid surface at the same time is certainly an approximation. Even so, the solution does agree with some experimental bubble growth data for bubbles growing on a solid surface.

Han and Griffith (21) started with the same problem analyzed earlier by Griffith (18) but in this case they assumed the superheated liquid layer was carried out into the bulk as the bubble grows. Using this assumption, the bubble radius as a function of time became:

$$R - R_c = \frac{\Psi_c \Psi_s}{\Psi_v}\left\{\frac{2}{\sqrt{\pi}} JA(\alpha_1 t)^{1/2} - \left(\frac{T_w - T_b}{T_w - T_{sat}}\right)\frac{d\,JA}{4}\left[\frac{4\alpha_1 t}{d^2}\,\mathrm{erf}\left(\frac{d}{2\sqrt{\alpha_1 t}}\right) + \frac{4}{d}\sqrt{\frac{\alpha_1 t}{\pi}}\,\exp\left(\frac{-d^2}{4\alpha_1 t}\right) - 2\,\mathrm{erfc}\left(\frac{d}{2\sqrt{\alpha_1 t}}\right)\right]\right\} + \frac{\Psi_b h_w (T_w - T_b) t}{\Psi_v \rho_v L} \qquad (4)$$

where

Ψ_s = surface factor = $(1 + \cos\theta)/2$,

Ψ_b = base factor = $\sin^2\theta/4$,

Ψ_v = volume factor = $[2 + \cos\theta\,(2 + \sin^2\theta)]/4$,

Ψ_c = curvature factor where $1 < \Psi_c < \sqrt{3}$

Han and Griffith also compared their theory to experimental data. They concluded that there is general agreement between theoretical and experimental results.

Golovin et. al. (17) experimentally measured bubble growth rates for several fluids as a function of pressure. They found a value of $C_1 = \sqrt{12\ JA}$ correlated the experimental bubble size data from 1 to 30 atmospheres.

The difference between the results of Golovin and the previous investigators has not been clarified. Except for the exact solution, which both Scriven and Birkhoff reported (Equation (2)), every other theoretical solution results in a linear dependence of Jakob number on the bubble size. This is the only solution that includes second order density effects, so it is the only one that has a chance of predicting anything but a linear relationship between R and JA.

4. <u>The Nature of An Active Site</u>

a. Role of Surface Conditions

Jakob (29) reported that boiling is affected by the surface conditions of the solid. When the surface was coated with oil, the bubble size at departure increased. The following equation, derived by Fritz (13), was used to explain the increased bubble size:

$$D_d = .0148\theta\sqrt{\frac{2\sigma}{g(\rho_1-\rho_v)}}\ . \tag{5}$$

He stated that θ increased when the surface was coated with oil. Based on equation (5), D_d increased accordingly. Jakob also reported that when the surface was artificially roughened, the number of active sites per unit area, n/A, increased. This also affected the heat transfer. Both these effects are attributed to a change in surface conditions.

Corty and Faust (9) measured the heat flux, wall superheat, and number of active sites on artificially roughened surfaces. In a quantitative manner they showed the importance of surface roughness. Clark, Strenge, and Westwater (6), observing the boiling surface with a low power microscope, found that pits with a diameter between 10^{-2} and 10^{-3} cm. were very active. Bubble nucleation was also observed from some scratches, a metal-plastic interface, and a mobile speck of material. Neither grain boundaries nor the various crystal faces of zinc (which is an anisotropic material) had any apparent effect on the nucleation characteristics of the surface.

If a vapor cavity is completely surrounded by a superheated liquid, thermodynamics requires that the equilibrium cavity radius be specified by the following relationship:

$$\frac{2\sigma}{R} = \frac{JL(T_l - T_{sat})\rho_v \rho_l}{T_{sat}(\rho_l - \rho_v)} \qquad (6)$$

Equation (6) is strictly applicable only if the vapor bubble is completely surrounded by a liquid. It is not evident what radius should be used if a bubble of radius R_o is in contact with a solid surface at a cavity of radius R_c. Using artificial cavities of known geometry, Griffith and Wallis (19) showed that R_c was the correct radius to use in equation (6). They also found that even though equation (6) was valid when R_c was used, there was no assurance that the cavity would be stable or even active at all.

Young and Hummel (51) distributed Teflon* spots randomly on a stainless steel surface. The spots covered only a small percentage of the surface area and each spot had a radius of between 10^{-2} to 10^{-3} cm. When water was boiled from the treated surface, the surface superheat required for bubble nucleation was less than 5°F.; whereas on the untreated portion, nucleation did not occur until the wall superheat was greater than 20°F. Gaertner (14) reported a similar result when Teflon spots of uniform size were distributed over the surface in a regular pattern.

b. Bubble Nucleation Criteria

Griffith and Wallis (19) stressed the importance of vapor existing at the surface but concluded that this condition alone does not insure the stability of the active site. The theories developed to judge the stability of a cavity originate from one of two initial assumptions. If liquid enters the cavity on the surface, then a valid criterion for stability can be based on the attainment of vapor-liquid equilibrium within the cavity. If, however, the departing bubble leaves sufficient vapor behind, so the liquid never enters the cavity, then the criterion for future nucleation depends on the recovery of the thermal boundary layer removed by the preceding bubble.

Bankoff (1) and Marto and Rohsenow (32) investigated the stability of a cavity containing both liquid and vapor. Bankoff proposed that a liquid could not rush into a stable cavity faster than a critical rate, which allowed time for thermal equilibrium to occur. He assumed that the wall was at a constant temperature; the liquid entering the cavity was initially at bulk liquid temperature. As the liquid rushed down the

---

*DuPont Trademark

cavity, slowed only by viscous drag, it began heating up to the wall temperature. Based on this analysis, the cavity with the optimum stability has a radius defined by the following equation:

$$R_c = \left\{ \frac{4k_1 \mu \sigma \rho_1 Cp_1 \cos\theta}{J^2} \left[\frac{T(\rho_1 - \rho_v)}{L^2 \rho_v^2 \rho_1} \right]_{avg} \right\}^{1/3} \qquad (7)$$

Marto and Rohsenow, by similar analysis, but with the knowledge that the wall temperature fluctuated in the region around an active site, derived the following expression:

$$\frac{y}{\ell} = \frac{2At}{\pi \ell B Kw}, \text{ where}$$

$$At = (1 + \frac{\varepsilon}{2})\, C \left(q\sqrt{\frac{f}{\alpha_w}} \right)^{-a} \frac{q\, T_{sat}\, 2\sigma \cos\theta}{k_w \rho_w L\, R_c}, \qquad (8)$$

$$B = \frac{bq}{\sqrt{\pi k_w \rho_w Cp_w}},$$

$$Kw = \frac{\rho_v L (1+\sin\theta)}{2\sqrt{\pi k_1 \rho_1 Cp_1}}$$

In equation (8), the constants ε, a, b, and C define the nature of the wall temperature recovery, ℓ is the depth of the cavity, and y is the maximum penetration depth of the liquid.

Hsu (28), and Han and Griffith (21) investigated nucleation controlled by the redevelopment of the liquid thermal boundary layer which was destroyed by the previous bubble. Hsu's analysis began with the departure of the bubble from the surface. At that time, the surface temperature is a constant and the thermal layer thickness d(0) is zero. Due to the difference between the bulk liquid temperature T_b and the wall temperature T_w, the thermal layer thickness d(t) gradually builds up. The temperature distribution in the thermal layer as a function of time and position can be specified by a solution of the heat conduction equation with the previous boundary conditions. Hsu assumed that at every point around a vapor cavity, which is connected to the surface at a cavity of radius R_c and has a spherical radius R_o, must be above the equilibrium temperature specified by equation (6) with $R=R_o$ before the cavity will nucleate. The maximum and minimum cavity size which can be active are specified by the following equation:

$$R_c \Big|_{min}^{max} = \frac{d \cos \theta}{2(1+\sin\theta)} \left[\left(\frac{T_w - T_{sat}}{T_w - T_b} \right) \pm \sqrt{ \left(\frac{T_w - T_{sat}}{T_w - T_b} \right)^2 - \frac{4\sigma T_{sat}(1+\sin\theta)}{JL\rho_v d(T_w - T_b)} } \right] \qquad (9)$$

If a cavity has a critical radius between the two values given by this equation, Hsu concluded it will be active and will only take a finite amount of time to nucleate. The solution for the maximum and minimum cavity radius when the boundary condition at the wall is a constant heat flux, can be obtained by replacing $T_w - T_b$ by qd/k_1 in equation (9).

Han and Griffith, using an approach similar to Hsu's, assumed the wall temperature was constant, the critical vapor bubble was a hemisphere, and the thermal boundary layer developed was governed by the following linear approximation to the heat conduction equation applied to an infinite liquid layer:

$$\left(\frac{\partial T}{\partial y} \right)_{y=0} = \frac{T_w - T_b}{(\pi \alpha_1 t)^{1/2}} = \frac{T_w - T_b}{d(t)} \qquad (10)$$

The first part of equation (10) is the exact definition of the temperature gradient at the wall when the liquid layer is of infinite extent. The second part of the equation is a convenient approximation for the thermal layer recovery. Using this approximation, the temperature profile becomes linear. The size range of active cavities is then given by the following maximum and minimum values:

$$R_c\Big|_{min}^{max} = \frac{d_m}{3}\left(\frac{T_w - T_{sat}}{T_w - T_b}\right)\left\{1 \pm \left[1 - \frac{12(T_w - T_b)T_{sat}}{(T_w - T_{sat})^2 d_m \rho_v L}\right]^{1/2}\right\} \tag{11}$$

For values of R_c between the maximum and minimum, the waiting time between bubble departure and the next nucleation is then:

$$t_w = \frac{9}{4\pi\alpha_l}\left[\frac{T_w - T_{sat}(1+2\sigma/R_c\rho_v LJ)}{(T_w - T_b)\,R_c}\right]^{-2} \tag{12}$$

The minimum waiting time and the corresponding optimum cavity size which can be obtained by differentiation of equation (12) are:

$$t_{wm} = \frac{144(T_w - T_b)^2 T_{sat}\,\sigma^2}{\pi J^2 \rho_v^2 L^2 (T_w - T_{sat})^4 \alpha_l}, \tag{13}$$

$$R_{cm} = \frac{4T_{sat}\sigma}{(T_w - T_{sat})\rho_v LJ} \tag{14}$$

c. Active Site Density

The effect of the number of active sites per unit area (n/A) on the overall rate of heat transfer is based almost entirely on experimental findings. The common method of determining the value of n/A as a function of other heat transfer variables consists in taking a series of photographs and counting the number of bubbles on the surface. At low fluxes, where the population of active sites is small, this method has been quite successful. Once the population density becomes greater than 5000 sites/ft^2 this method cannot be used because the surface is hidden by bubbles in various stages of the bubble cycle. Gaertner and Westwater (16) circumvented this problem by using electrolysis. At an active site, they found the metal plated on the surface at a much slower rate than over the remaining portion of surface where bubbles never interfere with the plating process. They reported the population density as a function of the total rate of heat transfer until the density became greater than 100,000 sites/ft^2. The results showed the effectiveness of each individual site continually decreased as the number of sites increased.

Summarizing the present research on the nature of an active site, it can be said that vapor must be present on the surface if a site is to become active at any reasonable temperature difference. If vapor is present, then the theories for predicting site activity can be used. On a normal boiling surface, even with the theories for predicting site activities, it is not possible to predict n/A because the number of vapor containing sites is much different from the number of possible vapor containing sites. On a specially prepared surface this is not the case because certain sites are made much more active than any naturally occurring sites.

5. Bubble Departure Criteria

Equation (5) has been used by many investigators to correlate bubble departure data. Cole and Shulman's (7) experiments at substmospheric pressures and Semaria's (42) experiments at pressures up to 20 atmospheres both showed unexpected deviations from equation (5). The departure size at subatmospheric pressure was bigger than the size predicted by equation (6); the departure size at high pressure was smaller. Cole and Shulman suggested the following equation, which will correlate both sets of data:

$$D_d = \left[\frac{\sigma \cdot}{g(\rho_l - \rho_v)}\right]^{1/2} \left(\frac{1000}{P}\right), \quad P \text{ is in mm of Hg} \tag{15}$$

Cole and Shulman discussed the corrections to the Fritz equation (5) that have been proposed by previous investigators. Except for a set of equations serived by Han and Griffith (20), Cole and Shulman found no equation which could correlate the existing data. They stated, "Han's equation is the most useful from the point of view of predicting the relative importance of departure velocity and acceleration, however its use to predict departure volumes is limited owing to the fact that Griffith (21) published another article almost concurrently with that of Cole and Shulman. In their report, Han and Griffith did not use the system of equations for departure. Instead they showed a plot of the receding bubble contact angle with the surface as a function of the bubble growth rate just before departure. The Fritz equation and this figure are used to determine when a bubble will depart in the second section of Han and Griffith's report (22). When they discussed proposed corrections to the Fritz equation they stated: "that these deviations were a result of an attempt to use a single mean contact angle for the whole bubble growth and departure process."

6. Boiling Temperature Distributions

a. Temperatures in the Solid

When two thermocouples are placed at known depths below the surface of a solid through which heat is being transferred, the heat flux can be determined from the recorded temperatures. If one temperature and the heat flux are known, then the temperature at the other point can be found by the same equation. This last procedure has been commonly used to obtain the surface temperature when the flux through a solid and the temperature at a certain depth below the surface is known.

Hsu and Schmidt (26), attempting to measure the surface temperature, by using a .040 in. thermocouple pressing against the surface, observed not only the surface temperature but also temperature fluctuations. They correlated the magnitude of the temperature fluctuations by the following expression:

$$\Delta T_{avg} = C\left[q\left(\frac{f}{\alpha_w}\right)^{1/2}\right]^{-a} q\,\frac{(T_w - T_{sat})}{k_w} \qquad (16)$$

They reported, in tabular form, the values of "C" and "a" for water boiling on several materials with known surface finishes. In an effort to explain the temperature fluctuations, Hsu and Schmidt proposed an efficient bubble departure mechanism as the cause.

Moore and Mesler (34) used a small cylindrical thermocouple with an outside diameter of .015". The second element of the thermocouple was a .005" diameter wire and was placed inside the outer tube. They press-fitted the thermocouple into the surface, ground it flat, and then plated metal on the surface to form a junction. By using the small sensing element and by displaying the temperature on an oscilliscope they discerned a regular, periodic temperature fluctuation. The analysis of the fluctuations showed the existence of a very high heat transfer rate for short time intervals. They concluded the only satisfactory explanation was a thin film vaporization model.

Three separate investigations show the correctness of Moore and Mesler's proposal. By synchronizing a strobe light with the temperature trace, Rodgers and Mesler (40) showed that the beginning of the fluctuation corresponded to bubble nucleation. Hendrichs and Sharp (24) obtained the same result in a motion picture study. They also observed almost no indication of either nucleation or departure in the region that never comes in contact with the bubble. Bonnet, Morin, and Macke (3) observed boiling off a small oil-heated tube in which a small thermocouple was brazed. Both an indication of the temperature being sensed by the thermocouple and photographs of the bubble above the temperature sensor were recorded on the same motion picture film; the results showed that Moore and Mesler's proposal is correct. Furthermore, they proposed the following equations as an explanation of the observed temperature fluctuations:

$$\Delta T_w(t) = \frac{-2\Delta q}{\sqrt{\pi k_w \rho_w Cp_w}} \sqrt{t} \qquad \text{when } t \leq te, \qquad (17A)$$

$$\Delta T_w(t) = \frac{-2\Delta q}{\sqrt{\pi k_w \rho_w Cp_w}} (\sqrt{t} - \sqrt{t-te}) \qquad \text{when } t \geq te \qquad (17B)$$

Part A of equation (17) is the temperature at the surface of an infinitely thick slab initially at a constant temperature after it is subjected to a constant surface heat flux Δq during the time interval [0,te]. The variable te is the time interval between nucleation and the occurrence of the minimum surface temperature. The second part of equation (17) is the temperature recovery of the surface after Δq has been removed and the surface is insulated.

Torikai et al. (47) photographed boiling from the undersurface of a glass plate. A conductive coating on the glass plate was used to generate the heat required for boiling. Since there is a difference in the critical angle for the reflection of light at glass-liquid and glass-vapor interfaces, they were able to show the existence of the liquid film photographically. They presented a theory for the microlayer thickness under a bubble. In the solution they assumed a linear velocity under the bubble, laminar flow, a hemispherical bubble shape, and a layer thickness determined by the diameter of the bubble adhesion area. The dynamic terms were grouped in a constant k_δ and a solution for just the surface tension force was given as:

$$\Delta(R_b) = R_b\sqrt{\frac{\mu_1 U_b}{2\sigma(1+k_\delta)}}\text{, and}$$

$$\Delta(R) = \frac{R}{R_b}\Delta\ (R_b) \qquad (18)$$

Sharp (45) used interference fringes, resulting from the reflection of monochromatic light off both the liquid-vapor interface and the liquid-solid interface. A flint glass plate, which was heated by a hot air jet, was used to boil water and methanol at various heat fluxes. The experimental measurements were obtained by observing a bubble through a piece of plastic mounted above the surface. After the bubbles grew to the height of the top plate, the base of the bubble was observable and the measurements were made. The height of the plate above the boiling surface was varied from .15 to .28 inches. The maximum bubble radius was between .25 and .37 inches. No estimate of the surface temperature could be obtained. Sharp concluded that the microlayer does exist, that no observable drying out of the film occurs at low fluxes, and that at high heat fluxes, it becomes the májor contributer to heat transfer. At an average flux of 42,000 Btu/ft^2-hr, he graphically showed the motion and the thickness of the layer.

Cooper and Lloyd (8) studied the boiling of toluene from a glass plate on which thermistors had been vapor-deposited. The liquid and the solid were superheated using radiant energy and then nucleation was induced by passing a small current through a thermistor of known distance from the thermistors being monitored. In addition to the initial temperature fluctuation associated with bubble growth, as others have also reported, they observed a smaller secondary fluctuation which started as the liquid-vapor interface passed back across the temperature sensor. From the temperatures at each of the four points being monitored, they calculated the amount of heat transfer and the amount of liquid evaporated. Two methods were used to calculate the liquid film thickness. A heat balance over the liquid layer gives the following differential equation:

$$\rho_1 L \frac{d\,\Delta(t)}{dt} \cong - \frac{k_1 (T_w - T_{sat})}{\Delta(t)} \qquad (19)$$

Integration over the duration of the temperature decrease results in the following equation for the initial film thickness:

$$\Delta_o = \left[\frac{2k_1}{\rho_1 L} \int_o^{te} (T_w(t) - T_{sat})\ dt \right]^{1/2} \qquad (20)$$

The other method, based on the properties of the solid, is not presented in the report. It is based on the observed temperature fluctuation of the wall being used as the boundary condition in the heat conduction equation, as applied to the solid. Tables, comparing the two methods of calculating microlayer thickness, are shown in their report.

Hospeti and Mesler (25) measured the average amount of vaporization under a bubble by measuring the amount of radioactive calcium deposited on the surface after 5000-10,000 bubbles have nucleated and departed. They found the average thickness of the layer evaporated was 120 μcm ±100%.

b. Temperature Measurements in the Liquid

Knowledge of the temperature patterns in the liquid around an active site is based entirely on experimental findings. Using Schlieren photography, Hsu and Graham (27), showed that the influence of an active site extended out to one bubble departure diameter away from the point of nucleation. Gaertner (15) saw interference patterns under a departing bubble in his photographs and concluded that a departing bubble sucks the liquid layer off the surface. A small moveable temperature probe enabled Marcus and Dropkin (31) to observe the behavior of the liquid thermal boundary layer as water boiled on the surface. They reported the thermal boundary layer thickness was a function of the surface heat transfer coefficient alone. When h_w was below 700 Btu/ft^2-hr, they found $h_w d = .619$; when h_w was above 700 Btu/ft^2-hr, they found $h_w d = .0224\ h_w^{1/2}$. Marcus and Dropkin reported the thermal boundary layer was linear out to .575d and then decreased according to an inverse power law. A maximum in the size of the temperature fluctuations in the boundary layer was observed at .64d.

It is difficult to imagine a more conclusive set of evidence to show the existence of the microlayer under a bubble growing on the surface. Sharp and Torikai have both developed the technique of showing the presence of the microlayer. Sharp has been able to measure the thickness of the layer. Cooper and Lloyd have presented two techniques for measurin the microlayer thickness from experimental surface temperature fluctuations. Torikai has presented a theory for predicting the microlayer thickness. Perhaps the only limitation of the theory is the absence of specific dynamic terms. The dynamic terms have to be important since surface tension has been overcome by the hydrodynamics when the bubble starts to grow.

Outside the region on the surface covered by a bubble, Hendricks and Sharp reported no temperature fluctuations. The study of liquid heat transfer during boiling by Marcus and Dropkin led to the same conclusion. The maximum in the temperature fluctuation in the liquid occurred at .64d and the fluctuation decreased as the probe was moved closer to the wall.

7. Nucleate Boiling Correlations

There are numerous boiling correlations available from the literature. Earlier correlations are summarized in a book by Tong (48), "Boiling Heat Transfer and Two Phase Flow."

Of all the equations Tong summarizes, only one correlation, by Rohsenow, even considers an effect of the liquid-solid combination on the overall heat transfer. This equation is:

$$\frac{Cp_1 \ \Delta T}{h_w} = C_6 \left(\frac{q}{\mu_1 L} \sqrt{\frac{\sigma}{g\ (\rho_1-\rho_v)}} \right)^{1/3} \left(\frac{Cp_1 \mu_1}{k_1} \right)^{1.7} \tag{21}$$

The values of C_6 for glass-alcohol and glass-toluene have never been determined. A lot of other data has been summarized by adjusting the value of C_6 in equation (21).

Correlationsby Chang (5) and Zuber (53) have used analogies between boiling and other heat transfer phenomena. Chang modified the natural convection equation to take account of turbulent agitation induced by boiling. Instead of using the molecular thermal conductivity in the natural convection equation, Nu = .145 $Gr^{1/3}$, he suggested the use of the effective thermal conductivity defined by the equation: $k_\varepsilon = k_1\ (1 + \varepsilon_1/\alpha_1)$. The ratio ε_1/α_1 was specified by the following equation which was derived using a dimensional analysis technique:

$$\frac{\varepsilon_1}{\alpha_1} = \frac{C_2 q}{(T_w - T_{sat})} \left(\frac{\Delta P \nu_1^2}{Cp_1 \mu \sigma k_1 \beta (T_w - T_{sat})} \right)^{1/2} \left(\frac{Cp_1 T_{sat} (\rho_1 - \rho_v) \Delta P}{L^2 \rho_v^2\ J} \right)^{1/5} \tag{22}$$

A value of C_2 = .343 was suggested by Chang after the equation was compared to experimental boiling data. Zuber presented a theory based on the trubulent natural convection investigations of Malkas (30) and Thomas and Townsend (46), (49). In the natural convection equation, Zuber modified the $\beta \Delta T$ term in the Grashof number to account for the additional buoyancy induced by the bubbles. The final result is:

$$\frac{h_w \ell}{k_1} = C_3 \left[\frac{g\ell^3}{\nu\alpha_1} \left(\beta(T_w - T_{sat}) + \frac{8nJA^2\alpha_1 D_d}{3A\ U_t} \right) \right]^{1/3} , \qquad (23)$$

$$\text{where} \quad U_t = C_4 \left[\frac{g(\rho_1 - \rho_v)}{\rho_1^2} \right]^{1/4} \qquad (24)$$

The equation for the rate of rise of lenticular-shaped bubbles, equation (24), has been reported in two articles: Peebles and Garber (36) suggested $C_4 = 1.18$; Harmathy (23) suggested $C_4 = 1.53$. A value of $C_3 = .34$, which Zuber used, is based on the turbulent natural convection studies.

Zuber (52) presented another correlation, which was an attempt to summarize some of the known experimental boiling facts. In this correlation, Zuber divided the surface into a region covered by bubbles and a region where only convection occurred. By assuming all the energy in the bubble comes from the surface, he obtained the following expression for the rate of heat transfer:

$$Q = C_5 k_1 (T_w - T_{sat})\ JA\ Pr^{1/3} \sqrt{\frac{n/A}{\pi Pr D_d}} \left(1 - \frac{\pi D_d^2 n/A}{4} \right) + \frac{\pi}{6} (n/A) L \rho_v D_d^2 f \qquad (25)$$

He states that: "this equation is valid as long as there is no lateral bubble interference on the surface." The experiments of Hsu and Graham (27) have shown that lateral interference occurs whenever $2(n/A)^{1/2} D_d > 1$. This is the upper limit on equation (25). The first part of equation (25) is the amount of energy transferred by agitation; the second part is the amount of energy transferred as latent heat. Thus, Zuber can show, from the equation (25), the effect of n/A on both agitation and latent heat transport.

8. Discussion of the Literature

Quantitative studies have never been reported for boiling off a glass surface. The major reason is probably because until recently it has been impossible to measure a surface temperature on a glass plate.

The theories for bubble growth presently assume that only liquid and vapor properties control bubble growth. The effect of the superheated liquid layer on the surface has been considered but only insofar as it contributes to vaporization on the outer bubble surface. The microlayer under the bubble, which has been shown to exist by physical measurements, has not been included in the bubble growth theories in any precise manner.

The effect of a glass substrate on the stability and activity of a site has been indirectly discussed. Since a glass surface is very smooth, there are very few vapor traps and therefore very few potentially active sites. Therefore, boiling might be unstable and in all likelihood it might be very difficult to nucleate on the glass surface at low superheats.

General correlations predict no effect of the thermal properties of the solid. The general feeling is that since a liquid has very poor heat transfer properties when compared to a solid, and since most of the heat transfer, until high fluxes, goes through the liquid, the major resistance to heat transfer is in the liquid layer.

Thus far, the studies of microlayer vaporization have been limited to describing the phenomenon and analyzing the temperature fluctuations induced by the evaporation of the microlayer. It has been shown that the sharp primary fluctuation, corresponding to microlayer vaporization, starts at the time the bubble spreads across a radial point on the surface. A smaller, secondary fluctuation has also been reported. This fluctuation can be interpreted as an indication of the liquid spreading back across the radial point if the microlayer has completely evaporated.

The total contribution of microlayer vaporization to the bubble volume at departure has not been calculated. In order to calculate the microlayer contribution, it is necessary to know the departure time, and the variation of the base contact radius with time. Until the microlayer theory was proposed, the region inside the base contact radius was not considered to be important. It has, therefore, not been well tabulated in the literature. The one theory which has been proposed for the microlayer thickness has never been compared with experimental data.

This study will attempt to determine if boiling heat transfer can be limited by a solid that does not have good heat transfer properties. The contribution of the microlayer will be estimated from experimental determinations of the bubble growth rate and the bubble base contact radius and from a theoretical study of microlayer thickness.

III. DESCRIPTION OF EQUIPMENT

1. Introduction

The goals of this study are to investigate the amount of heat transfer which occurs around a single active site. Microlayer vaporization is to be considered.

The temperature-time curves, for surface temperature sensors, are recorded from an oscilloscope screen and still photography gives the bubble size at a particular instant. An electrical measuring circuit pinpoints the time that these pictures are taken on the temperature-time curve. Based on at least 30 pictures of the boiling process, taken under the same experimental conditions, the geometric properties of the typical bubble are obtained as a function of time.

The following sections give a detailed description of the component parts which, when acting together, give all the necessary experimental information. The component elements are: the vapor-deposited surface resistors which serve as temperature sensors, the single-site heater which generates heat underneath the boiling plate, the boiling vessel which controls the environment around the single-site heater, the electrical triggering and measuring circuits which are used to relate the temperature trace to bubble size, and finally, the optical equipment for obtaining the boiling pictures.

2. Boiling Surface

The boiling surface is a piece of soda lime glass, .020" thick, and .460" square. On the top surface, as figure (1) shows, four nickel resistors, consisting of four parallel elements spaced .008" apart, are vapor deposited. Each element is .002" wide,.020" long, and nominally 200 A° thick. Each is connected in series to the other elements by gold conductor strips. From the end elements, gold bars are deposited out to square gold tabs at the edge of the plate. Two additional resistors with a different geometry are also deposited. A resistor located at the geometric center of the surface is similar to the previous resistors; the spacing between the two central elements is spread to .011" instead of a .008" spacing. In addition, a circular resistor is deposited, which has a radius of .043" about the geometric center of the surface. The resistance of each of the square resistors are nominally 7000Ω; the resistance of the circular resistor is about 14,000Ω. The centers of the square resistors are located at the following distances from the geometric center: .000", .065", .081", .125" and .153".

Beneath the resistors, which will be used as temperature sensors, is a layer of silicon monoxide followed by a strip of tantalum .154" wide. The direction of the strip which coats the central region is perpendicular to the gold leads connecting the temperature sensors to the side tabs. All but a square central region of this strip .154" square is overcoated with gold. The remaining tantalum square has

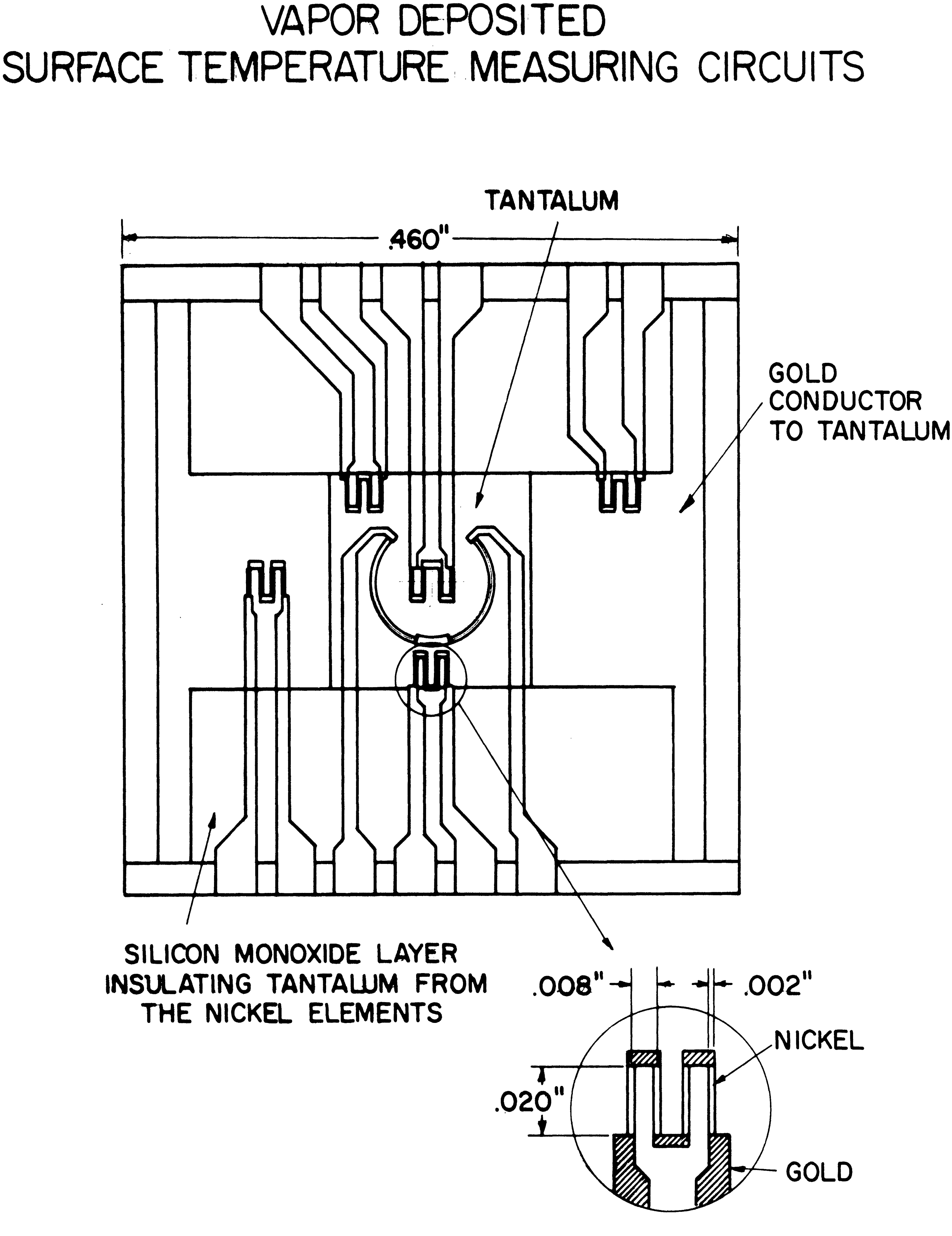

Figure 1 Geometric Arrangement of Vapor Deposited Resistors

CROSS-SECTIONAL VIEW OF THE SINGLE SITE HEATER

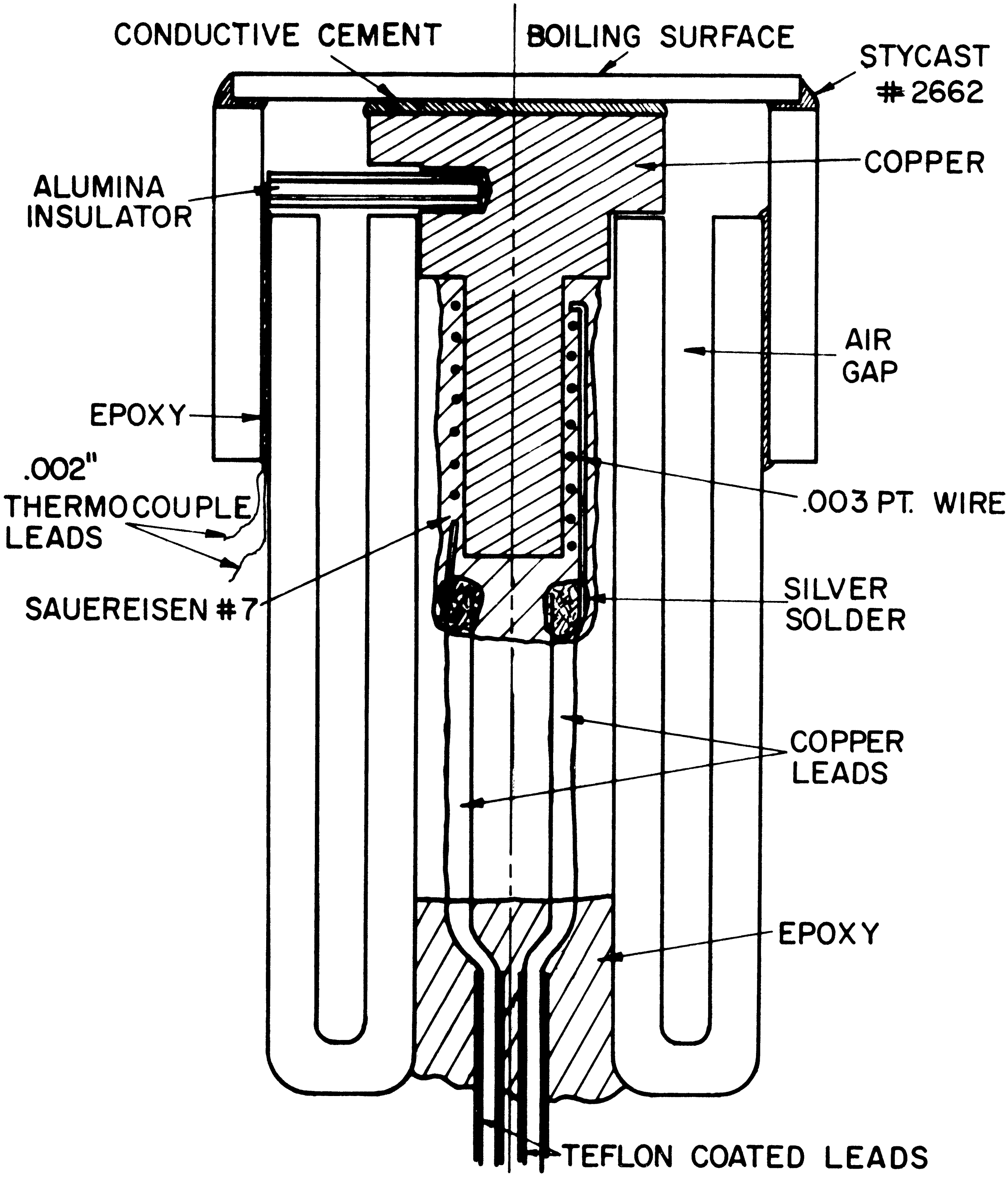

Figure 2 Cross-Sectional View of the Single Side Heater

a nominal resistance of 50Ω and it can serve as a surface heater. Above the temperature sensors was another layer of silicon monoxide, electrically insulating the surface resistor from the boiling fluid. Both insulating layers are about 1000 A° thick.

3. Single-Site Heater

A heating element, figure (2), capable of generating enough heat to boil the fluid on the glass plate, is glued to the bottom of the plate. The element consists of a copper core in the shape of a rivet. The head of the rivet, glued to the glass plate, is .350" in diameter; the shank is slightly under .100" in diameter. Electrical heat generation around the shank of the rivet is provided by a .003" platinum wire, embedded in Sauereisen cement. The cement insulates the wire from the copper core and serves as a heat transfer medium to transfer heat to the core. A glass fitting seals the heater from the boiling fluid. The fitting consists of two concentric pieces of glass tubing fused together at one end. The annular space between the tubes reduces the radial flow of heat from the heating element mounted in the inner tube. The heat must either flow up to the top surface or down the copper leads silver soldered to the platinum wire.

The glass fitting is not glued directly to the sides of the boiling surface. Instead, a piece of glass tubing with an ID slightly greater than the OD of the fitting is roughened and glued to the plate with Stycast* #2662. The heating element is then glued to the bottom of the glass plate. Several different materials are used to cut down the thermal resistance of this joint: Conductalute**, mercury, and a

*Emerson Cummings Tradename

**Sauereisen Tradename

silver filled epoxy glue made by Electro-Science Laboratories. After the heater is mounted to the boiling surface, the glass fitting is telescoped into the outer glass tube bonded to the top surface. The hole at the base of the glass fitting, where the leads to the heater enter, and the space between the outer tube and the glass base are sealed with epoxy.

Except for one heater, where the temperature of the heating element is determined by the resistance of the platinum wire, a .002" thermocouple, made by Omega, is placed in the head of the heating element. The leads from the thermocouple exit through the space between the outer glass tube and the glass fitting.

4. Boiling Chamber and Related Equipment

The completed heater, which includes lead wires which have been soft soldered to the tabs on the boiling surface, rests on the male end of a 16 hole, 3/4" diameter Conax gland. Four of the holes in the gland contain leads from two Chromel-Alumel thermocouples, two contain leads to the heating element, and ten contain leads connected to five of the six surface resistors. The assembled gland, figure (3) is inserted into the bottom part of a jacketed stainless steel test chamber.

The test chamber, as figure (4) shows, is a cylinder 2 1/4" in diameter and 3 1/4" long. The wall of the cylinder is a piece of 1/16" thick tubing; the ends are 1/2" thick, 3" diameter teflon sealed sight glasses, held by sets of 6" OD, 3/4" thick flanges.

The side of the cylinder is surrounded by a 3 1/2" diameter cylinder which is also welded to the end flanges. A top and a

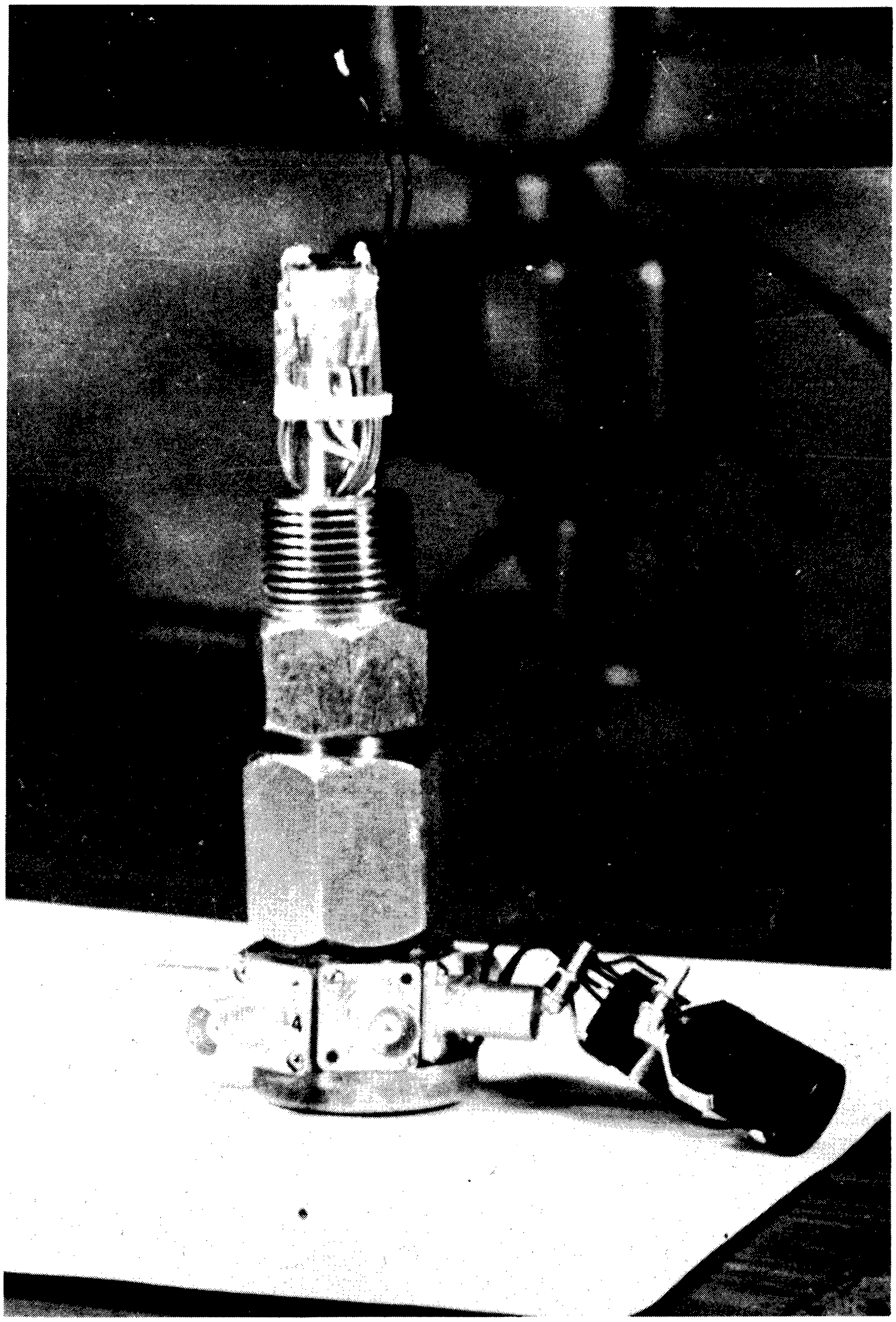

Figure 3 Photograph of the Assembled Conax Gland

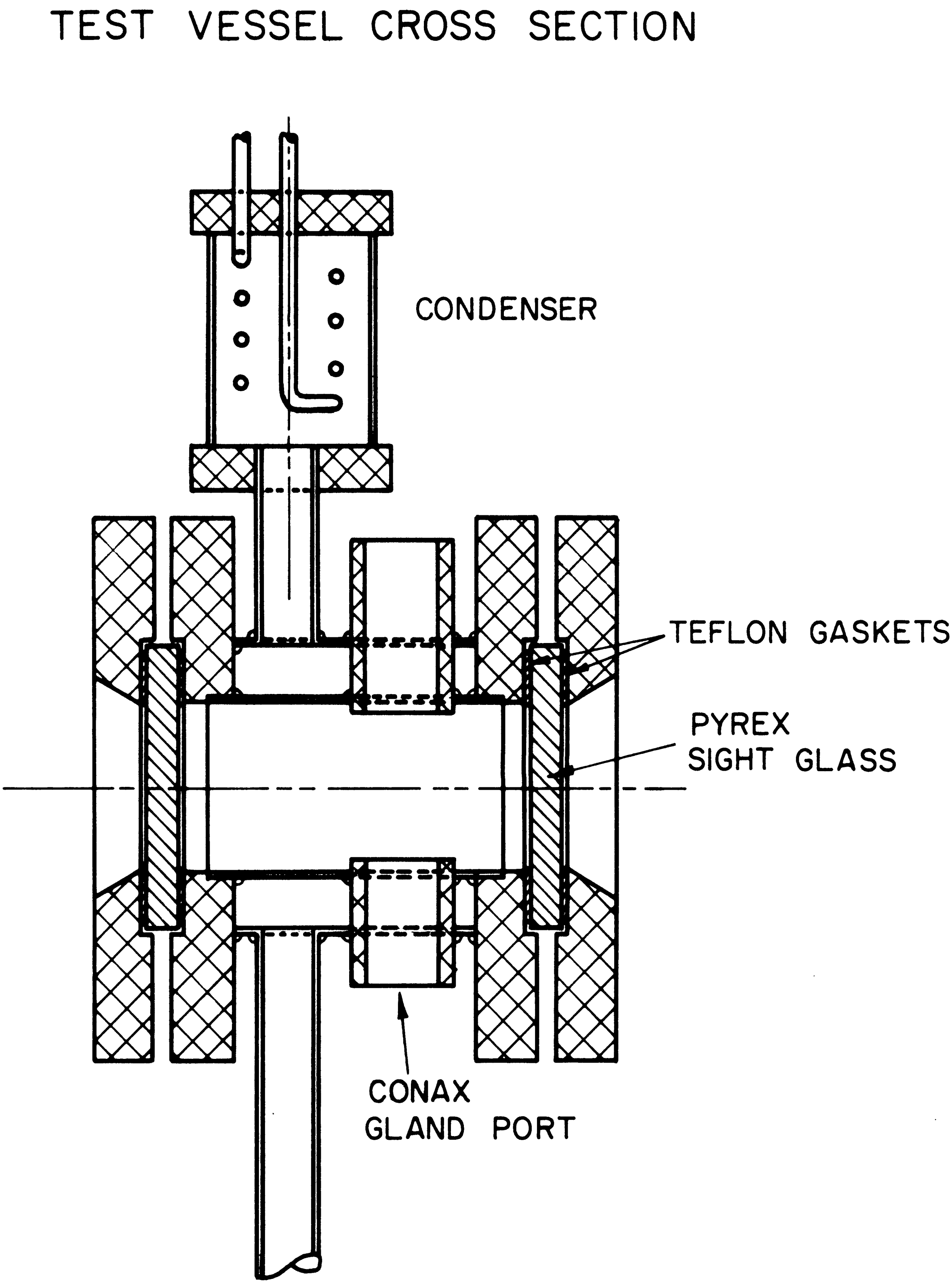

Figure 4 Cross-Secticnal View of the Test Chamber

bottom part with an ID of 29/32" pierce both the inner and outer tubes 1" from the end flanges. These port tubes, welded to both the inner and outer cylinders, provide the only quick access into the inner chamber. The outer jacket is pierced by two additional 3/4" tubes. Heat, generated along the tube joined to the underside of the jacket, boils the fluid in the jacket. The tube welded to the top of the jacket, leads to a water cooled condenser containing 6' of 1/4" stainless steel tubing.

Since the rate of heat generation in the inner chamber is less than 10 watts, no direct connection between the condenser and the inner chamber is required. Heat losses in the auxiliary piping can balance for the small amount of heat generated. Additional heating tapes are required around the flanges to compensate for the heat loss at these extended surfaces.

In addition to a condenser, a filling vessel controls the environment above the fluid during storage. High purity nitrogen from a gas cylinder supplies pressure; a water aspirator provides subatmospheric pressure. A schematic showing the valves and auxiliary equipment in relation to the boiling chamber is shown in figure (5).

5. Auxiliary Equipment

a. Electrical

A Tektronix, 502 oscilloscope is the basic instrument. On the screen of the oscilloscope, any two of the five surface resistors can be displayed. In addition, a modification kit from Tektronix provides a 25 volt square wave signal lasting for the duration of

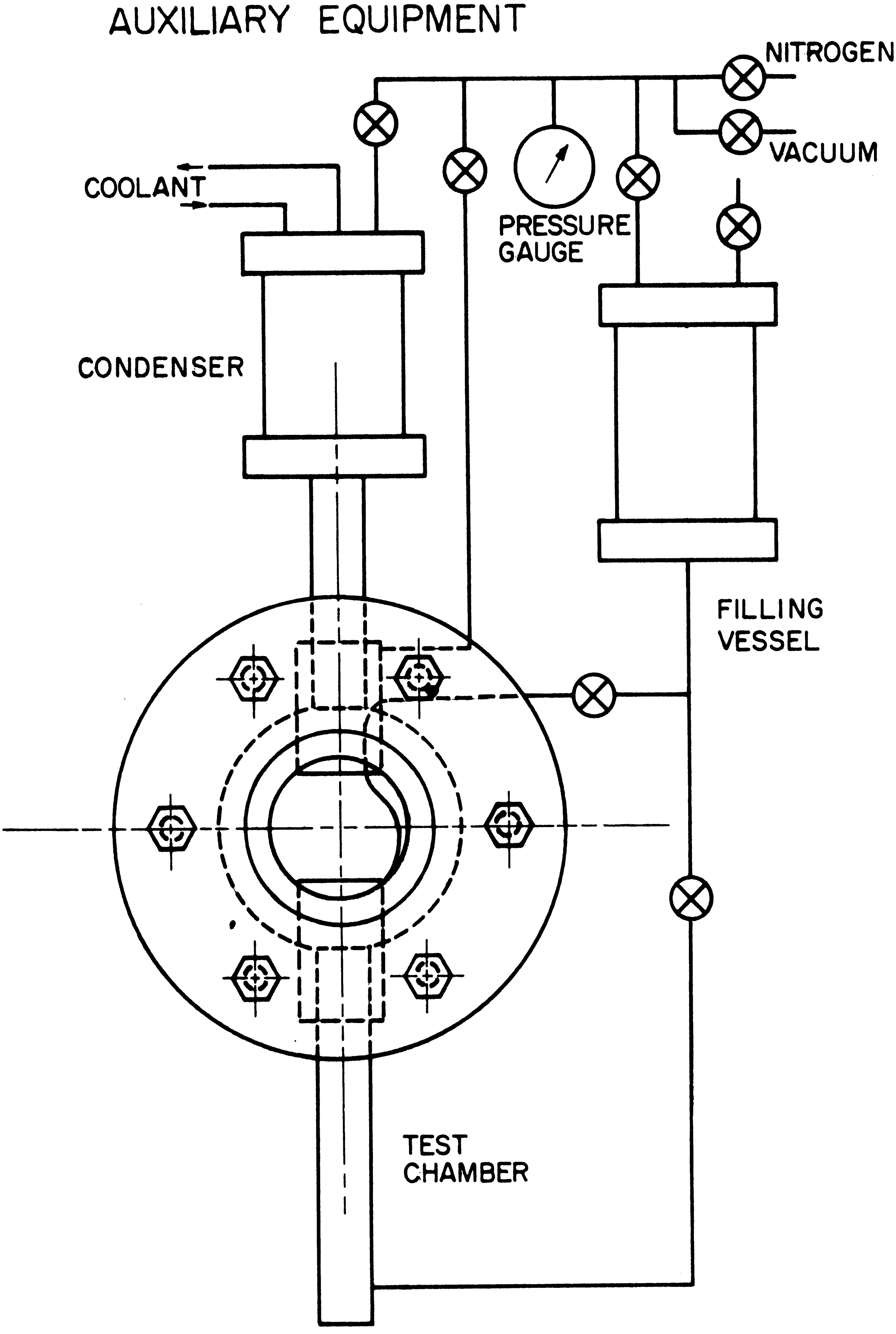

Figure 5 Auxiliary Equipment

any sweep across the oscilloscope screen. This provides a means of synchronizing other electrical equipment with the sweep of the oscilloscope.

The scope only measures voltage so the resistance of the temperature sensor has to be converted. Across a 10 volt mercury battery, a .9 meg Ω resistor is connected in series with one surface resistor. A change in resistance of the temperature sensor has a small effect on the current flow; a resistance change of 1000Ω is 1/1000 of the total current resistance. The voltage across the temperature sensor is proportional to the resistance of the element. The voltage fluctuation is only a small part of the total voltage drop across the element. A known amount of the total voltage drop across the surface film is bucked using a variable voltage source. The design of this voltage source differs between the first and last data obtained. The principle is the same; a resistor in series with a 10 turn potentiometer is connected across a mercury battery. In the original design, the battery is Zenér stabilized and the resistance of the potentiometer is 100KΩ. After use, the Zenér stabilization has been discarded as unnecessary and the total resistance of the potentiometer has dropped to 25Ω.

Two Edgerton, Gremehausen and Grier (EGG) microflash units are used to obtain doubly exposed boiling pictures. After the input signal is received, the occurrence of the flash can be delayed up to 1 msec. Another time delay unit, based on the same design principles used in the EGG units, provides time delays up to 20 msec. The auxiliary unit is placed electrically in front of one of the EGG units. Two phototubes, one in front of each flash unit, control a

Hewlett Packard interval timer which is capable of measuring the time interval between flashes to within .01 milleseconds.

The sweep trigger in the oscilloscope provides a way of starting the beam sweep across the screen only when two preset conditions are satisfied simultaneously on the monitored channel. The preset conditions are a voltage level and the slope of the voltage-time curve.

During boiling, the surface temperature is fluctuating rapidly. The conditions necessary to trigger the oscilloscope are satisfied soon after the last sweep is completed. This means almost a continuous stream of 25 volt pulses, separated only by the time necessary for the beam to sweep across the oscilloscope screen, are emitted by the modification put on the oscilloscope. Only one of these pulses must trigger the flash tubes if doubly exposed pictures are to be obtained. A single pulse generator, figure (6) shows the schematic, is placed between the oscilloscope output and the flash units. The single pulse generator operates in the following way. Once the DC voltage is applied to the thyratron tube, the next pulse emitted by the oscilloscope fires the tube which in turn generates an output pulse. Subsequent incoming signals do not change the state of the tube since it will continue to fire until the DC voltage is removed.

The power supply to the single site boiler is an 8 amp. 8 volt DC source with a .25% ripple. The current and voltage applied to the heater are measured by calibrated meters with mirror backed scales and knife edge pointers.

A Leeds and Northrup potentiometer measures the output signal from Chromel-Alumel thermocouples placed in the test assembly.

SINGLE PULSE GENERATOR

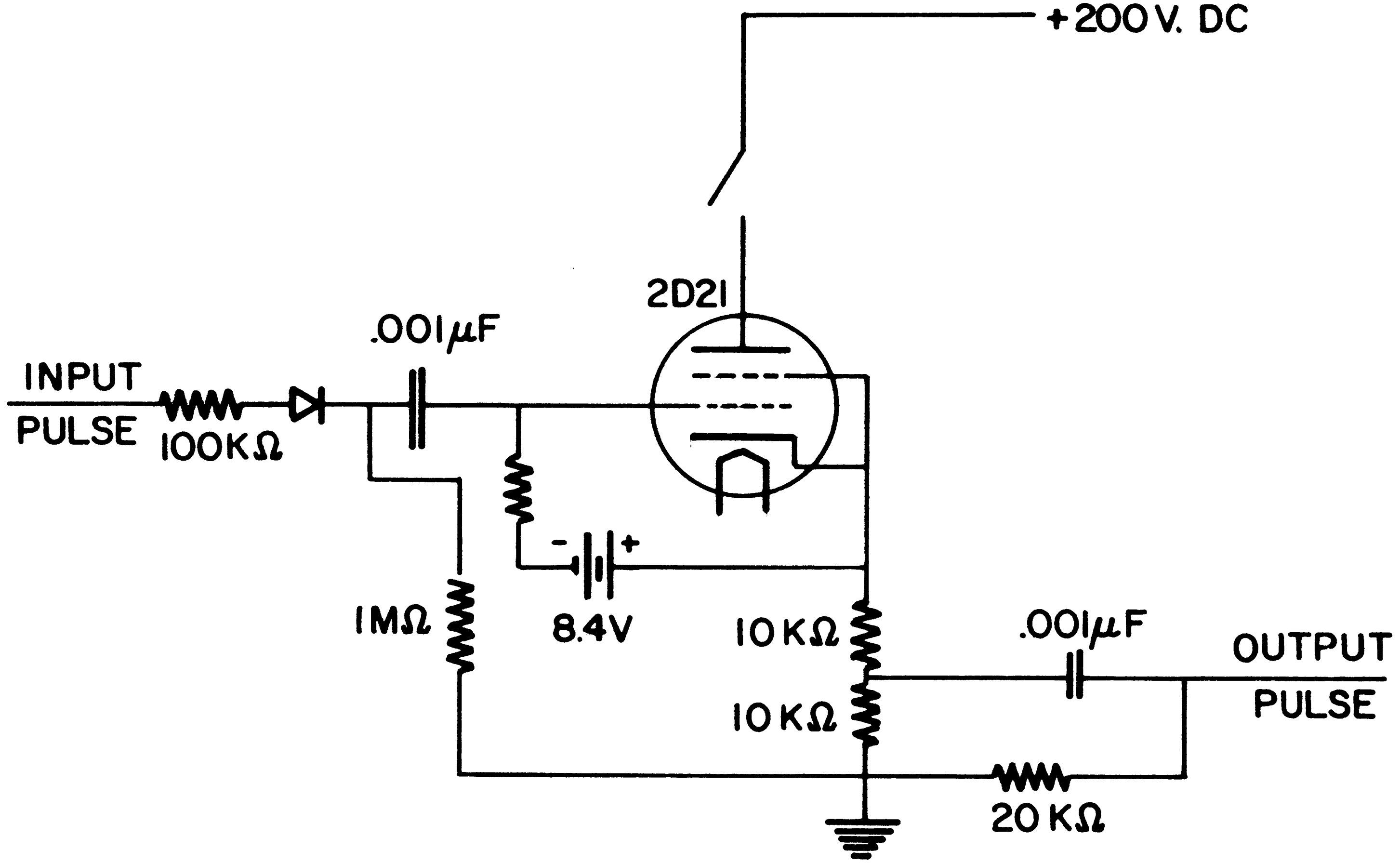

Figure 6 Electrical Circuit for the Single Pulse Generator

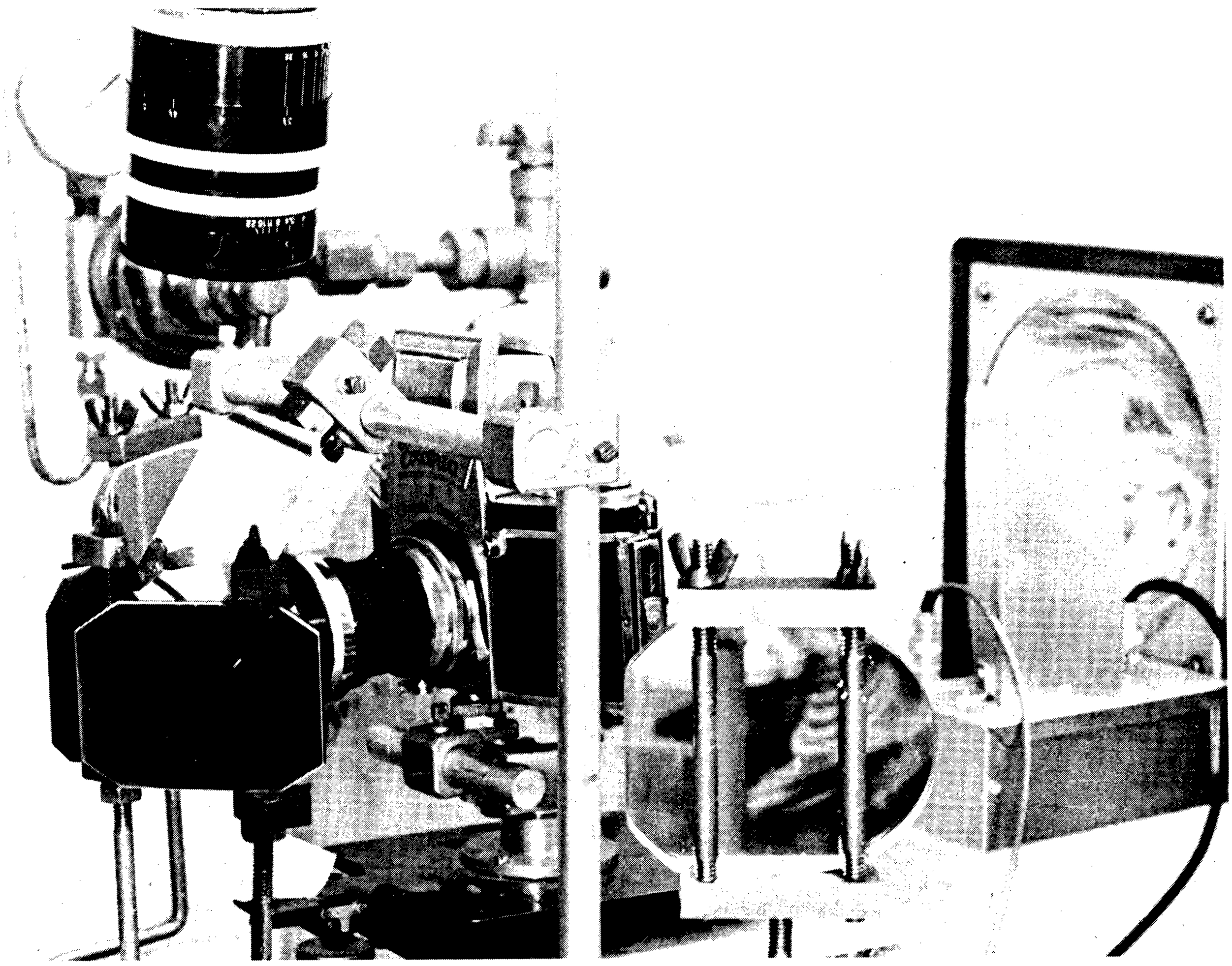

Figure 7 - Mirror Arrangement: Extreme Right - One of the flash units, Lower Right - Front surface mirror converging light from a flash unit toward test chamber, Lower Left - Second front surface mirror in optical path directing light onto the boiling surface, Center - Side view camera, Upper Left - Top view camera below which is the final mirror in the light path which directs the reflected light off the bubbles into the camera lens.

b. Optical Equipment

Pictures of the oscilloscope screen are taken with a 35 mm oscilloscope camera. Photographs of the boiling surface are obtained by an Exacta camera. Aluminum overcoated, flat, front surface mirrors are used to direct the light from the flash units into the test chamber. The arrangement of the mirrors, as figure (7) shows, serves two purposes; the test chamber is illuminated and the cameras are shielded from the flashes. A piece of polished nickel about 3/4" square is mounted within the test chamber. This polished surface provides a top view of the boiling surface. Initially, one camera was switched between side and top view. Later, a second camera and another front surface mirror, permit both views to be recorded at the same time. The arrangement of the flash units, cameras, mirrors, and test vessel on the optical bench is shown in figures (8) and (9).

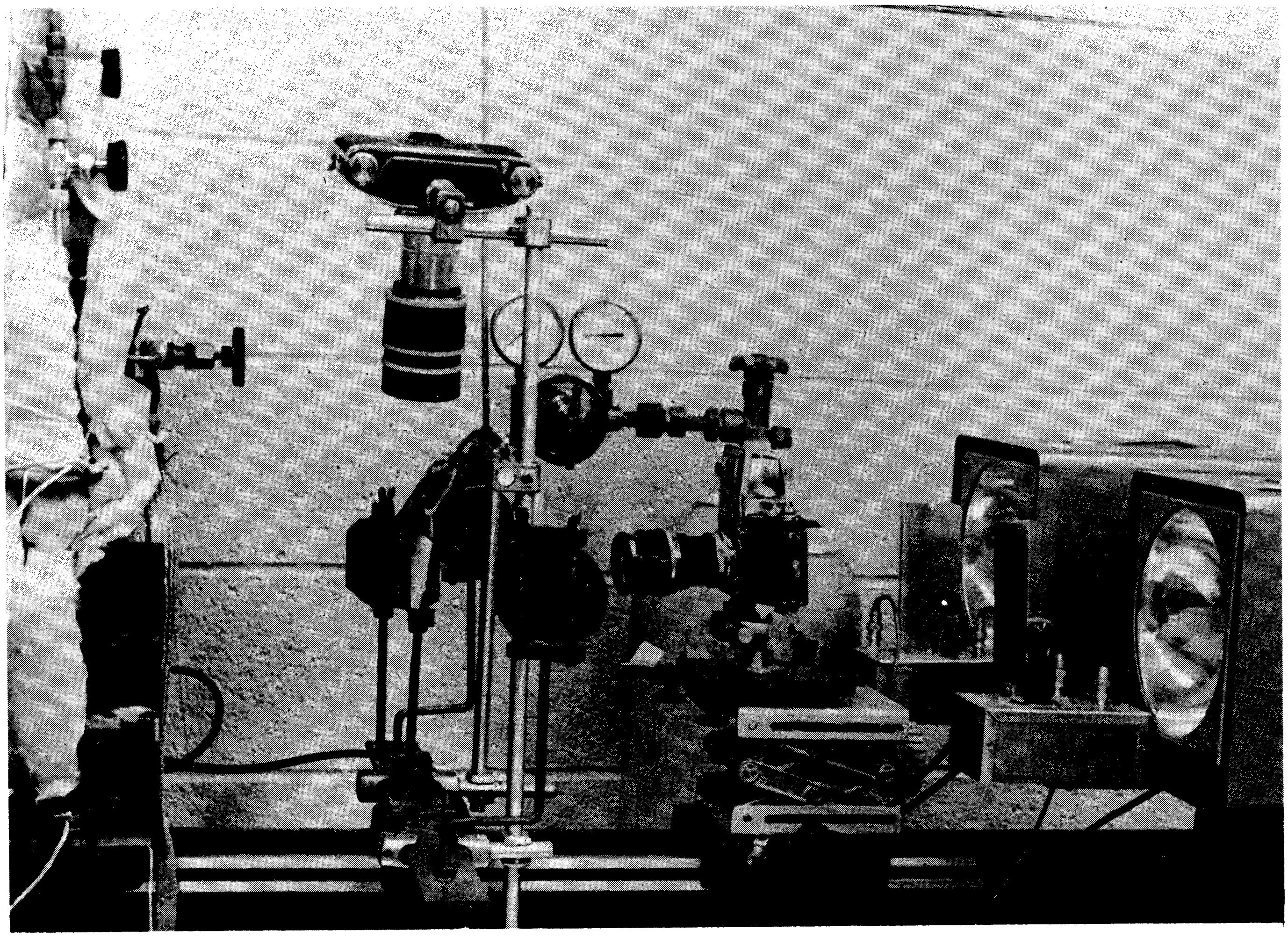

Figure 8 Photograph Showing the Mirror, Camera and Flash Mounts

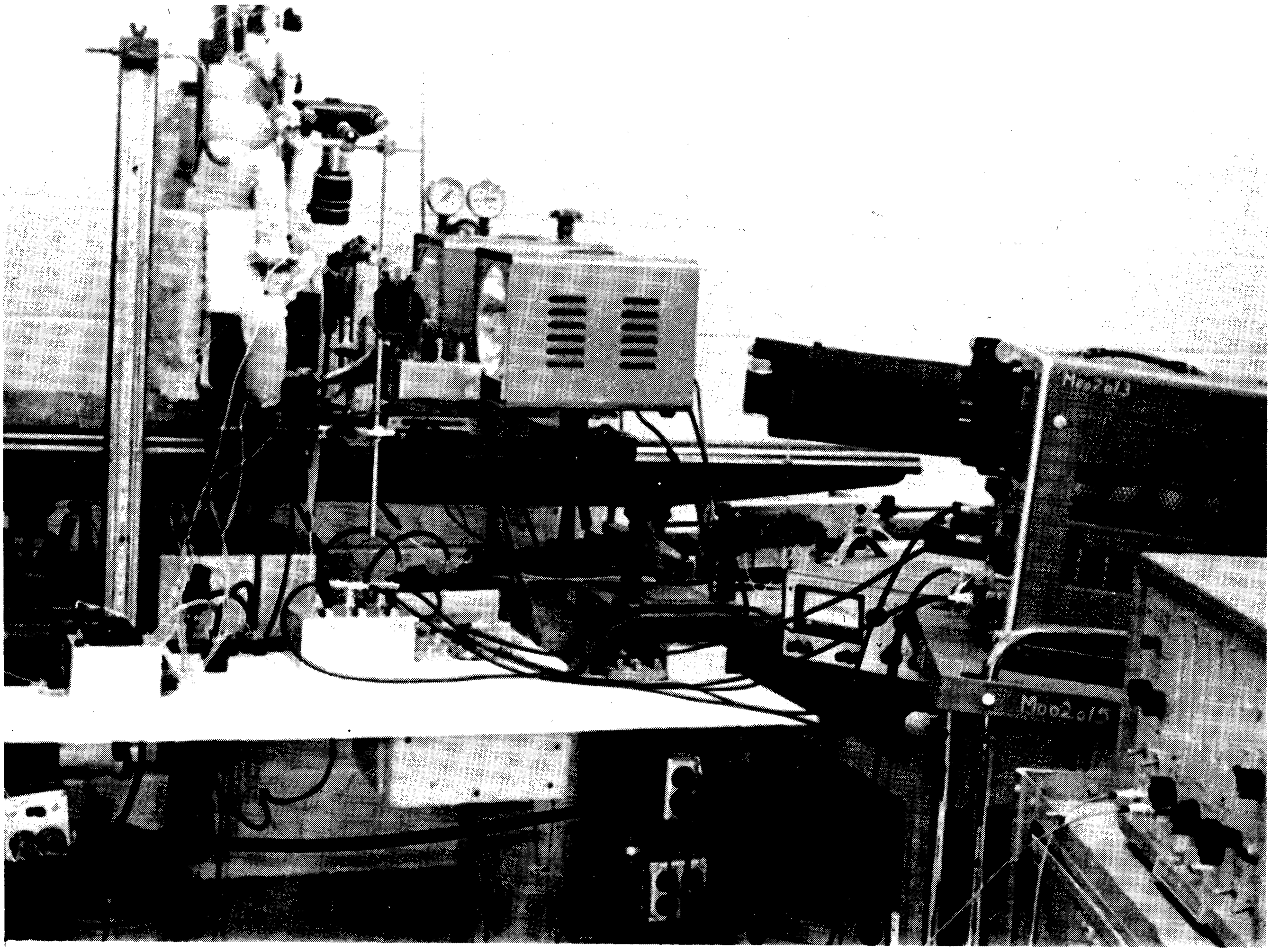

Figure 9 Photograph Showing the Relative Position of the Mirrors, Cameras, Flash Units and Auxiliary Equipment in Position for Taking Data

IV. EXPERIMENTAL PROCEDURES

The electrical circuit for the measurement of element resistance is shown in figure (10). The method of calibrating each surface element is explained in Appendix A. This calibration procedure continues until the surface is replaced.

Before boiling data is obtained, the equipment has been preheated and the liquid in the supply tank has been degassed by pulling a vacuum on it for 15 minutes. The liquid is then charged into the inner chamber of the test vessel. Normally the depth of the liquid is 1" above the boiling surface if the mirror showing the top view is used. The power to the single-site heater is turned on and gradually increased until nucleation occurs on the surface. After the start of nucleation, the power to the heater is turned down until only a few active sites are nucleating on the surface. An attempt is made to get only one active site but this is not always possible. During this adjustment period the cameras are positioned, and focused and all the remaining electronic equipment is turned on. A steady temperature in the inner chamber signals the completion of the startup procedure.

All the settings on the power supply to the heater, the resistance measuring circuit, and the oscilloscope are recorded. The pressure and bulk liquid temperature are also recorded. Two additional thermocouples, one in the vapor and another within the heater, are also noted in the log book.

The room is darkened, the camera shutters are opened, and the oscilloscope trigger level is adjusted. Simultaneously the voltage to the single pulse generator is applied and the shutter on the oscilloscope camera is opened. The next sweep of the oscilloscope triggers the flash

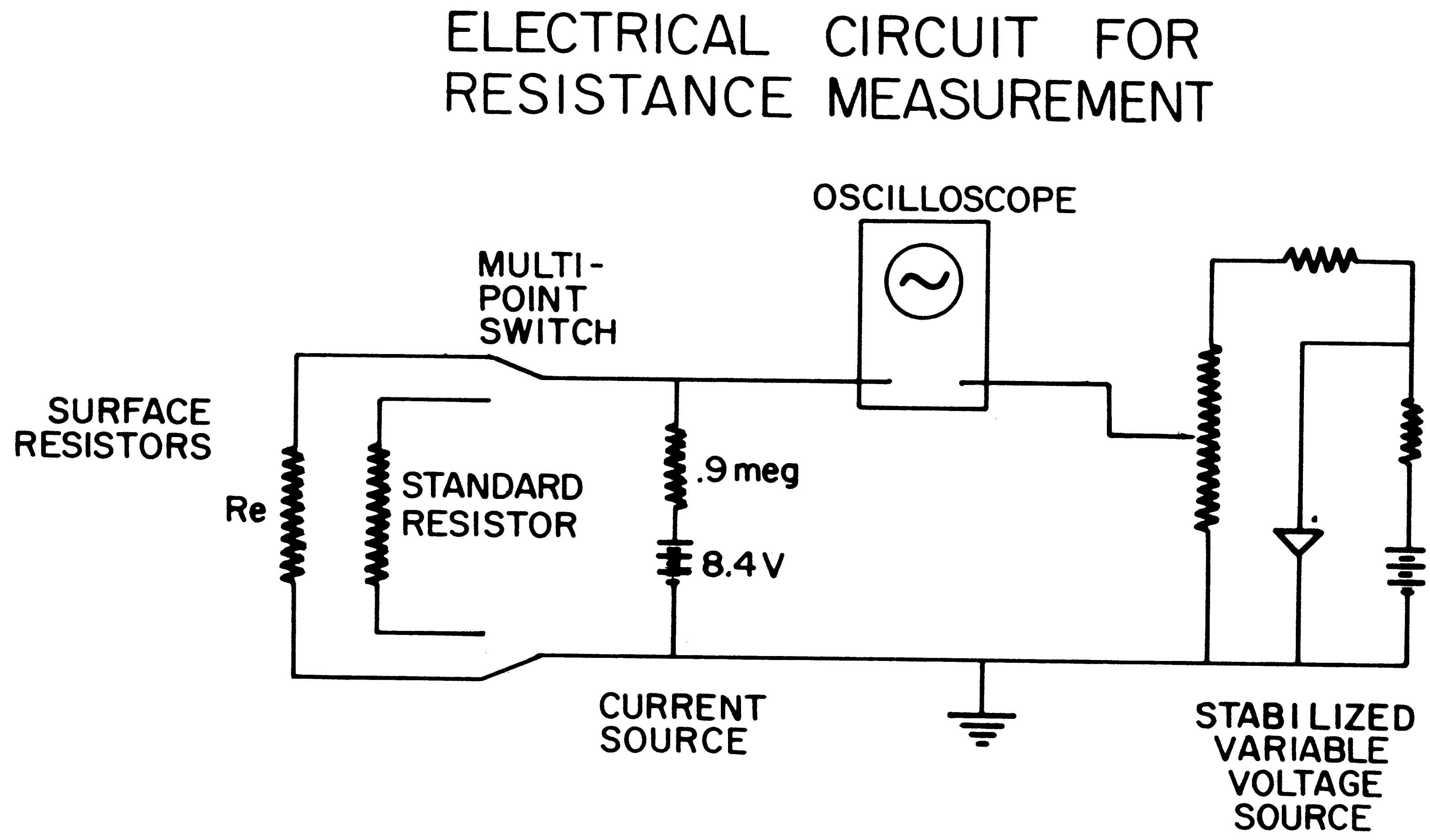

Figure 10 Electrical Circuit for Measuring Resistance

units and exposes the film in the cameras focused on the boiling surface. The voltage to the single pulse generator is removed only after all the camera shutters are closed and the reading on the interval timer is recorded. The winding of the camera starts the process again.

After a series of six to ten pictures have been taken, the cameras are indexed twice. This produces a blank space on all three rolls of film so the relation between the rolls is clear. At this time all the temperatures, pressure, surface resistor settings, power input to the single site heater, and the oscilloscope adjustments are recorded.

Each 35 mm roll of film contains about 39 frames. When the rolls are completely exposed, the power to the heater is turned off and another resistivity value for each element at the bulk liquid temperature is obtained.

The rolls of film are developed and printed using standard procedures. All the results are obtained from the enlarged prints.

V. EXPERIMENTAL RESULTS

1. Analysis of Boiling Photographs

The boiling photographs and corresponding pictures of the oscilloscope screen are obtained from 35 mm negatives. The boiling photographs which are to be analyzed, are enlarged to about eight times actual size during the printing process. The exact degree of enlargement, which is the same for each series of pictures on one roll, is determined by measuring the amount of enlargement of objects in the prints whose actual size is known.

From the photographs, the bubble shape is determined by tabulating five bubble measurements. The parameters which have been tabulated are shown in Figure (11A). In addition, the bubble volume has been obtained by numerically integrating the expression $2\pi R \Delta H(R)$. This expression assumes axial symmetry. If the photograph is a double exposure then bubble size and volume are calculated for both bubbles.

The oscilloscope photographs have subdivided grid lines superimposed on the traces so it is never difficult to determine a time or voltage level from any size enlargement. It is necessary to convert the voltage-time traces to temperature-time traces. This procedure is explained in Appendix B. Once the converted traces have been obtained they are processed in two ways. There are several variables that can be used to characterize the temperature trace. Figure (11B) shows the parameters that have been used in analyzing the temperature traces. In addition, the initial sharp decrease in temperature is tabulated by determining the temperature every 1/4 msec. from the start of the temperature decrease until the minimum temperature occurs. This is necessary if calculations of the microlayer thickness are to be made.

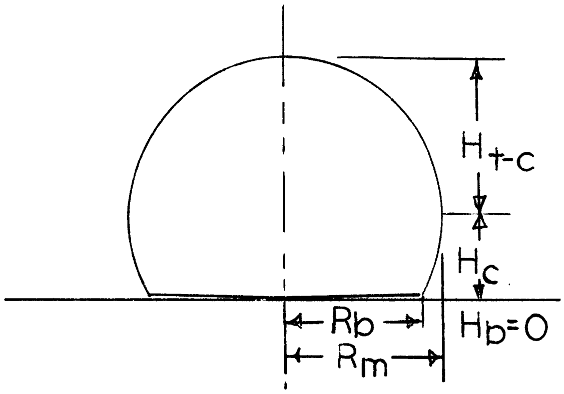

(11A)

Bubble Parameters

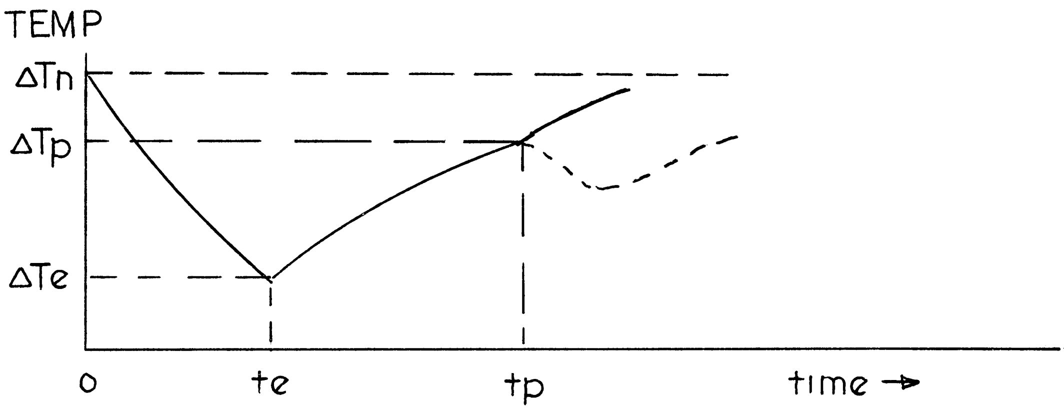

(11B)

Temperature Trace Characteristics

It is necessary to mark the temperature trace to indicate the time the pictures are taken. Fortunately, it was not required to build a special electronic device. The first oscilloscope pictures showed there is an inductive effect imposed on the measuring circuit at the time the flash tubes discharged. The flash tubes operate by storing charge in two 10 μf capicators at a potential difference of 20,000 volts. When the capicators discharge in 1/2 microsecond, there is an inductive effect observed which temporarily blanks out the millivolt level trace on the oscilloscope.

This marking of the temperature trace for every flash, as Figure (39) on page 128 shows, not only indicates the time of the flash but also distinguishes which trace on the oscilloscope corresponds to the picture when several traces are shown. In the case of double exposures, it is possible even to measure the time delay between flashes independently of the interval timer,but the accuracy is not as great.

Tables I and II summarize the values for bubble size and the temperature trace characteristics for boiling ethyl alcohol. Toluene boiling data is summarized in Table III. The system variables: pressure, liquid bulk temperature, saturation temperature, and average heat flux from the single-site heater are also noted in tables whenever they are changed. The method of calculating the average heat flux is shown in Appendix C.

2. Relation Between Bubble Parametes and the Temperature Trace Characteristics

Based on one still photograph of the boiling process, it is very difficult to draw conclusions. Each picture tells only part of the story. A few have some real significance. For example, the picture designated as 9-3-32 and its companion temperature trace show a very small bubble and also the start of the temperature fluctuation. The actual temperature trace is reproduced in Appendix B as Figure (39). This trace shows that the point of nucleation corresponds to the start of the dip in temperature. Without this information, the estimated time after nucleation could not have been estimated. For all other pictures, the time after nucleation can now be estimated from the temperature traces. In many cases, the nucleation temperature is missing because the oscilloscope trigger is usually set just below the nucleation temperature. Since the initial temperature decrease is sharp,

TABLE I. BOILING DATA FOR ETHYL ALCOHOL

Notation	Time After Nucleation (msec)	BUBBLE GROWTH PARAMETERS R_b cm	R_m cm	H_c cm	ΔH_{t-c} cm	H_b cm	Volume mm^3	TEMPERATURE TRACE CHARACTERISTICS — CENTER RESISTOR ΔTn °C	te msec	ΔTe °C	tp msec	ΔTp °C	SIDE RESISTOR ΔTn °C	te msec	ΔTe °C	tp msec	ΔTp °C	P mm	Tsat °C	Tb °C	Flux $\frac{cal}{cm^2\text{-sec}}$
9-1-1A		.039	.116	.093	.093	0	6.3											500	68	66	1.17
B		.000	.136	.134	.134	.077	10.8														
9-1-2		.196	.253	.155	.385	.252	53.0														
9-1-6		.196	.253	.250	.250	.000	72.0			6			23		23		23				
9-1-12		.214	.291	.155	.405	.272	67.0	21	8.7	0	18	16	30		30		30				
9-1-13A	4.5	.105	.156	.134	.103	.000	11.5						24		24		24				
B	10.0	.105	.184	.184	.159	.000	22.6														
9-1-24A	3.5	.047	.126	.097	.078	.000	4.0	23	11.7	6	18	15	28		28		28				
B	9.0	.126	.214	.147	.115	.000	19.8														
9-1-32A	2.0	.066	.079	.080	.065	.000	1.8	35	8.7	8			30		30		30				
B	7.5	.131	.237	.159	.131	.000	34.6														
9-1-33	6.5	.262	.262	.058	.134	.000	47.4	50	1.0	30	30	53	40	5	10	20	31				
9-1-34	35.0	.242	.242	.097	.663	.390	52.0	29	10.0	9	20	18	29		29		29				
9-1-35	28.0	.242	.242	.360	.230	.290	42.0	29	8.7	9	15	20	29		29		29				
9-1-36A	6.0	.132	.264	.146	.149	.000	47.4	38	8.8	12			31		31		31				
B	11.5	.158	.264	.225	.239	.000	79.5														
9-2-15	15.0	.155	.252	.195	.233	.000	61.6	18	13.7	0	20	7	26		26		26				
9-3-2		.125	.175	.136	.174	.000	19.3						24	8.3	4	15	22				
9-3-3	10.0	.126	.223	.195	.183	.000	41.0	22	8.7	3	16	11	29		29		29				
9-3-4	5.0	.128	.135	.058	.127	.000	8.1	41	7.1	12	18	25	24		24		24				
9-3-22	38.0	.290	.290	.311	.429	.152	66.0	25	8.7	3	18	15	28		28		28				
9-3-24A	6.0	.132	.200	.105	.211	.000	33.8	22	9.6	2			33		33		33				
B	11.5	.132	.218	.212	.200	.000	45.0														
9-3-28	25.0	.066	.237	.277	.163	.000	52.0	23	8.7	4	21	15	28		28		28				
9-3-30A	4.6	.118	.158	.079	.158	.000	14.3	21	8.7	5			27		27		27				
B	10.0																				
9-3-32A	.5	.076	.082	.052	.053	.000	1.1	23	14.0	5	22	12	26		26		26				
B	5.9	.118	.185	.132	.158	.000	21.2														
9-3-35A	3.0	.105	.145	.066	.144	.000	10.4	22	9.2	2	19	7	27		27		27				
B	8.4	.145	.264	.156	.214	.000	50.5														
9-3-37		.196	.196	.076	.328	.076	26.1														
14-7-1	7.4	.072	.104	.078	.103	0	4.64	27	4.9	12			45		45		45	623	73	72	1.13
3A	4.0	.078	.117	.065	.091	0	4.68				19	16	49		49		49				
3B	14.0	0	.143	.176	.104	.104	8.72														
11A	1.5	.065	.118	.052	.061	0	1.77			5	12	14	27		27		27				
11B	12.0	0	.117	.156	.098	.078	5.30														
15	~22	0	.117	.182	.104	.048	6.55				22	22	40		40		40	645	74	73	
17A	8.0	.081	.098	.091	.090	0	4.02	26	5.0				28		28		28				
17B	18.7	0	.117	.188	.092	.110	4.70														
19	13.8	0	.111	.214	.098	.110	5.25	27	5.1	12	13.8	23	30		30		30				
22A	3.0	.117	.126	.078	.104	0	6.88	23	8.2	11	13.0	13	40		40		40	603	72	70	
22B	13.0	0	.188	.195	.150	.072	22.30														
23A	8.5	.120	.146	.081	.115	0	9.41	24	10	5	16	11	42		42		42	557	70.5	69	
23B	18.6	0	.156	.195	.146	.092	12.80														
26	3.0	.139	.130	.078	.104	0	6.25	26	6.9	10	13	18	43		42		42	480	66.5	66	1.11
27A	3.0	.143	.162	.091	.117	0	12.80	16	18.3	7	20.5	12	42	9.8	16	13	24				
27B	13.1	0	.247	.195	.195	.052	46.60														
28	14.2	0	.107	.162	.124	.120	4.00	26	5.8	7			38		38		38				
30A	3.0	.101	.117	.039	.104	0	4.47			8	14	16									
31A	3.0	.113	.126	.585	.095	0	5.28			8	13.4		32		31		32				
31B	13.4	0	.142	.162	.150	.091	10.00														
32	8.8	.137	.182	.156	.169	0	17.22	19	11	8.8			36		34		36				

TABLE II. BOILING DATA FOR ETHYL ALCOHOL

	BUBBLE GROWTH PARAMETERS							TEMPERATURE TRACE CHARACTERISTICS CENTER RESISTOR					TEMPERATURE TRACE CHARACTERISTICS SIDE RESISTOR								
Notation	Time After Nucleation (msec)	R_b cm	R_m cm	H_c cm	ΔH_{t-c} cm	H_b cm	Volume mm^3	ΔTn	te	ΔTe	tp	ΔTp	ΔTn	te	ΔTe	tp	ΔTp	P	Tsat	Tb	Flux $\frac{cal}{cm^2\text{-sec}}$
14-8-7A	3.5	.169	.185	.082	.162	0	20.2	30		10	27	31	42	14	18			463	66	65.5	.70
7B	14.0	.191	.310	.224	.199	0	91.0														
10A	3.0	.131	.152	.059	.129	0	10.5	30		10	19	29	42		42		42				
10B	14.0	.161	.218	.145	.178	0	36.10														
29A	2.0	.145	.148	.040	.119	0	7.65	40	1.5	20	25	42	*42	14	25						1.11
29B	12.5	.222	.310	.191	.198	0	82.60														
30A	2.0	.092	.102	.040	.080	0	2.79	38	2.5	19	19.5	40	*48	14	38	18	42				
30B	12.8	.204	.262	.145	.145	0	51.30														
31A	1.7	.119	.125	.041	.110	0	5.41	38	2.3	19	16.5	39	*43		43		43				
31B	12.3	.159	.250	.172	.178	0	45.00														
33A	5.0	.092	.110	.059	.076	0	3.94	28	7	9	15.7	18	40		40		40				
33B	15.7	0	.109	.158	.076	.079	4.63														
36A	4.0	.080	.108	.073	.080	0	4.40	24	10	5			34		34		34				
36B	14.7	0	.125	.178	.112	.105	6.90														
37A	3.0	.066	.095	.073	.069	0	3.10	24		8	13.6	18	33		33		33				
37B	13.6	0	.092	.171	.069	.105	2.54														
14-9-2	11.4	.293	.336	.192	.244	0	106.00	**33	1.4	15	15.5	40	45	15	40	15	42	439	64.8	62.5	1.17
7B	11.0	.324	.390	.211	.278	0	156.00	**36	1.3	18	26	43	45	20	18						
9A	.5	.077	.102	.063	.058	0	2.84	**30	1.3	12	26	45	39	20	8						
9B	11.0	.306	.378	.304	.178	0	158.10														
11A	5.5	.119	.185	.119	.132	0	19.78	23	7.9	5	16	18	32		32		32	448	65	62.5	1.09
11B	16.0	.119	.240	.198	.218	0	46.50														
16B	11.5	0	.092	.172	.086	.099	2.61	18	3.0	10			39		40		41	472	66	63	1.37
23A	7.8	.158	.212	.132	.158	0	28.80	**19	9.2	2			15		18		20				
28A	6.2	.132	.139	.066	.112	0	8.55	25	(7.0)	7			48		48		48	492	67	65.5	1.23
14-9-30A	2.0	.108	.132	.069	.103	0	7.03	18	6.9	0	16.5	7	38		38		38				
30B	12.5	.105	.238	.198	.182	0	42.40														
34A	1.5	.086	.116	.060	.075	0	3.83	18	7.0	2			39		39		39				
34B	12.2	(.092)	.170	.204	.088	0	17.55														
35	2.0	.092	.099	.053	.079	0	3.10	20	3.8	5			42		42		42				
36	2.0	.092	.106	.040	.066	0	2.92	18	7.5	4			42		42		42				

** Point of Nucleation on Side Resistor (Center-Side Columns Switched)
* Oscilloscope Sweep Triggered on Side Resistor Fluctuation

TABLE III. BOILING DATA FOR TOLUENE

		BUBBLE GROWTH PARAMETERS						TEMPFRATURE TRACE CHARACTERISTICS: CENTER RESISTOR					TEMPFRATURE TRACE CHARACTERISTICS: SIDE RESISTOR								
Notation	Time After Nucleation (msec)	R_b cm	R_m cm	H_c cm	ΔH_{t-c} cm	H_b cm	Volume mm^3	ΔTn °C	te msec	ΔTe °C	tp msec	ΔTp °C	ΔTn °C	te msec	ΔTe °C	tp msec	ΔTp °C	P mm	Tsat °C	Tb °C	Flux $\frac{cal}{cm^2\text{-sec}}$
14-3-8	3.5	.076	.089	.051	.064	0	2.15	47	2.00	34	5.0	39	54		54		54	531	98	90	1.09
11A	1.2	.084	.084	.028	.076	0	1.94				11.0	37	51		51		51				
11B	11.0	.077	.109	.125	.082	0	4.74														
14A	1.2	.097	.079	.028	.111	0	3.05			35	14.0	47	51		51		51				
14B	11.0	.167	.160	.167	.117	0	19.30														
20A	7.5	.026	.036	.035	.048	0	.28	48	1.50	31			51		51		51	504	96	90	1.09
20B	17.0	0	.070	.097	.069	.028	.89														
23	8.2	.084	.170	.164	.114	0	15.80	45	1.50	31	8.2	42	51		51		51				
26A	.2	.055	.063	.035	.064	0	11			33	5.0	40	50		50		50				
26B	9.5	0	.090	.160	.082	.014	3.70														
27	2.3	.128	.139	.063	.111	0	7.96	42	1.75	28	14.5	41	48		48		48				
34	2.8	.070	.070	.031	.066	0	1.25	43	1.50	33			49		49		49				
14-4-2	7.0	.073	.090	.044	.080	0	2.48	36	1.50	20	10.0	33	48		48		48	523	98	96	.825
4	9.5	.124	.190	.131	.131	0	18.25			18	14.5	34	43	3.5	30	9.5	37				
5	10.6	0	.088	.161	.101	.070	3.48			16											
12	9.2	.117	.313	.102	.066	0	6.30	32	1.25	19			48		48		48	514	97	95	.825
17A	—	.117	.137	.058	.108	0	6.90														
17B	—	.058	.160	.161	.109	0	14.12			22			47		47		47				
17C	—	0	.204	.248	.136	.146	20.78														
19A	6.0	.088	.133	.102	.120	0	9.20	34	1.50	18	12.5	32	48	45	3.5	8.0	44				
19B	6.0	.083	.146	.102	.121	0	9.50														
21	11.0	.029	.088	.117	.095	0	3.03			15	11.0	28	46		46		46	490	96	94	.77
26	8.6	0	.073	.117	.048	.073	1.23	32	1.25	23	7.0	28	40		40		40				
39	3.6	.131	.146	.058	.137	0	8.50	30	1.75	19	15.0	33	46		46		46				
31	1.0	.045	.045	.022	.036	0	.35	37	1.75	25	4.0	30	47		47		47				
33	9.3	.073	.124	.107	.098	0	6.82	33	2.00	18	11.3	31	43		43		43				
14-5-5	11.0	.114	.123	.038	.114	0	5.42						48		48		48	413	90	87	.71
20A	.4	.089	.089	.019	.081	0	1.93	31	1.2	17.5	23	36	44	4.25	22	19	39.5				.64
20B	9.2	.218	.260	.128	.179	0	49.40														
17A	.5	.089	.114	.102	.076	0	5.88	31	1.0	18	18	36	45	5.5	28	11	38				
17B	9.0	.153	.203	.146	.133	0	25.60														
25A	8.4	.164	.206	.114	.140	0	26.10									11	32				
25B	17.0	0	.210	.204	.140	.102	23.20														
26A	.5	.067	.074	.025	.051	0	.94	30	1.0	15	15	30	40	5.0	31.5	9	34.5				
26B	9.1	.146	.186	.108	.20	0	17.90														
27	10.0	.074	.076	.070	.108	0	4.16	31	1.2	17	16	33	39.5	6.0	36.5	7	38				
29A	.5	.064	.082	.064	.047	0	1.90	31	1.0	17	18	33.5	43	5.5	31	11	37				
29B	9.1	.127	.172	.089	.114	0	13.95														
31	.5	.076	.082	.025	.070	0	1.535	31	1.0	18	19	35	41	7.0	23	12	32				
33A	.5	.066	.069	.025	.051	0	.78	31	1.2	18	15	34	46	5.5	30	11	40				
33B	8.9	.127	.127	.144	.085	0	11.72														
14-6-11	2.5	.092	.079	.038	.071	0	2.62	26	1.9	13	13.5	19	46		46		46	553	100	98	.87
21	9.4	.089	.089	.089	.102	0	6.38	28	1.0	14	13.5	24	42		41		41	503	97	92	.77
23A	.5	.102	.121	.076	.102	0	6.20	28	1.0	13	19	28	43	5.5	22	13.5	37				
23B	11.0	.127	.216	.165	.165	0	25.35														
26A	.6	.102	.103	.038	.084	0	10.40	32	1.0	19	19	35	51	4.5	28.8	17	47	412	90	86	
26B	10.7	.287	.305	.076	.290	0	71.40														
29A	3.5	.254	.311	.127	.254	0	82.10				13.5	30				11	43				
29B	13.5	0	.333	.248	.278	.076	93.50														
32	6.5	.175	.203	.114	.146	0	25.20	30	1.6	20	14	32	46		46		46				.75

it is only a slight error to draw a straight line up to the average nucleating temperature and from the intersection of the two lines estimate the time the pictures are taken.

Thus far, the cause of the initial rapid decline in temperature has been related to the bubble nucleation and growth. To be consistent with the microlayer theory, the time interval, measured by t_e in Figure (11B), is the period during which microlayer vaporization exists. Also, the value of t^e must either measure the time required to vaporize the microlayer completely or it must measure the interval before the base contact radius R_b passes back across the temperature element.

The variable t_p has been tabulated as a temperature-trace characteristic. For ethyl alcohol, an abrupt change in slope of the smooth recovery rate is frequently observed. The surface temperature difference, $\Delta T_p = (T_w - T_{sat})$, and the time after nucleation, t_p, when this break is observed are tabulated in Tables I and II. For toluene, an actual secondary fluctuation is observed. This fluctuation is much smaller and slower than the primary fluctuation, which has been related to bubble growth. It will be shown that t_p can be interpreted in the same way for both toluene and ethyl alcohol.

Consider first, the large toluene bubbles for which fluctuations on two surface elements are observed. In data point # 14-5-26 shown in Table III, R_b is .146 cm when the "B" picture is taken. The start of the secondary fluctuation began .1 msec. before this picture. The outer resistor lies between .140 cm and .190 cm from the center, with an average distance of .165 cm. Therefore, the fluctuation starts with the vapor-liquid interface, measured by R_b, passing over the temperature sensor. A detailed sketch of a similar temperature trace is shown in Figure (19) on page 62 . This sketch shows that the secondary fluctuation lasts several milliseconds. Since it starts with the passing of the liquid-vapor interface and lasts for several milliseconds, secondary fluctuation is due to liquid flow and not vaporization. The same conclusion also explains the fluctuations of the center resistor. For the pictures labeled #14-4-26, the secondary fluctuation in the temperature curve at the center resistor occurs at 7 msec; the time of departure for this bubble, as indicated by the value of H_b, is sometime before 8.6 msec. The composite photographs labeled 14-4-21, show the bubble at the time the secondary fluctuation begins; the value of R_b indicates the bubble is very close to departure. These two photographs are within 1 msec. of tp; in one, the bubble has almost departed and in the other the bubble has departed. Figure (21) on page 64 shows that this secondary fluctuation also lasts several milliseconds. Therefore, the secondary fluctuations of the center element are induced by bubble departure. Suction of the liquid from the surface would be the most reasonable force for inducing this heat transfer at departure.

The cause of the break in the recovery of the ethyl alcohol temperature fluctuations can be investigated in the same way. First, note that a break cannot always be observed. Several pictures have been taken at a point close to where the temperature break can be seen. Data points 14-7-19, 22, 23, and 31 all occur close to the observed break in the temperature curve. In every case, the bubble has departed. Therefore, although the break is a measure of bubble departure time, in all likelihood the bubble departs slightly before the change in the slope of the central element is observed.

There are some cases, such as 9-1-36, no break in temperature of the central element can be observed. Since it has been found that tp is a measure of departure, then te should equal tp, if the microlayer has not completely vaporized. In the case of 9-1-36, te= 8.8 msec the bubble is still on the surface at 11.5 msec. and R_b at that time is .158 msec. This must simply be a case of the two curves matching perfectly so no change in slope can be observed.

For the large ethyl alcohol bubbles which cover the outer sensor .165 cm from the center, a value of tp can seldom be obtained. The most reasonable explanation in this case is that the microlayer vaporization is stopped by the vapor-liquid interface passing back across the point. Data point #14-8-7 shows that the minimum surface temperature of the outer element occurs at 14 msec. At that time R_b is .191 cm, which closely corresponds to the maximum radial distance of the outer element from the center. The outer element senses an averaged temperature between .140 and .190 cm for the center. Since tp cannot be noted, it must be concluded that tp=te and an unknown fraction of the microlayer has evaporated.

The temperature trace characteristics and the bubble parameters, shown in Figure (11), can be related in the following manner. The temperature trace characteristic tp measures the interval that elapses after nucleation for the bubble base contact radius, measured by R_b, to recede back across the temperature element. At the central temperature sensor, tp can be associated with bubble departure. The curve characteristic te is the interval of time required to evaporate the microlayer completely providing that te is less than tp. Finally, if the microlayer has vaporized completely, it is usually possible to determine tp from the temperature curves.

3. Boiling and Nucleation Characteristics of Ethyl Alcohol and Toluene on Soda Lime Glass.

In the previous section, the temperature trace characteristics have been linked to bubble parameters. Hence, it is possible to explain the nature of boiling on a glass surface. In this section, the composite photographs which are made up of one or two views of the boiling surface and the transposed temperature traces will be used. The voltage-time curves have been changed to temperature-time curves by the method explained in Appendix B. In addition, the disturbances caused by the flash discharges have been smoothed and then replaced by a cross-hatch and an arrow at the bottom of the sketch. The arrows therefore indicate the time when the pictures have been taken. The vertical scale has just been converted to a temperature scale so the fluctuations are as close as possible to the original voltage-time traces.

Experimentally it has been found that wall superheats of 40-50°C are required to initiate boiling of ethyl alcohol on a glass plate; toluene requires an even higher superheat. A spot of Floro Glide,made by Chemplast, has been dropped onto the surface in an effort to start nucleation. The spot, shown in Figure (12), covers most of the center resistor with a thin flaky coating. All the toluene and ethyl alcohol data for heater #14 have been taken with this spot on the center resistor. After looking at all the photographs and temperature traces for toluene, it may be concluded that nucleation occurs only from the Teflon*like material.

The toluene data show two characteristic temperature traces. At an average heat flux of 1.10 cal/cm^{-2}sec, a pressure of 504 mm, and 8°C subcooling these two types of traces are shown in Figures (13) and (14).

*DuPont Tradename

Figure 12 Floro Glide Spot Over the Center Resistor

Side View

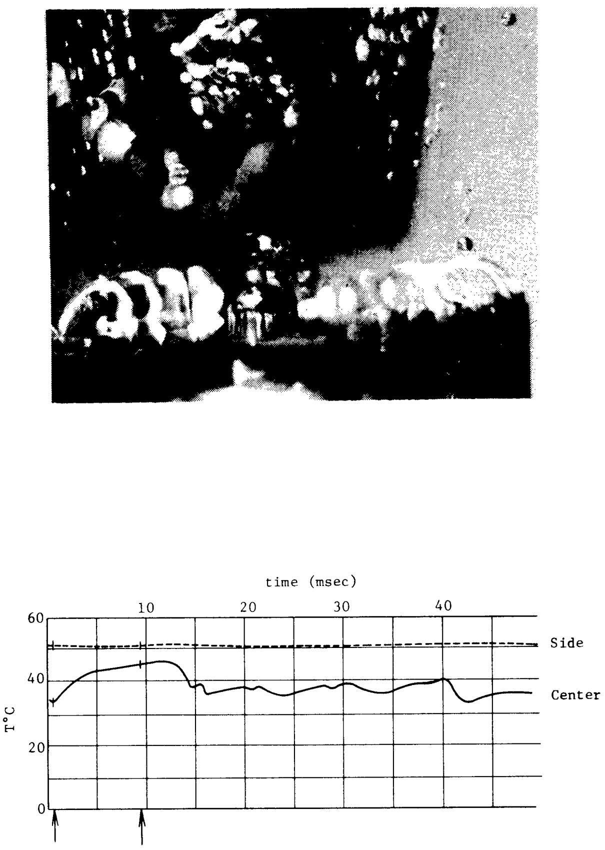

Figure 13 Boiling of Toluene #14-3-19, P = 531, q = 1.09 and Tsat-Tb = 8 °C

Side View

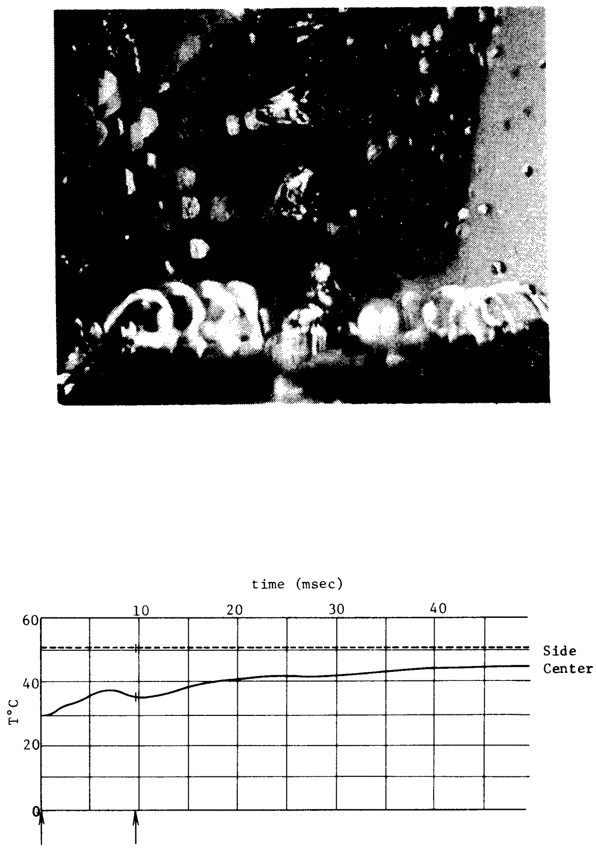

Figure 14 Boiling of Toluene #14-3-11, P = 531, q = 1.09 and Tsat Tb = 8 °C

Both photographs show a double exposure of large bubbles growing on the surface. The rate at which the temperature recovers after the minimum temperature is quite different. In Figure (13), the rate of recovery is very high and departure is followed by a sharp temperature drop which could only be secondary nucleation. In Figure (14) the temperature recovery after the minimum temperature is very slow and no secondary nucleation occurs. The small fluctuations in Figure (13) closely resemble the fluctuations shown in Figure (15). Judging from this figure, the small fluctuations in Figure (13) are due to many small bubbles nucleating on the surface. Figure (16) shows the smallest bubbles which have been observed in 14-3. It indicates there is quite a size range of bubbles growing from the same region on the surface.

Run #14-4 shows toluene boiling at from 1-2°C subcooling, 500mm of pressure, and at a heat flux of .75 cal/cm^2-sec. The same two types of temperature traces, which have been described in 14-3, appear at these conditions also. Figure (17) shows the surface temperature recovering very rapidly (at departure, $\Delta T_p \simeq \Delta T_n$) and Figure (21) shows a much slower recovery rate. Figure (18) indicates the secondary nucleation, which occurs whenever the surface temperature recovery is very rapid, thus increasing the value of ΔT_p. It is impossible to tell the interaction of the bubbles within this picture; it is definite that there is vertical interference between bubbles.

The difference between Run #14-4 and #14-5 is a change in pressure and a slight change in the heat flux. In 14-5, where the pressure and the heat flux are lower, the tendency to form large irregular bubbles greatly

SIDE VIEW

TEMPERATURE TRACES

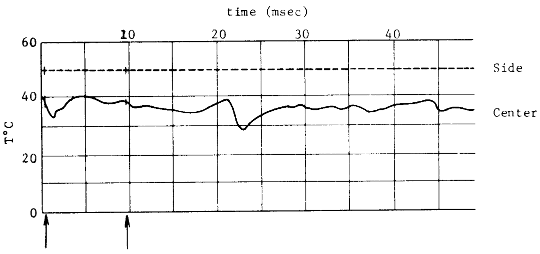

Figure 15 Boiling of Toluene #14-3-26, P = 504, q = 1.09 and Tsat-Tb = 6 °C

SIDE VIEW

TEMPERATURE TRACES

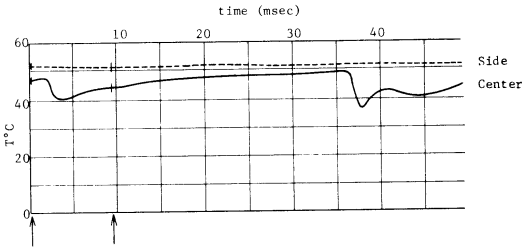

Figure 16 Boiling of Toluene #14-3-20, P = 504, q = 1.09 and Tsat-Tb = 6 °C

TOP VIEW

SIDE VIEW

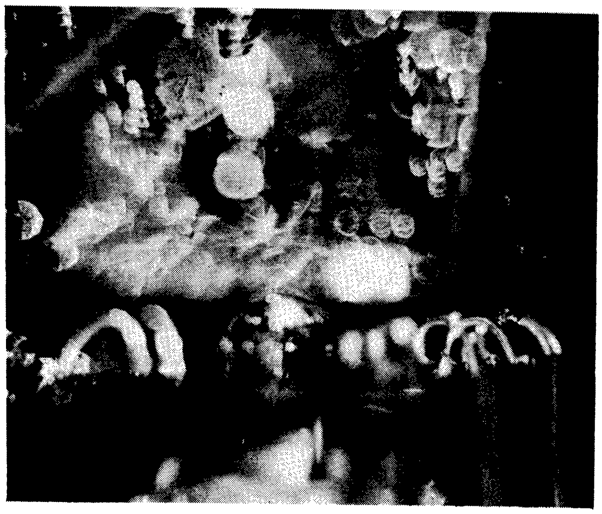

TEMPERATURE TRACES

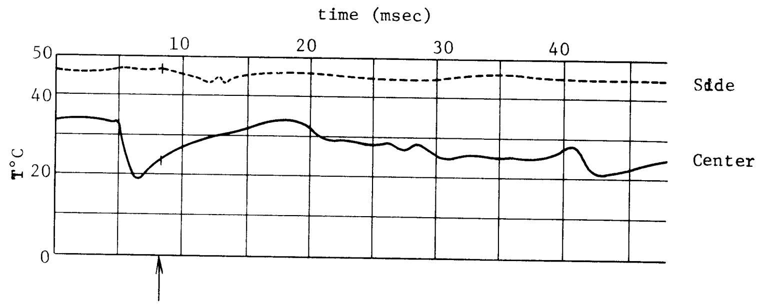

Figure 17 Boiling of Toluene #14-4-39, P = 490, q = .77 and Tsat-Tb = 2 °C

TOP VIEW

SIDE VIEW

TEMPERATURE TRACES

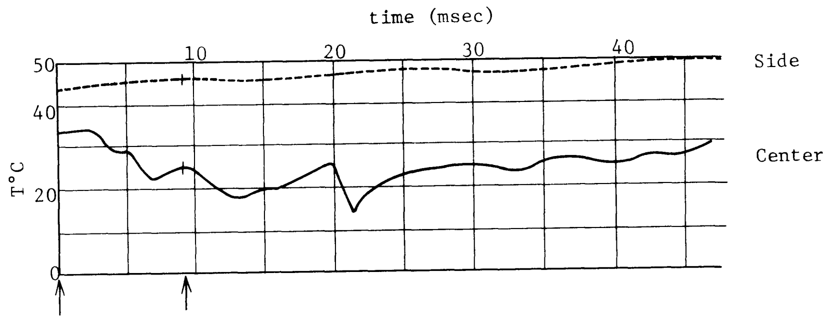

Figure 18 Boiling of Toluene #14-4-17, P = 514, q = .82 and Tsat-Tb = 2 °C

TOP VIEW

SIDE VIEW

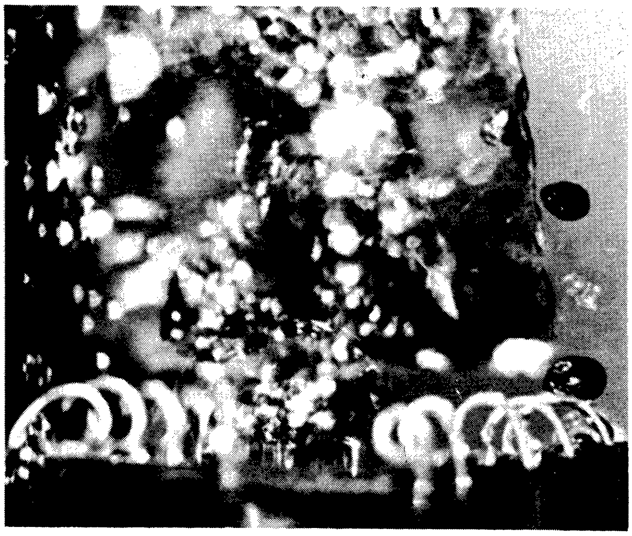

TEMPERATURE TRACES

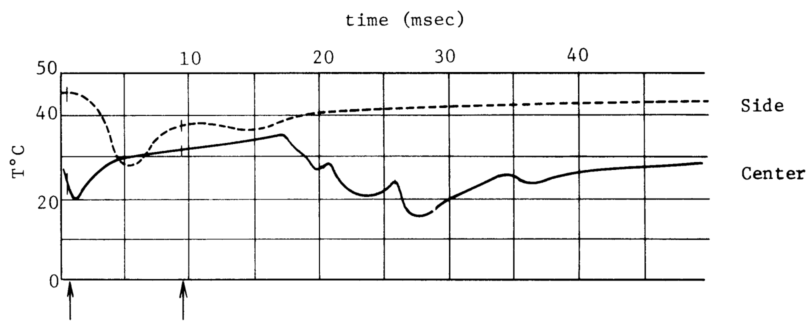

Figure 19 Boiling of Toluene #14-5-17, P = 413, q = .64 and Tsat-Tb = 3 °C

TOP VIEW

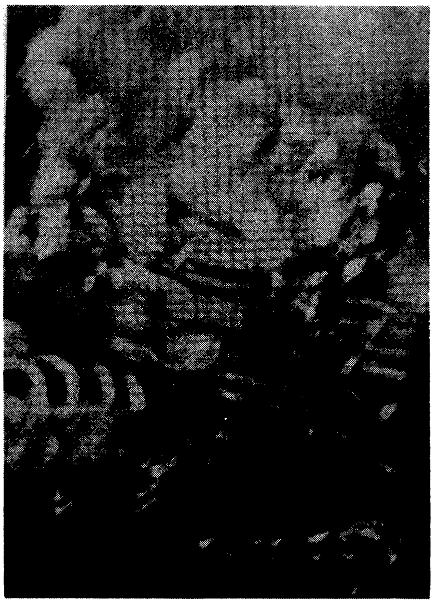

SIDE VIEW

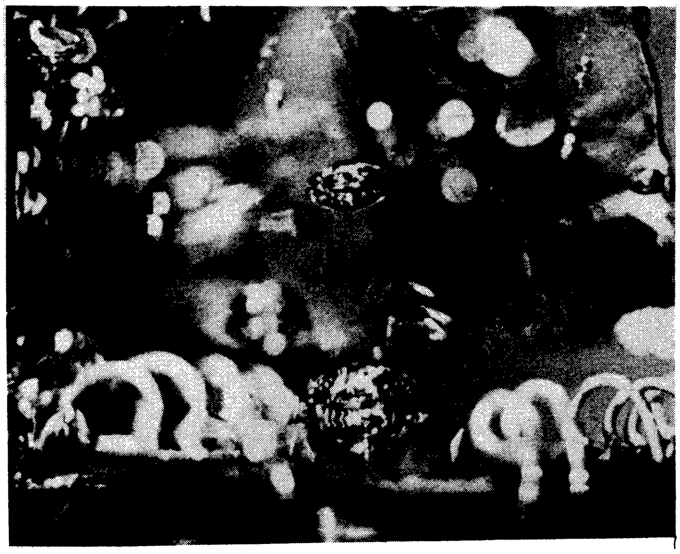

TEMPERATURE TRACES

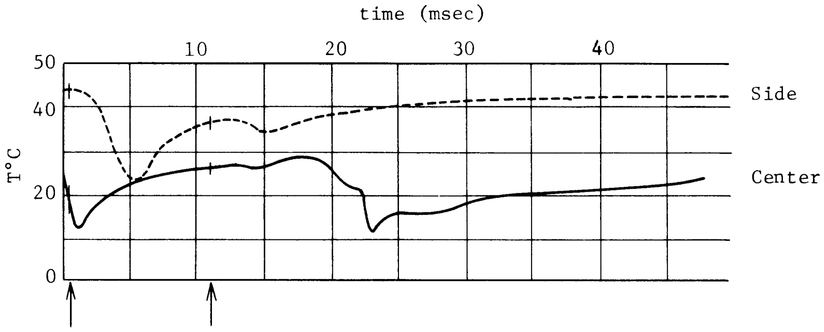

Figure 20 Boiling of Toluene #14-6-23, P = 503, q = .75 and Tsat-Tb = 4 °C

TOP VIEW

SIDE VIEW

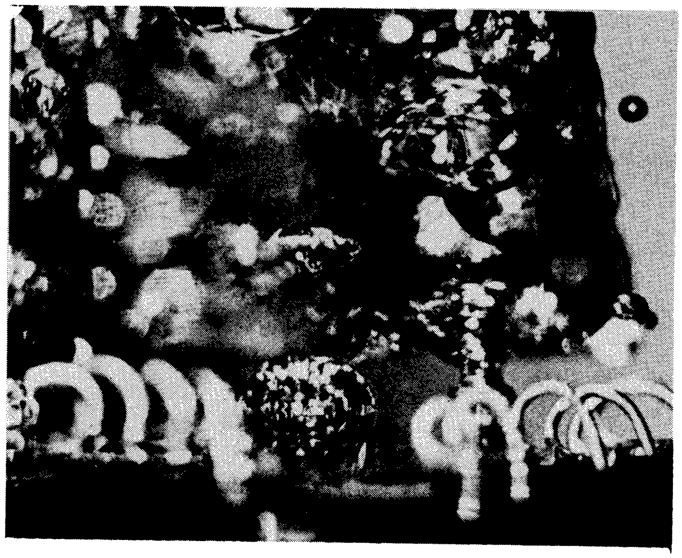

TEMPERATURE TRACES

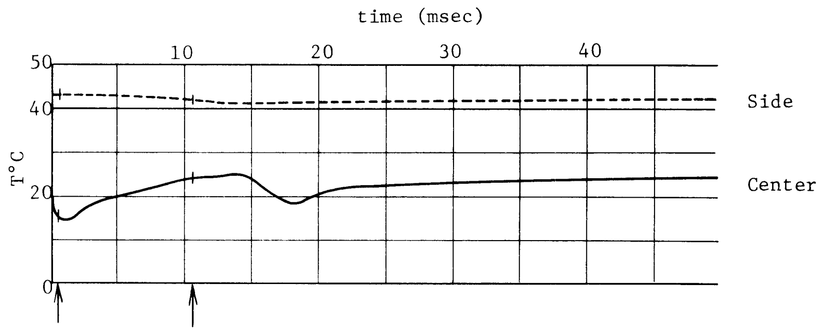

Figure 21 Boiling of Toluene #14-6-21, P = 503, q = .77 and Tsat-Tb = 5 °C

increases. Figure (19) shows a typical bubble which is observed in 14-5. Figure (20) has been included to show that the big bubbles are occasionally observed at higher pressures. The interaction of pressure and heat flux, which appears in the differences between #14-4 and #14-5, is not well understood. Certainly, if the heat flux is not sufficient to sustain continuous boiling at a nucleating temperature at around 30°C above the saturation temperature, the boiling, if it exists, would have to be intermittent. These results show there is an interaction of pressure and heat flux on the bubble size which up to now has not been clearly described. At the same time in Run # 14-6, the last series of photographs, pressure is the same as #14-5 and the flux almost equal to #14-4. This shows the bigger bubbles are caused predominatly by the change in pressure.

In summary, it has been found that at the pressures, heat fluxes, and degrees of subcooling which have been studied, the boiling of toluene is a very irregular process. Secondary nucleation is likely if at departure, the surface temperature has almost fully recovered from the primary temperature fluctuation. Bubble size can be affected by changes in pressure and heat flux by a mechanism which is not well defined.

The ethyl alcohol data at one pressure and heat flux are very extensive. At a pressure of 500 mm of Hg and a flux of 1.2 cal/cm^2-sec a regular form of boiling has been observed. Figures (22) and (23) show this type of regular boiling. Under the bubble in Figure (23), interference fringes can be seen. These indicate strong temperature gradients. If the liquid temperature is 4°C subcooled, the interference fringes become very evident as Figure (24) shows. The temperature trace shown in Figure (25) indicates there are to active sites existing within .165 cm of each other. This condition lasted for 10-15 seconds.

TOP VIEW

SIDE VIEW

TEMPERATURE TRACES

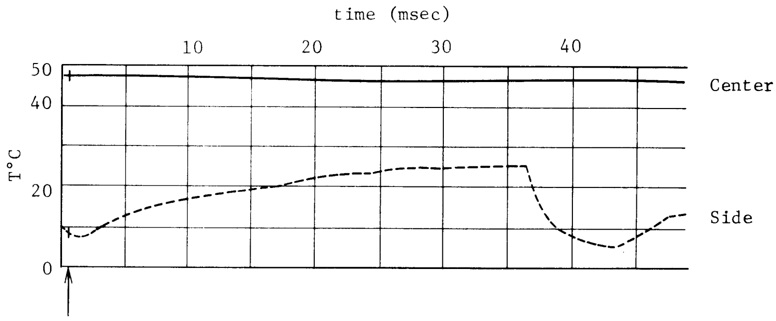

Figure 22 Boiling of Ethyl Alcohol #14-9-28, P = 492, q = 1.23 and Tsat-Tb = 1.5 °C

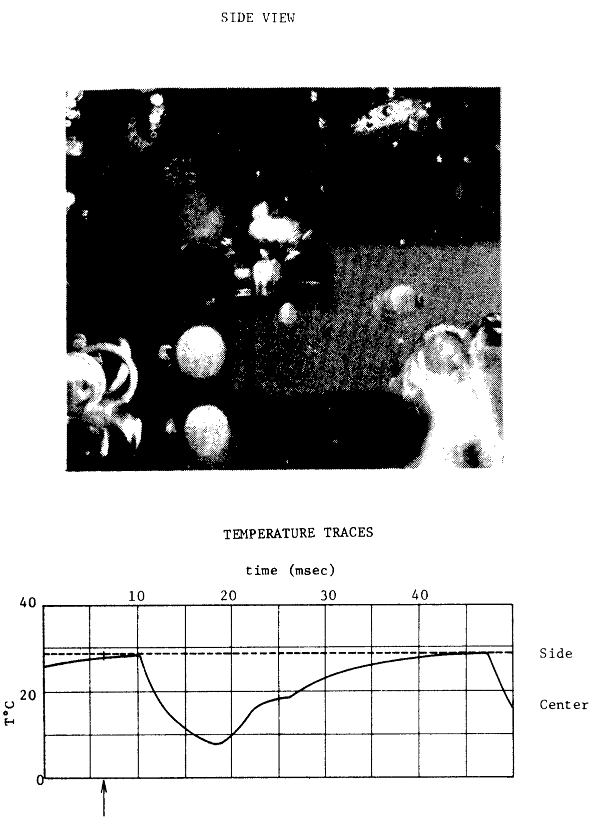

Figure 23 Boiling of Ethyl Alcohol #9-1-13, P = 500, q = 1.17 and Tsat-Tb = 2 °C

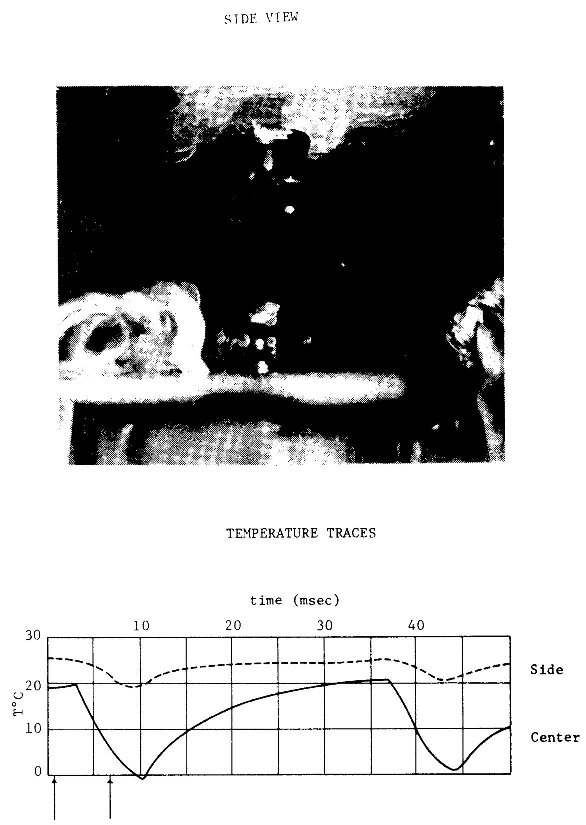

Figure 24 Boiling of Ethyl Alcohol #9-7-19, P = 500, q = 1.2 and Tsat-Tb = 4 °C

TOP VIEW

SIDE VIEW

TEMPERATURE TRACES

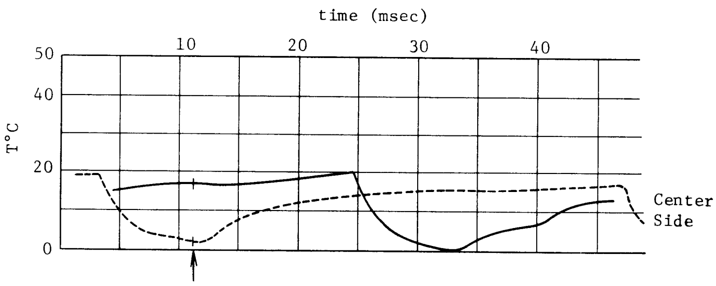

Figure 25 Boiling of Ethyl Alcohol #14-9-23, P = 472, q = 1.37 and Tsat-Tb = 3 °C

SIDE VIEW

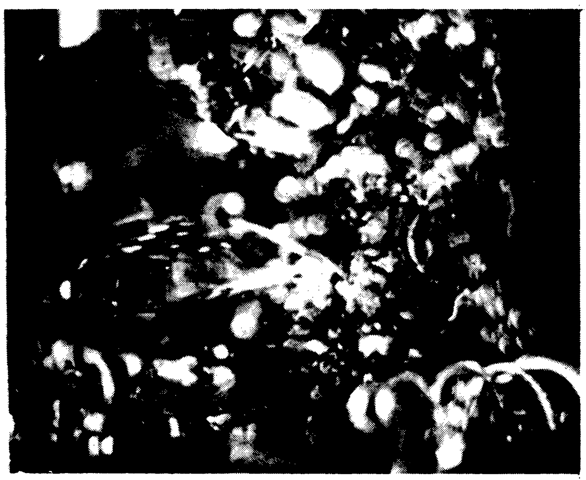

TEMPERATURE TRACES

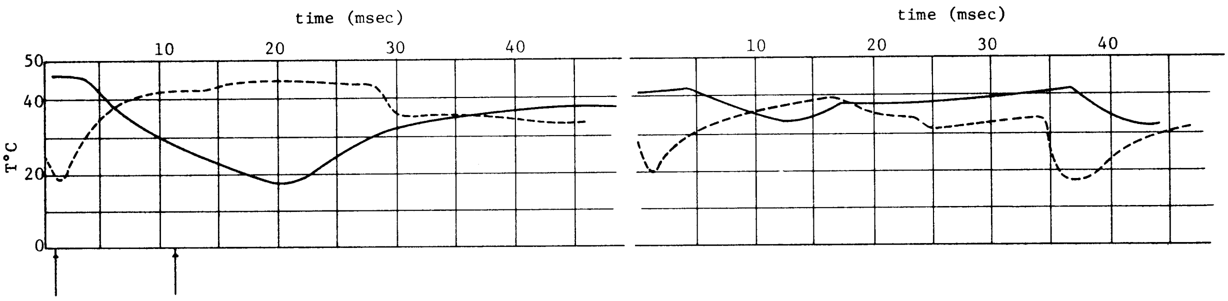

Figure 26 Boiling of Ethyl Alcohol #14-9-7, P = 439, q = 1.17
and Tsat-Tb = 2.5 °C

This regular boiling has been observed at pressures above 500 mm of mercury also. At higher pressures there is more of a tendency toward multiple sites on the surface. At pressures below 500 mm of Hg, there is a much greater tendency toward big irregular bubbles. Figure (26) shows the trace that triggered the picture and another which occurred some time afterward. It can be seen that the bubble is very large.

As with toluene, the tendency to form the large irregular bubble is probably the interaction between heat flux and pressure which prevents the surface from maintaining boiling at the temperature differences required for nucleation.

In summary, the ethyl alcohol data are significantly different from the toluene data. First, there is an absence of secondary nucleation, even in the case of the big alcohol bubble shown in Figure (26). Secondly the boiling of ethyl alcohol is extremely regular. The only apparent similarity is the effect of lowering the pressure and heat flux which once again increases the bubble size.

VI. ANALYSES OF RESULTS

1. Introduction

A great deal has been learned by looking at the many composite bubble photographs and temperature-time curves. A more complete understanding of boiling can only be obtained by grouping series of photographs taken at the same experimental conditions and then studying how the bubble parameters and temperature-trace characteristics change as the experimental conditions are varied.

The next section summarizes in graphical form the two bubble parameters $R_b(t)$ and $R_m(t)$. These two variables, $R_b(t)$ in particular, are important in any consideration of heat transfer at the surface. The following section contains an analysis of the observed surface temperature fluctuations. These fluctuations will be related to an evaporating microlayer thickness.

2. Bubble Parameters

Based on Tables I, II and III, graphs for the various bubble growth parameters can be drawn. Figure (27) gives the maximum bubble diameter as a function of time for ethyl alcohol boiling at a system pressure of 500 mm of Hg and at an average heat flux of 1.2 cal/cm^2-sec. The solid line drawn through the data points in this figure is assumed to have the following form.

$$R_m(t) = \eta\sqrt{t} \qquad (26)$$

In this case $\eta = 2.34$ $cm/sec^{1/2}$. For very short times after nucleation the bubble grows as a hemisphere. Thereafter the base contact radius begins to lag behind the maximum. It reaches a maximum and then decreases to zero at departure. An equation which behaves in this manner is:

$$R_b(t) = \eta\sqrt{t} \left[1 - \frac{1}{2n+1} \left(\frac{t}{t_m}\right)^n\right] \qquad (27\ )$$

At "t_m," $R_b(t)$ is forced to be a maximum by the (2n+1) term. At very small times, relative to "t_m," $R_b(t) = R_m(t)$. A value of $n = 1$ fits the data presented here. The equation which is used to correlate the data is:

$$R_b(t) = \eta\sqrt{t} \ [1 - 1/3\ (t/tm)] \qquad (28\ )$$

where η is the same value which correlates the maximum bubble radius expression. It should be noted that equation (28) forces $R_b(t_m)$ to be equal to 2/3 $R_m(t_m)$ and it also requires the time of departure to equal $3t_m$. The data for the base contact radius vs time for ethyl alcohol, which is a companion to figure (27) showing the data for $R_m(t)$, is shown in figure (28). The value of $\eta = 2.34$ cal/sec$^{1/2}$ and $t_m = .007$ sec are used to correlate the data.

Figures (29) and (30) show the maximum and base radii as a function of time after nucleation for toluene boiling at 520 mm of Hg and at an average heat flux of .75 cal/cm^2-sec. The correlating parameters are $t_m = .004$ sec and $\eta = 2.6$ cm/sec$^{1/2}$. Figures (31) and (32) show the maximum and base radii as a function of time for toluene boiling at 410 mm of Hg and at an average heat flux of .64 cal/cm^2-sec. The correlating parameters are $t_m = .005$ sec and $\eta = 4.25$ cm/sec$^{1/2}$.

Figures (27) to (32) summarize most of the data in Tables I, II and III. There are several isolated conditions where only a few pictures have been taken. These isolated points are not used.

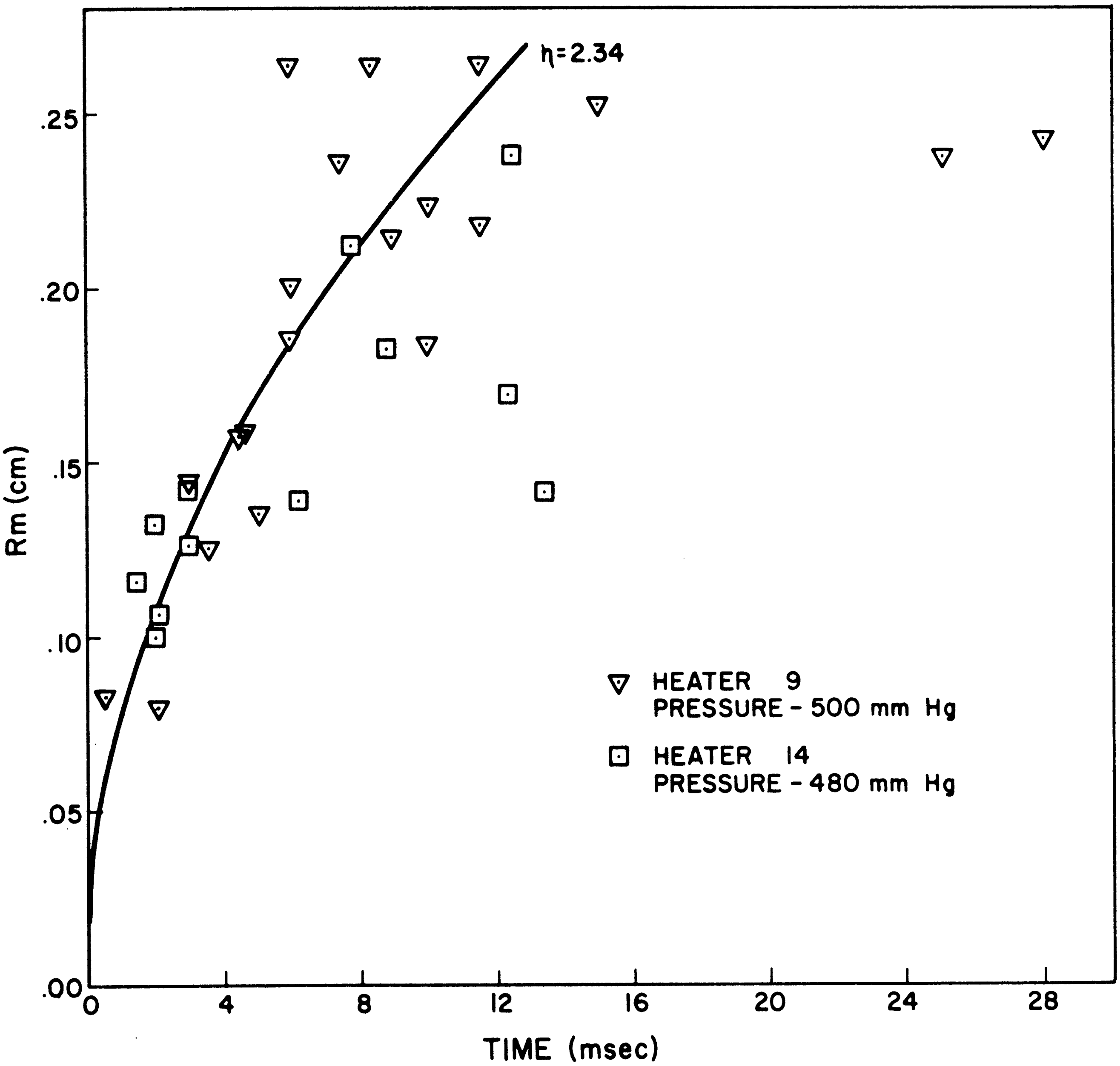

Figure 27 **MAXIMUM BUBBLE RADIUS**
ETHYL ALCOHOL
HEAT FLUX - 1.2 cal/cm^2-sec

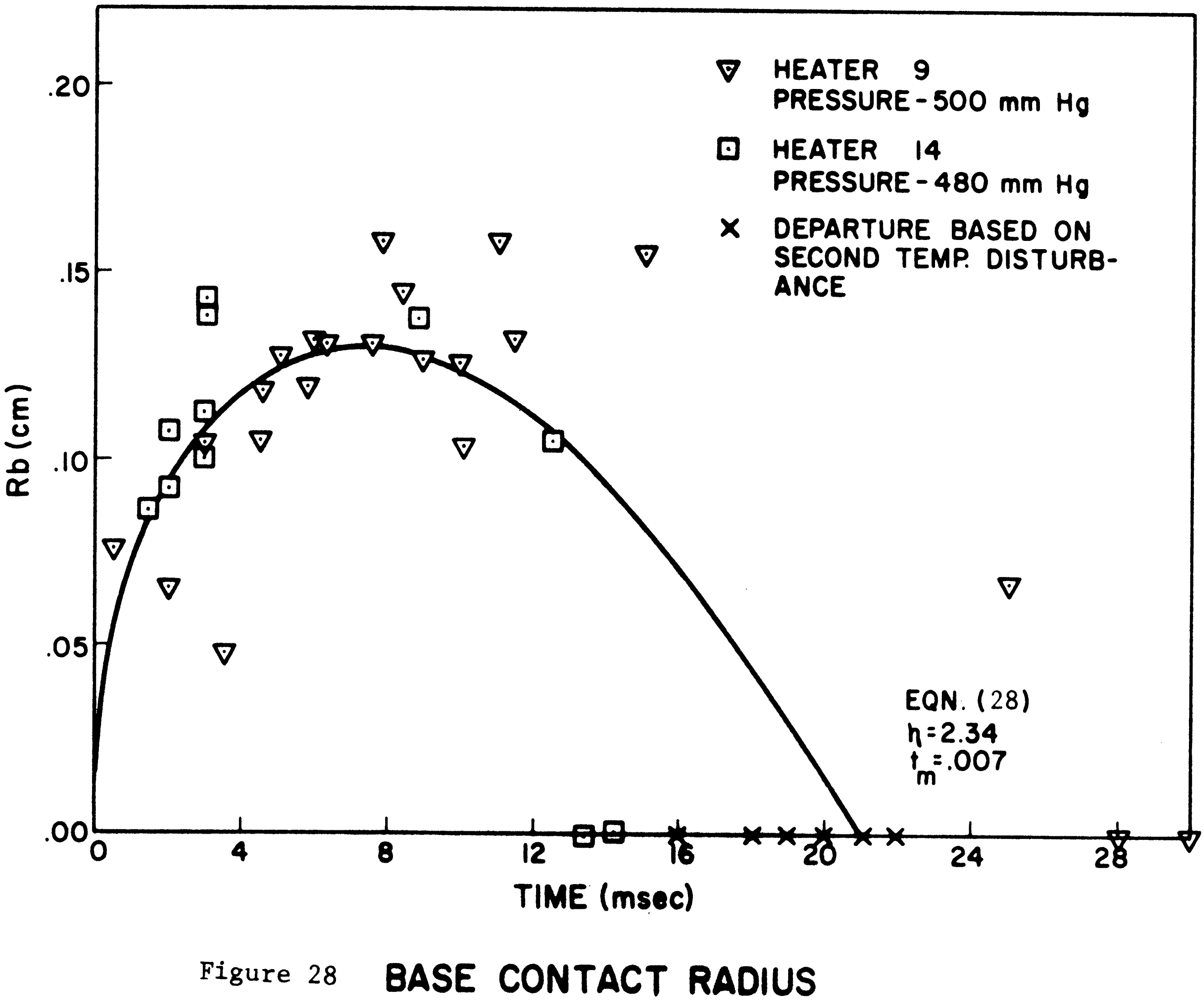

Figure 28 **BASE CONTACT RADIUS**
ETHYL ALCOHOL
HEAT FLUX - 1.2 cal/cm^2-sec

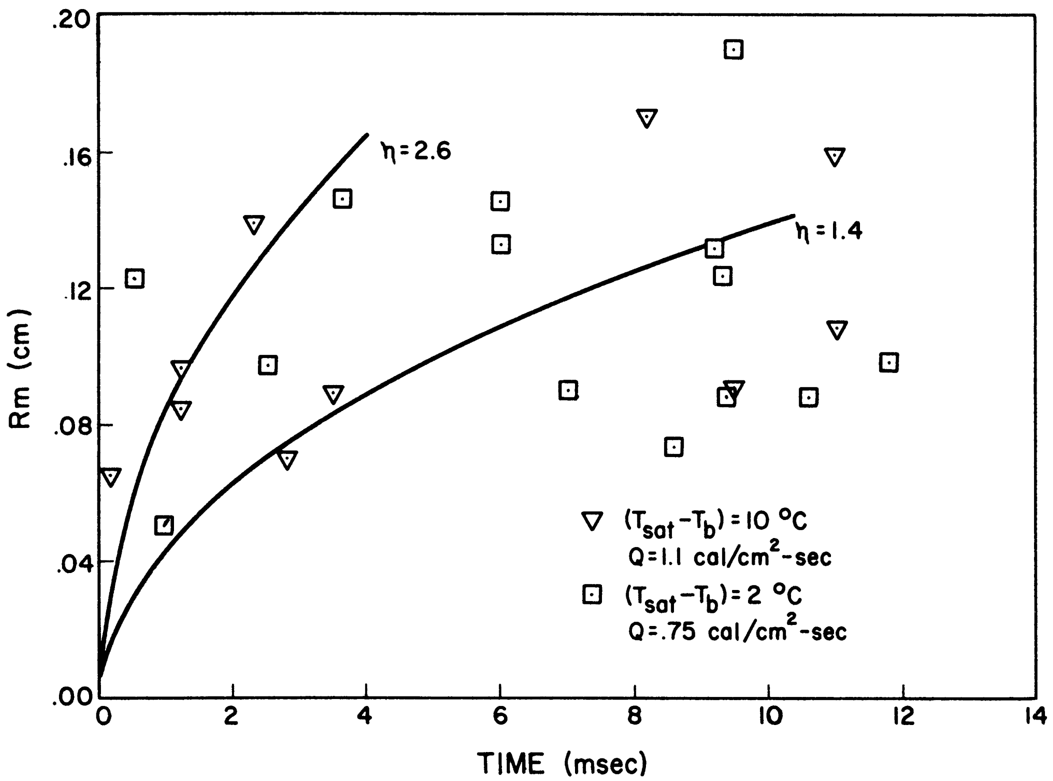

Figure 29 **MAXIMUM BUBBLE RADIUS**
TOLUENE at 520 mm Hg

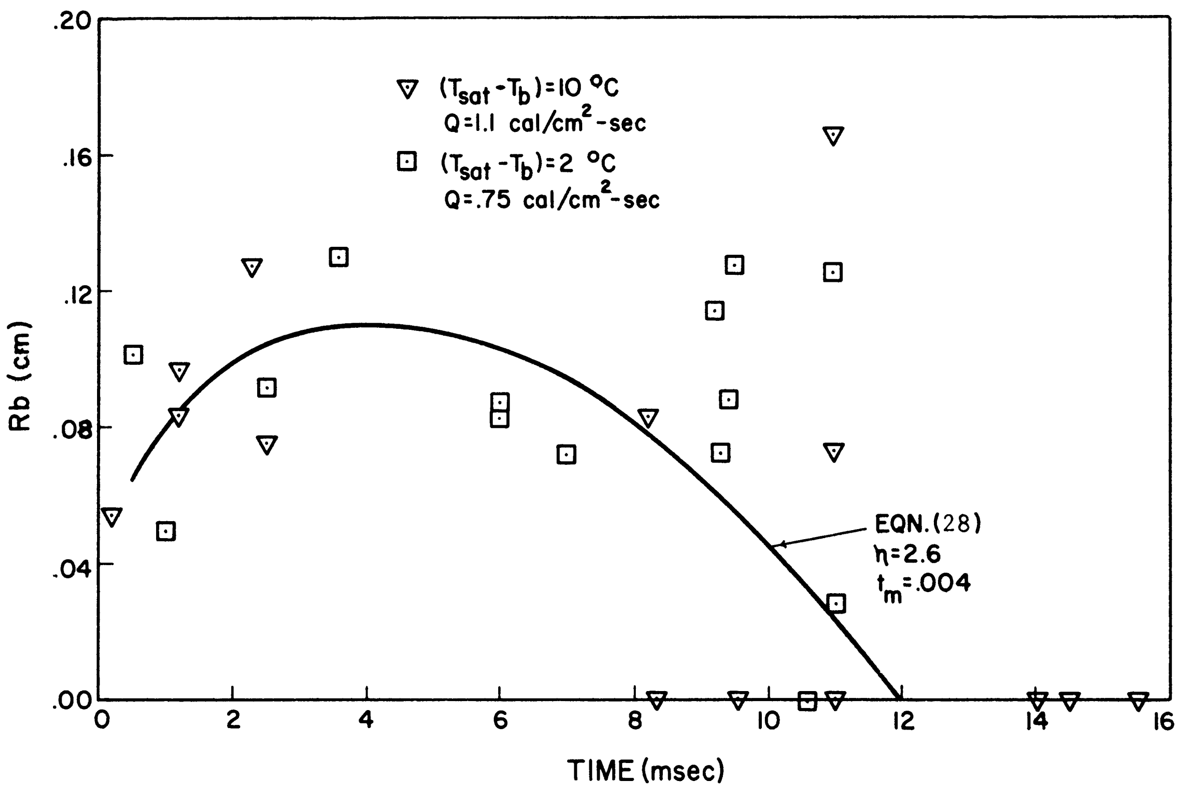

Figure 30 **BASE CONTACT RADIUS**
TOLUENE at 520 mm Hg

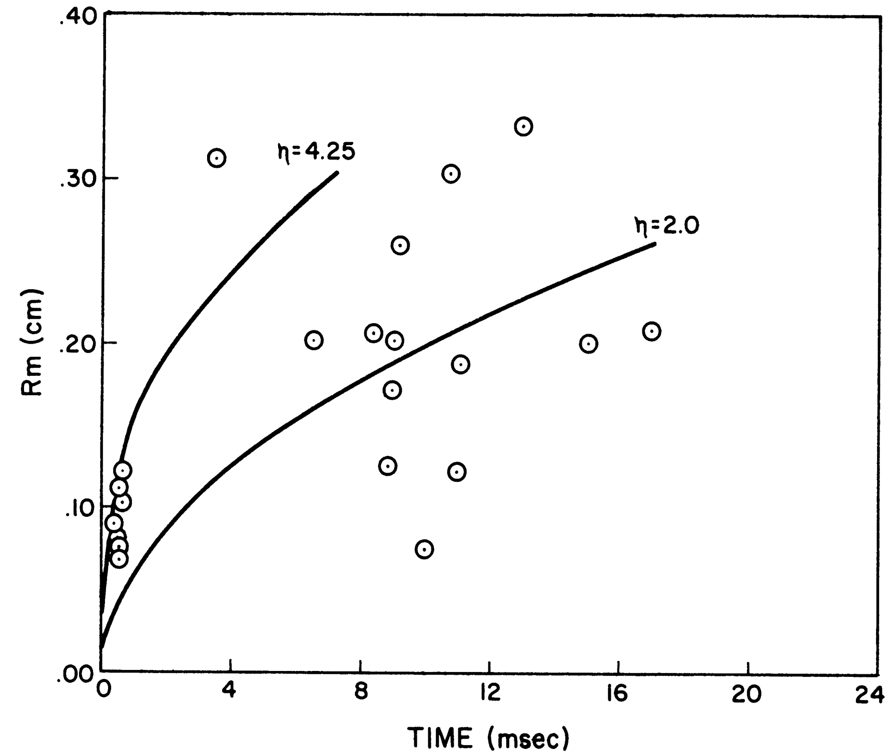

Figure 31 **MAXIMUM BUBBLE RADIUS**
TOLUENE at 410 mm Hg
Q=.64 cal/cm^2-sec

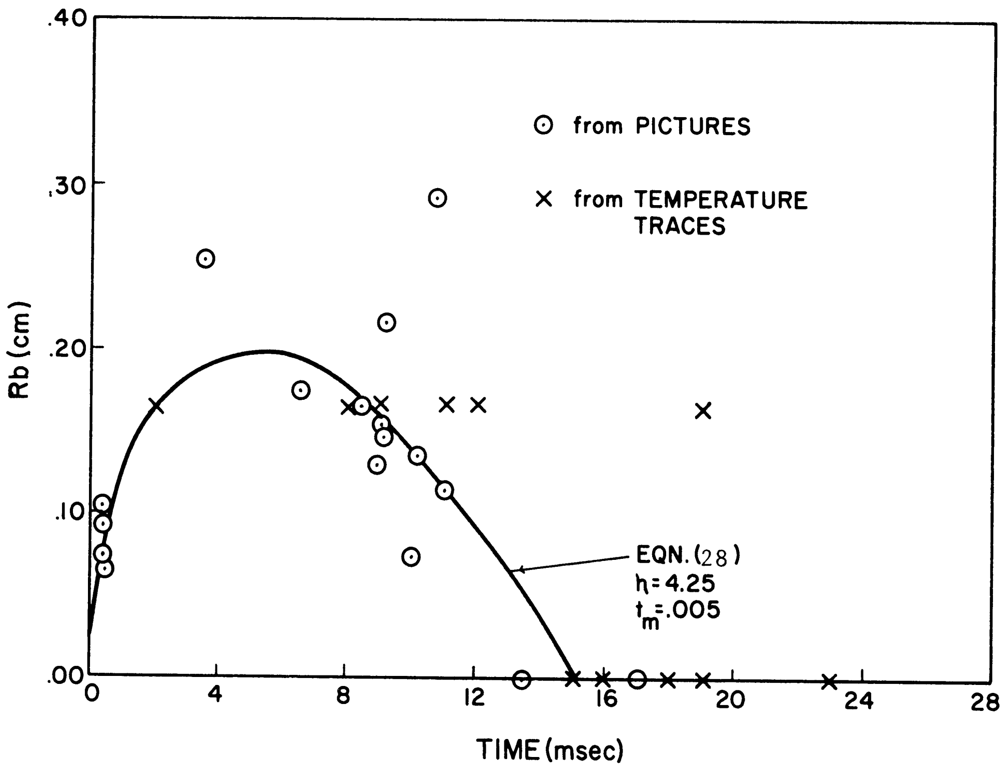

Figure 32 **BASE CONTACT RADIUS**
TOLUENE at 410 mm Hg
Q=.64 cal/cm^2 - sec

Figures (27) to (32) reveal several unexpected features. In Figures (29) and (30), the data seems to be independent of the amount of subcooling. Referring to Table III, the subcooled data comes from Run #14-3 and the data at a very slight subcooling is from #14-4 . The nucleating temperature is at least 10°C higher for the subcooled boiling. Any effect of subcooling must be compensated for by the higher nucleation temperature. In this data there seems to be a difference between the initial rate of bubble growth, measured by equation (26), and the average rate of bubble growth based on the maximum radial bubble size at departure. This effect is so pronounced in Figures (29) and (31) that two curves are shown on the graph. The higher value of η on the top curve is the initial rate of bubble growth and that on the lower curve is an average bubble growth rate. A good curve through the data for $R_m(t)$ would result from specifying the maximum radial bubble size by the initial growth rate up until the base contact radius is a maximum, and then specifying no further radial growth until departure.

The following table compares the theories for experimental growth rate.

TABLE IV

COMPARISON OF THEORETICAL AND EXPERIMENTAL GROWTH RATES

Fluid	Pressure mm of Hg	η Experimental	η Forster & Zuber	η Plesset & Zwick	η Zuber
Ethyl Alchol	500	2.34	2.4	2.6	1.5
Toluene	520	2.6	3.0	3.3	1.9
Toluene	410	4.3	3.5	3.8	2.2

Based on the TableIV,none of these theories predict the pressure effect which has been observed for Toluene. The equation derived by Han and Griffith, equation (4), requires an additional experimental variable - the liquid thermal layer thickness;d - even with this additional variable, which is unknown, the initial growth rate from the equation is the same as the last column in Table IV.

It is very difficult to obtain any correlation with the bubble departure theories because of the scatter in the experimental data and also the lack of enough pictures at departure to obtain the departing contact angle. Based on the experimental equation proposed by Cole and Shulman, equation (15), the departure radii for the three cases summarized in the graphs are: R_d = .14 cm at 500 mm of Hg for ethyl alcohol, R_d = .13 cm at 520 mm of Hg for toluene, and R_d = .17 cm at 410 mm of Hg for toluene. The equation approximately predicts the departure size but no real agreement is present.

Once nucleation begins, the power has to be turned down to get bubbles which nucleate more uniformly. Even if the site becomes inactive, it is never necessary to go above the original power setting before the site will reactivate. Therefore, vapor in some form must be present on the surface. At the observed nucleating temperature, the critical bubble dimension can be obtained from equation (6). For toluene, the critical radius at 30°C superheat is 6 x 10^{-4}cm; for ethyl alcohol at 20°C superheat the critical radius is 8 x 10^{-4}cm. The theories for predicting the active cavity radius show that any cavity between 10^{-4}cm and 10^{-2}cm could be active.

The comparisons of the experimental results with the theories for bubble growth, nucleation, and departure show some agreement but the theories are unable to describe fully the experimental results that are summarized in this section.

From the experimental results, it is possible to also check the general boiling correlations, described in the Literature Review, at a single active site. Since most of these equations assume the liquid flow controls boiling heat transfer, the ΔT which will be used in checking the validity of these correlations at a single active site will be the difference between the surface temperature outside the maximum bubble base contact radius ($R_{b\ max}$) and saturation temperature. For ethyl alcohol boiling at 500 mm of Hg, the wall temperature outside $R_{b\ max}$, is around 30°C superheated. The equation by Chang, equation (22), predicts $q = 1.25$ cal/cm^2-sec. The equation by Zuber, which is based on buoyancy, equation (23), predicts $q = 1.38$ cal/cm^2-sec. The experimental value is: $q = 1.20$ cal/cm^2-sec. These equations both predict the liquid heat-transfer rate in the liquid quite well.

3. Analysis of the Experimental Temperature Fluctuations

The primary temperature fluctuations indicate microlayer vaporization. Cooper and Lloyd (8) devised two methods of relating the temperature fluctuations to a microlayer thickness. Both require the surface temperature to be known as a function of time. The first method, based on the thermal resistance of the liquid, assumes all the liquid film evaporates. The second method, based on the thermal reaction of the solid to the change in surface temperature is not limited by the assumption that all the liquid film evaporate but does require that the temperature not only at the surface but also within the solid be known at the time of nucleation. The microlayer thickness which is calculated from the liquid thermal resistance is designated as Δ_1. The deviation starts with the equation governing the rate of evaporization of the film:

$$k_1\left(\frac{\partial T}{\partial y}\right)\Bigg|_{\Delta} = \rho_1 L\left(\frac{d\Delta(t)}{dt}\right) \qquad (29)$$

If the specific heat of the liquid is neglected then:

$$k_1\left(\frac{\partial T}{\partial y}\right)\Bigg|_{\Delta} \cong -k_1\frac{\left[T_w(t)-T_{sat}\right]}{\Delta(t)} \qquad (30)$$

When equation (30) is substituted into equation (29), the resulting differential equation can be integrated over the following limits: at $t = 0$, $\Delta = \Delta_o$, and at $t = t_e$, $\Delta = 0$. The final equation is:

$$\Delta_o = \sqrt{\frac{2k_1}{\rho_1 L}\int_o^{te}\left[T_w(t) - T_{sat}\right]\,dt} \qquad (20)$$

In all subsequent references to equation (20), this value of the initial microlayer thickness will be referred to as Δ_1 since it is based on the liquid properties and the experimental surface temperature fluctuation.

The other method of calculating a microlayer thickness is based on calculation of the total heat flow to the surface from within the solid

Assume the heat flow in the solid can be described by one dimensional heat conduction equation, i.e., :

$$\frac{\partial T(y,t)}{\partial t} = \frac{k_s}{\rho_s Cp_s} \frac{\partial^2 T(y,t)}{\partial y^2} \qquad (31)$$

The boundary conditions are:

$$T(0,t) = T_w(t) \qquad (32)$$

$$T(y,0) = T_o(y) \qquad (33)$$

$$T(y_b,t) = T(y_b,0) \qquad (34)$$

Equation (32) is the experimental wall temperature fluctuation, equation (33) is the initial temperature distribution in the solid at the time of nucleation, and equation (34) specifies that the temperature at some depth within the solid does not change with time. Of these boundary conditions, the last two cannot be specified experimentally during boiling. First assume it is possible to specify all the boundary conditions. Then equation (31), subject to the three boundary conditions given as equations (32) through (34), can be solved and the temperature at any point in the solid at any time can be determined. The heat flux at the wall can also be determined from temperature solution. The following equation relates the wall heat flux to the evaporated microlayer thickness during the fluctuation.

$$\rho_1 L \Delta_s = \int_o^{te} - \left[k_s \left(\frac{\partial T(y,t)}{\partial y} \right) \Bigg|_{y=o} \right] dt \qquad (35)$$

Whenever equation (35) is used to calculate a microlayer thickness the subscript "s" is used. If it is possible to specify the initial temperature distribution down to a point where the temperature is constant, it is possible to calculate Δ_s.

In the case where boiling initiates, it is possible to select an initial temperature distribution from a measured heat flux. The initial distribution would be:

$$T(y,0) = T_w(0) - qy/k_s. \qquad (36)$$

This equation also specifies the temperature at y_b. Once boiling begins, it is not possible to specify an initial temperature distribution unless the complete history of the surface from the first bubble onward is known. Of the infinite number of possible initial conditions two linear profiles are used. The first uses the average heat flux in equation (36) and the value , which is calculated after solving the temperature problem ,is jus designated as Δ_s. The second solution is obtained by changing q in equation (36) until the temperature, at some time after the microlayer has evaporated, matches the experimental temperature at that time. This value of q is designated as q_r; the value of Δ_s obtained from equation (35) is designated as Δ^*_s.

Table V summarizes the analysis of many of the toluene and ethyl alcohol temperature traces. The microlayer thicknesses Δ_1, Δ_s and Δ^*_s have been calculated by a computer program which is shown in Appendix E. The method of solving the one dimensional transient heat conduction equation is a simplification of a method described in Appendix D. A sample set of results is shown in Appendix G.

In this table, the notation is slightly different from the first three tables. The final number, added to the original notation designates the temperature trace. The number "1" represents the fluctuation of the center channel which triggered the flash. The number "2" is the

Table V. Estimation of the Microlayer Thickness Evaporated from the Temperature Traces

Notation	Δl cm x 10^6	Δs cm x 10^6	q cal/cm^2-sec	Δs* cm x 10^6	qr cal/cm^2-sec
			FOR TOLUENE		
14-3-23-1	647	123	1.09	113	1.075
27-1	672	129	1.09	95	0.762
14-4-1-1	515	87	.82	100	0.950
2-1	582	150	.82	121	0.700
19-1	506	123	.82	99	0.700
24-1	479	116	.77	89	0.575
29-1	529	129	.77	107	0.638
30-1	448	92	.77	99	0.825
32-1	525	130	.77	140	0.825
39-1	523	128	.77	110	0.638
14-5-26-1	397	64	.64	87	0.850
26-2	1112	82	.64	39	0.284
29-1	442		.64	120	1.100
29-2	1256	167	.64	166	0.639
29-3	524	119	.64	140	0.725
29-4	1118			290	0.725
30-1	408		.64	124	1.600
30-2	1143		.64	288	0.350
30-3	413	54	.64	32	0.936
33-1	458	76	.64	102	0.850
33-2	1287	171	.64	166	0.618
14-6-9-1	505	161	.87	68	0.288
11-1	501	125	.87	97	0.600
21-3	410	140	.76	121	0.600
21-4	1020	166	.76	233	1.084
21-5	400	104	.76	76	0.475
26-1	555		.76	85	1.100
26-2	1210	222	.76	250	0.979
27-1	939	110	.76	116	0.795
27-3	626		.76	101	1.100
27-4	1266			325	1.178
27-5	495	75	.76	84	0.850
32-1	579	61	.76	40	0.475
			FOR ETHYL ALCOHOL		
14-7-1-1	679	170	1.13	59	.25
22-1	830	285	1.11	142	.32
27-1	615	212	1.11	90	.19
27-2	1027*	233*	1.11	170*	.69
28-1	649	261	1.11	170	.49
30-1	631	339	1.11	163	.28
14-9-9-1	321		1.17	162	2.00
9-2	1430*	743*	1.17	536*	.55
23-2	436	410	1.37	258	.36
36-1	446	272	1.23	139	.29
9-9-3-13-1	514	406	1.2	118	.10
18-1	804	432	1.2	233	.33
28-1	870	392	1.2	291	.65
28-2	809*	451*	1.2	212*	.30
36-1	750	393	1.2	324	.73
9-7-8-1	538	315	1.2	145	.29

*No evidence of complete vaporization

fluctuation of the side channel corresponding to number "1". In like manner "3" and "4" are companion traces which are shown on the negatives of the temperature traces but have no corresponding boiling pictures. The odd number always designate fluctuations of the center resistor.

A comparison of Δ_1 with the Δ_s's shows that Δ_1 is always higher. The assumption that a linear profile in the solid represents the actual situation partially explains the difference. The physical size of the temperature sensor can also have an effect when the fluctuations are very sharp. If the parts of the sensor are exposed to different conditions, the resistor indicates only an average. Figure (33) shows an assumed fluctuation for two parts of the element. The dotted line is the average value.

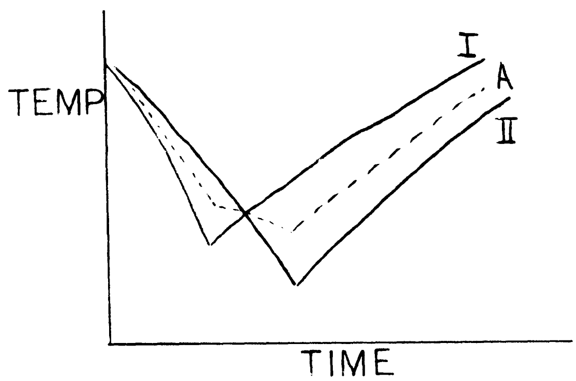

Figure (33)

Effect of the Sensor Size on the Measurement of Temperature Fluctuations

It can be seen that the averaging not only broadens the curve but also raises the minimum. If the minimum is raised, then the gradient in the solid, evaluated at the wall is underestimated because of the reduced driving force for heat flow in the solid. Furthermore, $(T_w(t)-T_{sat})$ is overestimated. It can also be seen that if the heat removed from the wall is too small, the wall will recover faster. This can partially explain the low values of Δ^*_s. This effect can also explain the difference between Δ_s and Δ_1.

Since Δ_1 appears to overestimate the evaporated microlayer thickness and Δ_s underestimates the thickness, the actual evaporated microlayer thickness should be between Δ_1 and Δ_s.

VII. THEORETICAL MICROLAYER THICKNESS

1. Introduction

The theoretical analysis of the microlayer thickness is based on the following mechanism of bubble growth in saturated boiling. Nucleation of a bubble on the surface is followed by rapid growth of the bubble both across the surface and up into the liquid. As the bubble travels across the surface, a thin film, called the microlayer, is left behind. The vaporization of this layer plus vaporization at the remaining bubble surface facilitates growth. As the microlayer evaporates it may vanish altogether in a particular region under the bubble.

This physical model of the bubble growth mechanism is based on a number of previous investigations. Moore and Mesler (34) postulated the existence of the microlayer to explain some experimentally observed temperature traces. Sharp (45) and Torikai (47) observed a microlayer under a bubble. Hence, in the classical picture of a bubble growing on the surface, as figure (11A) shows, the base contact radius $R_b(t)$ must be interpreted as indicating the maximum extent of the microlayer, not as a dry region.

The following theoretical analysis evaluates the microlayer thickness from experimental growth rate data and then proceeds to show that the vaporization rates from such a microlayer, as interpreted by wall temperature measurements, are consistent with the observed bubble growth rates and temperature traces.

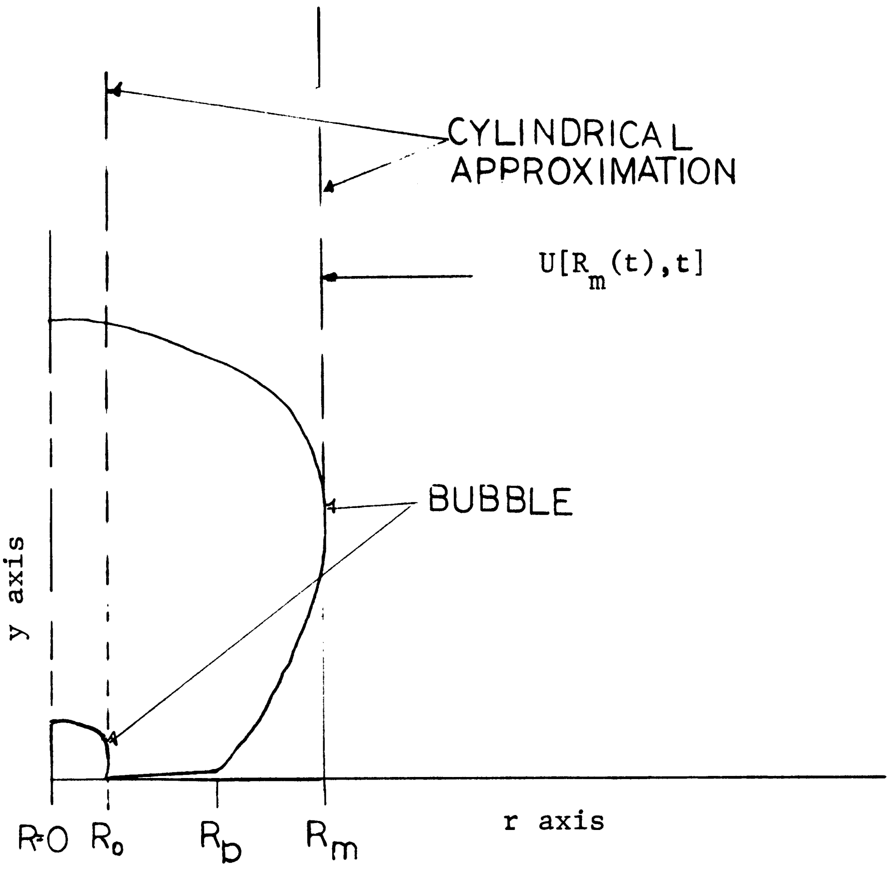

Figure (34) Mathematical Boundary Layer Model

2. Assumptions

Figure (34) shows the hydrodynamic model which is assumed to govern the formation of the microlayer. It is based on the following assumptions:

(1) The actual bubble growth on a solid surface can be analyzed in cylindrical coordinates by substituting a cylindrical tube of vapor for the bubble at all points above the height, H_c (see Figure (11A)), where the bubble ratios is a maximum. (2) Only radial axisymmetrical flow of liquid exists. (3) An incompressible one-fluid model can be substituted for the actual two-phase model for studying development of the viscous boundary layer constituting the microlayer. The position of the vapor-liquid interface is obtained by following

the motion of a fluid particle. (4) The boundary layer approximation is valid. (5) Initially, the fluid is at rest and the vapor cavity has a radius R_o. Subsequently, the free stream velocity imposed on the boundary layer is governed by the growth of the maximum radius $R_m(t)$.

3. Mathematical Formulation

The formulation is in terms of the continuity equation and the unsteady boundary layer equation for axisymmetrical flow. These equations are 11.3 and 11.1 in Schlichting's book on "Boundary Layer Theory" (43) and are shown as equations (37) and (38).

$$\frac{\partial u}{\partial t} + u\frac{\partial u}{\partial r} + v\frac{\partial u}{\partial y} = -\frac{1}{\rho}\frac{\partial p}{\partial r} + \nu\frac{\partial^2 u}{\partial y^2} \qquad (37\ )$$

$$\frac{\partial (ur)}{\partial r} + \frac{\partial (vr)}{\partial y} = 0 \qquad (38\ )$$

These equations can be simplified for small values of time by ignoring, to a good approximation, the connective terms. Only the first perturbation will be considered here. The equations become:

$$\frac{\partial u(r,y,t)}{\partial t} - \nu\frac{\partial^2 u(r,y,t)}{\partial y^2} = \frac{\partial U(r,t)}{\partial t} \qquad (39\ )$$

$$\frac{\partial [ru(r,y,t)]}{\partial r} = 0 \qquad (40\ )$$

In these equations, u(r,y,t) is the velocity of a particle in the fluid and U(r,t) is the free stream velocity. Equation (39) and (40) are subject to the following initial and boundary conditions:

$$u(r,y,0) = 0 \qquad (41)$$

$$u(r,0,t) = 0 \qquad (42)$$

$$u(r,\infty,t) = U(r,t) \qquad (43)$$

$$R(y,0) = R_o \qquad (44)$$

$$R(\infty,t) = R_m(t) = R_o + \eta\sqrt{t} \qquad (45)$$

The first three equations specify the boundary and initial conditions on velocity. Initially, the fluid is at rest, for all times the velocity at the wall is zero, and the velocity at infinity is specified by the free stream velocity. Equations (44) and (45) describe the position of particles which serve to indicate the liquid-vapor interface in the one-fluid model.

The free stream velocity U(r,t) is obtained from the fluid motion resulting from the expansion of the vapor cavity radius $R_m(t)$ which is initially at R_o. From the continuity equation (40) the free stream velocity is given by:

$$U(r,t) = \frac{R_m(t)\,\dot{R}_m(t)}{r} \qquad (46)$$

Substituting equation (45) gives:

$$U(r,t) = \frac{\eta R_o}{2r\sqrt{t}} + \frac{\eta^2}{2r} \qquad (47)$$

This equation, when substituted into equation (39) produces:

$$\frac{\partial u(r,y,t)}{\partial t} - \nu\frac{\partial^2 u(r,y,t)}{\partial y^2} = -\frac{R_o\eta}{4r(t)^{3/2}} \qquad (48)$$

The boundary conditions on u(r,y,t) are:

$$u(r,y,0) = 0$$

$$u(r,0,t) = 0, \text{ and}$$

$$u(r,\infty,t) = \frac{R_o\eta}{2r\sqrt{t}} + \frac{\eta^2}{2r} \qquad (49)$$

Equation (48) is solved by Laplace transforms after introducing the substitution,

$$u_1(r,y,t) = u(r,y,t) - \frac{R_o \eta}{2r\sqrt{t}} - \frac{\eta^2}{2r} \quad , \tag{50}$$

yielding the solution for u(r,y,t) as:

$$u(r,y,t) = \frac{\eta^2}{2r}\left[1 - \text{erfc}\left(\frac{y}{2\sqrt{\nu t}}\right)\right] + \frac{R_o \eta}{2r\sqrt{t}}\left[1 - \exp\left(\frac{-y^2}{4\nu t}\right)\right] . \tag{51}$$

Equation (51) is a general equation which holds for every point in the fluid at anytime. If R(y,t) is the radial position of a particle indicating the liquid vapor interface, then the velocity of this particle is given by substituting R(y,t) for r in equation (51). Since $u[R(y,t), y,t] = \partial R(y,t)/\partial t$, equation (51) may be integrated directly after rearranging to yield the particle position R(y,t) as a function of time. The resulting integral is:

$$\int_0^t \left[R(y,t) \frac{\partial R(y,t)}{\partial t}\right] dt = \int_0^t \left\{\frac{\eta^2}{2}\left[1 - \text{erfc}\left(\frac{y}{2\sqrt{\nu t}}\right)\right] + \frac{R_o \eta}{2r\sqrt{t}}\left[1 - \exp\left(\frac{-y^2}{4\nu t}\right)\right]\right\} dt \tag{52}$$

The right-hand side of equation (52) can be integrated by Laplace Transforms (see for example Roberts and Kaufman (39)). The final result is:

$$R^2(y,t) - R_o^2 = \eta^2 t\left[1 - \left(1 + \frac{y^2}{2\nu t}\right)\text{erfc}\left(\frac{y}{2\sqrt{\nu t}}\right) + \frac{y}{\sqrt{\pi\nu t}}\exp\left(\frac{-y^2}{4\nu t}\right)\right]$$

$$+ R_o \eta\sqrt{t}\left[1 - \exp\left(\frac{-y^2}{4\nu t}\right) + \frac{y\sqrt{\pi}}{2\sqrt{\nu t}}\text{erfc}\left(\frac{y}{2\sqrt{\nu t}}\right)\right] \tag{53}$$

Based on the one-fluid model, the value of y which satisfies equation (53) at $R = R(y,t)$ is the definition of $\Delta(R,t)$. The one-fluid model imposes a restriction on the flow in the microlayer which is not realistic. In the physical case, once the interface passes above any point R, the shear stresses imposed by fluid flow must be replaced by normal forces since the liquid-vapor interface can impart only very small shear stresses. Therefore, it is assumed that once the interface passes, the flow in the microlayer can be neglected.

It is not possible to solve equations (53) explicitly for $\Delta(R_b(t),t)$. This would be the microlayer thickness at the radial point R when the base contact radius passes over the point. An approximate, linear solution, is obtained by an indirect method. First, all the terms of order y^2 or greater are neglected in equation (53). This makes it possible to obtain an expression for $\Delta(R,t)$ in terms of the radial position, time, and R_o. Then R_o is neglected and the equation for $\Delta(R,t)$ is evaluated at $R_m(t)$. It can then be shown by substituting the final equation back into equation (53), exactly what the above approximations infer.

Neglecting all the terms of order y^2 or greater in equation (53) results in:

$$\Delta(R,t) = \frac{\left(R^2 - R_o^2\right)\sqrt{\pi\nu}}{2\eta^2\sqrt{t} + \pi R_o \eta} \qquad (54)$$

The values of R much greater than R_o, the terms containing R_o can be neglected. The equation becomes:

$$\Delta(R,t) = \frac{R^2\sqrt{\pi\nu}}{2\eta^2\sqrt{t}} \qquad (55)$$

The thickness at $R_m(t)$ based on the first term approximation for $\Delta(R,t)$ is:

$$\Delta[R_m(t),t] = R_m(t)\,\frac{\sqrt{\pi\nu}}{2\eta} \qquad (56\ )$$

A comparison of equation (56) with the exact equation is made by expressing $R_m(t)$ as $\eta\sqrt{t}$ in equation (56). The resulting equation can be expressed as: $\Delta[R_m(t),t]\ /2\sqrt{\nu t} = \sqrt{\pi}/4$. When this equation is substituted into equation (53), neglecting the R_o part, all the non-linear terms can be evaluated and the equation becomes: $R = .81\ R_m(t)$. Based on the experimental equations for $R_b(t)$ and $R_m(t)$, the average amount $R_b(t)$ lags behind $R_m(t)$ is $.80\ R_m(t)$. Thus, in an approximate manner, an expression which takes into account the slower motion of $R_b(t)$ has been obtained. The equation for the thickness of the liquid film left behind at a radial point R, where $R < R_b(t)$ is therefore:

$$\Delta(R) = R\sqrt{\pi\nu}/2\eta \qquad (\ 57)$$

The following diagram summarizes the results of this analysis:

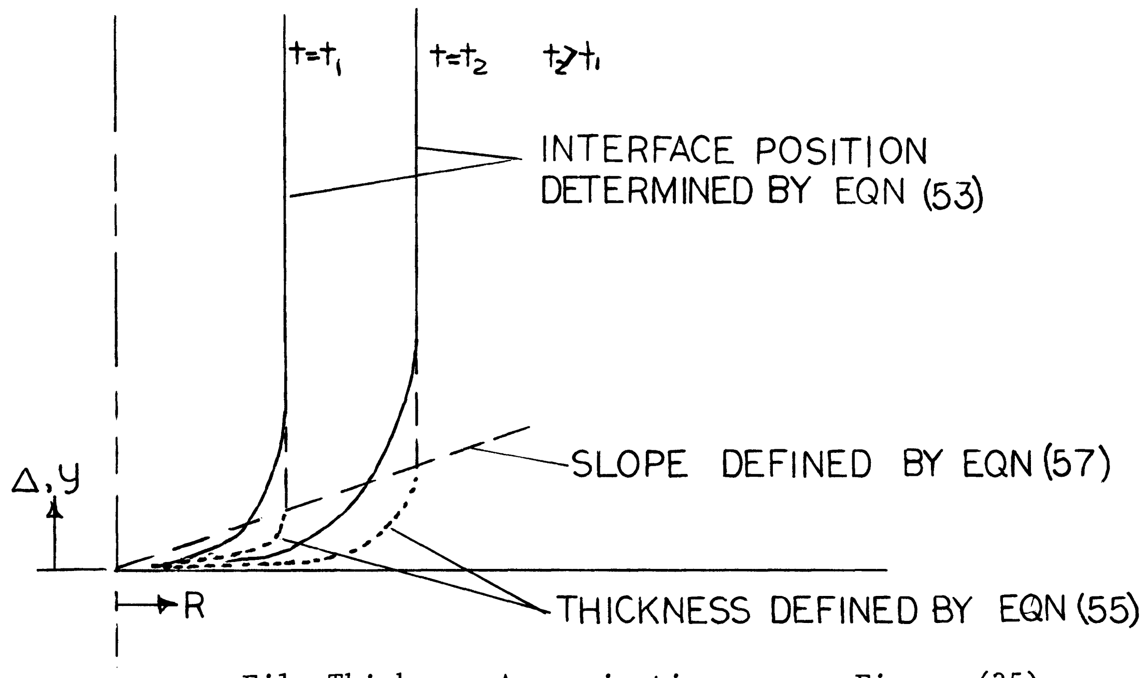

Film Thickness Approximations Figure (35)

The above model considers shear stress to control the flow in the microlayer up to the time when the bubble base passes the point. After this time flow is neglected because of the inability of a liquid-vapor interface to impart shear forces. The results of this analysis will now be compared with experimental results.

4. Comparison with Experimental Results

Based on equation (57) it is possible to compare the microlayer thickness, measured by the temperature trace, to the theoretical microlayer thickness. The average experimental microlayer thickness is based on Table V, shown on page (83). For the center resistor, the average radial distance from the point of nucleation has been determined by consideration of the resistor geometry. The resistor bars of the temperature sensor are spaced at .011 and .032 cm. from the point of nucleation. The average value, which will be used to calculate the experimental microlayer thickness, is R = .021 cm. The values of η and $R_{b\ max}$, which are needed in order to obtain the slope of equation (57), are based on the experimental data summarized by figures (27) through (32). The comparison of experimental and theoretical results are shown in Table IV. The data of Cooper and Lloyd (Run #1) are also shown. In their data, a value of $\eta = 9.5$ and $R_{b\ max} = 1.00$ cm. appears to fit their sketches of bubble size as a function of time.

TABLE VI

COMPARISON OF EXPERIMENTAL AND THEORETICAL FILM THICKNESS MEASUREMENTS

Fluid	Experimental Notation	Radial Portion of Temperature Sensor From Point of Nucleation		Average Experimental Microlayer Thickness from Temperature Traces			Theoretical Microlayer Thickness
	(Run #)	R	$R/R_{b\ max}$	Δ_1	Δ_s	η	Δ
		cm		$cm \times 10^6$	$cm \times 10^6$		$cm \times 10^6$
Toluene	14-3,14-4	.021	.18	542	120	2.6	450
Toluene	14-5	.021	.10	436	78	4.3	250
	14-5	.0165	.80	1183	140	4.3	2000
Ethyl Alcohol	14-7,14-9 9-3,9-7	.020	.14	627	338	2.3	570
Toluene Cooper & Lloyd	Run #1	.038 .190 .340	.038 .190 .340	575 1065 1990	340 1020 1620	9.5 9.5 9.5	236 1180 2100

There are several ways of checking for agreement between the theoretical and experimental results. At the same radial distance from the point of nucleation, the theory agrees with the theoretical results over a three fold change in η. Since the kinematic viscosity of ethyl alcohol is about 50% higher than toluene, the microlayer should be thicker for ethyl alcohol films when the bubble grows at the same rate. Within the Δ_1's and Δ_s's, the results show this trend.

In this investigation, some measurements of the microlayer have been computed at values of R very close to the maximum extent of the bubble base contact radius $R_{b\ max}$. It is only at this point where the experimental measurements, which are based on temperature fluctuations, differ from the theory. The use of the linear expression for the microlayer thickness as a function of radius could be inaccurate at this point. As Figure (19) indicates, the temperature at this radial point is 45°C. above the saturation temperature. Since the analysis of the temperature traces neglects liquid superheat, an error of 25% in the experimental results is possible.

The results of Sharp (45) have shown that at low superheats, only a small amount of the film vaporizes completely. At low fluxes, most of the vaporization occurs in the central region. It is in this region that the theory agrees with the experimentally determined film thickness.

5. Microlayer Vaporization

a. Introduction

In the previous section, ignoring vaporization, an expression has been derived for the microlayer thickness. In the present analysis, when vaporization is allowed, the microlayer thickness, defined by equation (57), is an initial condition. The evaporating microlayer thickness, $\Delta_e(R,t)$, is a boundary condition on the heat transfer problem. The previous section showed that from temperature measurements, the microlayer thickness agrees with the theory; in this section, the theory is used to show that starting with the microlayer thickness and known experimental bubble growth parameters, it is possible to approximate the observed fluctuations. Based on these results, it is then possible to extend the results to show the influence of microlayer vaporization on boiling heat transfer at low fluxes.

b. Assumptions

1. The liquid thermal inertia in the microlayer can be neglected.
2. Heat transfer in the solid is governed by the two dimensional axisymmetric radial heat conduction equation.
3. The surface is insulated after the microlayer has evaporated.
4. The maximum extent of the microlayer is $R_b(t)$.
5. In the region not covered by the microlayer, the heat transfer rate can be described using a constant heat transfer coefficient at the surface.
6. No flow in the microlayer is allowed.
7. Bubble growth begins whenever the temperature of the surface at the point of nucleation exceeds a specified value.

c. Mathematical Formulation

The radial axisymmetric heat conduction equation in the solid is:

$$\rho_s \, Cp_s \, \frac{\partial T(r,y,t)}{\partial t} = k_s \left[\frac{\partial^2 T(r,y,t)}{\partial r^2} + \frac{1}{r}\frac{\partial T(r,y,t)}{\partial r} + \frac{\partial^2 T(r,y,t)}{\partial y^2} \right] \qquad (58)$$

The initial and boundary conditions are:

$$k_s \left. \frac{\partial T(r,y,t)}{\partial y} \right|_{y=0} = 0 \qquad \text{Whenever } \Delta_e(r,t) = 0 \text{ and } r<R_b(t) \qquad (59)$$

$$k_s \left. \frac{\partial T(r,y,t)}{\partial y} \right|_{y=0} = k_s \frac{[T(r,o,t) - T_{sat}]}{\Delta_e(r,t)} \qquad \text{Whenever } \Delta_e(r,t)>0 \text{ and } r<R_b(t). \qquad (60)$$

$$k_s \left. \frac{\partial T(r,y,t)}{\partial y} \right|_{y=0} = h_w \left[T(r,0,t) - T_b \right] \qquad \text{Whenever } r>R_b(t) \qquad (61)$$

$$k_s \left. \frac{\partial T(r,y,t)}{\partial y} \right|_{y=0} = \rho_l L \frac{d\Delta_e(r,t)}{dt} \qquad \text{Whenever } \Delta_e(r,t)>0 \text{ and } r<R_b(t) \qquad (62)$$

$$R_b(t) = \eta\sqrt{t} \, (1 - t/t_d) \qquad (63)$$

$$\Delta_e[r, t^{-1}(R_b)] = r\sqrt{\pi\nu}/2\eta \qquad \text{Whenever } t \leqslant t_d/3 \qquad (64)$$

$$\left. \frac{\partial T(r,y,t)}{\partial r} \right|_{r=0} = 0 \qquad (65)$$

$$\left. \frac{\partial T(r,y,t)}{\partial r} \right|_{r=r_{max}} = 0, \text{ where } r_{max} >> R_{b\,max} \qquad (66)$$

$$T(r, y_b, t) = T_{base} \qquad (67)$$

$$T(r,y,0) = T(r,y,t_n) \text{ , Whenever } t_n > t_d \text{ and } T(0,0,t_n) \geqslant T_n \qquad (68)$$

The first three boundary conditions describe the rate of heat transfer from the top surface. These conditions depend on whether the microlayer has evaporated completely and whether the bubble contact radius $R_b(t)$ still extends beyond the radial point. The rate of microlayer vaporization can be related to the thermal gradient in the solid at the surface as equation (62) shows. Equation (63) is the experimentally determined equation for $R_b(t)$. The boundary condition described by equation (64) is the initial film thickness which is formed at the time $R_b(t)$ passes r. Thus, $t^{-1}(R_b)$ is the inversion of equation (63) for $R_b(t)$. Equations (65) and (66) give the boundary conditions governing the radial flow of heat. The temperature at the base of the plate is a constant as equation (67) specifies. The final boundary condition is the initial temperature distribution, which is specified only by the initial condition for the start of bubble growth.

One of the assumptions is that a bubble nucleates whenever the temperature at the point of nucleation exceeds a specified temperature T_n. The variable t_n is the first time after departure, t_d, where this condition is satisfied. It is still necessary to specify an initial temperature before the first bubble nucleates. The actual choice depends on the method of solution. In this case, a finite-difference technique is used on the digital computer. It is therefore important to specify any known temperatures. Experimentally, a temperature outside $R_b(t)$ is

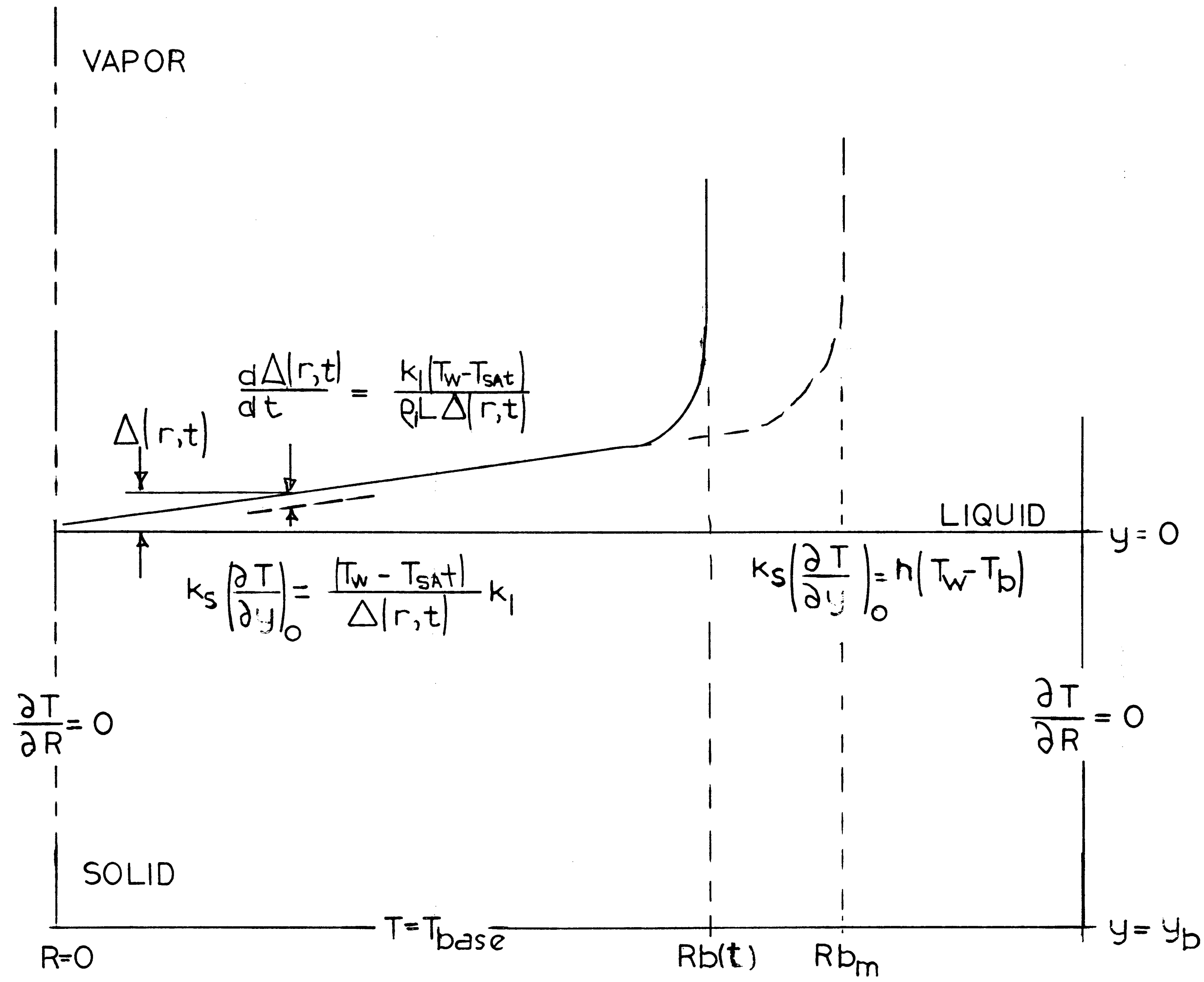

Figure 36 Heat Transfer Model Governed by the Liquid Film

known. Since the base temperature is also known or can be specified from a known average heat flux, the initial condition which is used is that of a uniform surface temperature equal to temperature of the outer resistor. At any intermediate point in the solid, linear interpolation between the base temperature and the outer surface temperature is used. Figure (35) summarizes the boundary conditions governing heat transfer and vaporization.

d. Dimensional Analysis

The equations governing heat transfer in the solid can be made dimensionless by defining the following variables: $\theta = (T-T_{sat})/(T_n-T_{sat})$, $z = y/y_b$, $\tau = t/t_m = 3t/t_d$, $x = r/R_{b\,max}$, and $\delta[x,\tau^{-1}(x_b)] = \Delta[r,t^{-1}(R_b)]/\Delta_o$ where $\Delta_o = \Delta[R_{b\,max}, t^{-1}(R_{b\,max})]$.

The equation governing heat transfer in the solid becomes:

$$\left(\frac{\rho_s Cp_s}{k_s}\right)\left(\frac{9\eta^2}{4}\right)\frac{\partial\theta(x,z,\tau)}{\partial\tau} = \frac{R^2_{b\,max}}{y_b^2}\frac{\partial^2\theta(x,z,\tau)}{\partial z^2} + \frac{\partial^2\theta(x,z,\tau)}{\partial x^2} + \frac{1}{x}\frac{\partial\theta(x,z,\tau)}{\partial x} \quad (69)$$

The initial and boundary conditions become:

$$\left.\frac{\partial\theta(x,z,\tau)}{\partial z}\right|_{z=0} = 0 \qquad \text{Whenever } \delta(x,\tau) = 0 \text{ and } x<x_b(\tau) \quad (70)$$

$$\left.\frac{\partial\theta(x,z,\tau)}{\partial z}\right|_{z=0} = -\left(\frac{k_1\, y_b}{k_s\,\Delta_o}\right)\frac{\theta(x,0,\tau)}{\delta(x,\tau)} \qquad \text{Whenever}\begin{cases}\delta(x,\tau) > 0\\ x<x_b(\tau)\end{cases} \quad (71)$$

$$\left.\frac{\partial\theta(x,z,\tau)}{\partial z}\right|_{z=0} = \frac{h_w \Delta T_n}{k_s}\left[\theta(x,0,\tau) - \theta_b\right] \text{ Whenever } x > x_b(\tau) \qquad (72)$$

$$\left.\frac{\partial\theta(x,z,\tau)}{\partial z}\right|_{z=0} = \left(\frac{k_1 y_b}{k_s \Delta_o}\right)\left(\frac{9\rho_1 \nu_1 L}{\pi k_1 \Delta T_n}\right)\frac{d\delta(x,\tau)}{dt} \quad \text{Whenever } \delta(x,\tau) > 0 \text{ and } x < x_b(\tau) \qquad (73)$$

$$x_b(\tau) = \frac{3}{2}\sqrt{\tau}\,(1 - \tau/3) \qquad (74)$$

$$\delta_e\,[x,\tau^{-1}(x_b)] = x \qquad (75)$$

$$\left.\frac{\partial T(x,z,\tau)}{\partial x}\right|_{x=0} = 0 \qquad (76)$$

$$\left.\frac{\partial T(x,z,\tau)}{\partial x}\right|_{x=x_{max}} = 0 \qquad \text{Where } x_{max} >> \underline{1} \qquad (77)$$

$$\theta(x,-1,\tau) = \theta_{base} = (T_{base} - T_{sat})/(T_n - T_{sat}) \qquad (78)$$

$$\theta(x,z,0) = \theta(x,z,\tau_n), \text{ Whenever } \tau_n > 3 \text{ and } \theta(0,0,\tau_n) > 1 \qquad (79)$$

The order in the list of boundary conditions is identical to the original dimensional set of equations, thus equation (70) is the dimensionless form of equation (59), etc.

There are two relationships that are implied by realizing that $x[1,t^{-1}(1)] = 1$ and $\delta_e(1,1) = 1$. They are: $R_{b\ max}\,\eta/\sqrt{t_m} = 3/2$, and $\Delta_o = \sqrt{\pi\nu_1 t_m}/3$. With these relationships it is possible to eliminate Δ_o and t_m

from all equations. In equations (71) and (73), the Δ_o is actually specified when $R_{b\ max}$ is set. The dimensionless group in equation (80) can be written as:

$$\left(\frac{k_1 y_b}{k_s \Delta_o}\right) = \left(\frac{k_1 y_b}{k_s R_{b\ max}}\right)\left(\frac{3\eta}{\sqrt{\pi \nu_1}}\right) \qquad (80)$$

Equation (69), subject to the boundary conditions described by equations (70) through (80), is solved by finite-difference techniques on a digital computer. The difference equations and the method of solving the equations are shown in Appendix D; the actual program, written in MAD, is shown in Appendix F.

e. Comparison of Temperature Traces with Experimental Traces

Two of the three cases described in the experimental results section have been programmed into the computer. These are the boiling of ethyl alcohol at a pressure of 500 mm of Hg and a heat flux of 1.2 cal/cm^2-sec, and boiling of toluene at a pressure of 500 mm of Hg and a flux of .75 mm of Hg.

Because of the size of the temperature sensors in relation to the grid size, which has been used in the computer solution, the central sensor averaged the heat flux from zero to 1.6 grid spaces for both cases studied. An area average has been used to obtain the average surface temperature for the computer results. For the zero, first and second grid space the area average is:

$$\bar{T} = \frac{T_o A_o + T_1 A_1 + T_2 A_2}{A_o + A_1 + A_2} \qquad (81)$$

TABLE VII

COMPARISON OF THE THEORETICAL RESISTOR AVERAGED TEMPERATURE WITH AN EXPERIMENTAL TEMPERATURE CURVE FOR ETHYL ALCOHOL

t msec	T_o Temperature at Grid Space #0	T_1 Temperature at Grid Space #1	T_2. Temperature at Grid Space #2	$\bar{T}$ Area Averaged Temperature	Experimental Curve 9-1-13
0	20	18.8	20.4	19.8	18.6
1	11.3	17.5	20.0	17.4	11.6
2	.01	11.4	16.3	10.2	8.4
3	5.2	8.3	14.0	8.9	5.9
4	8.9	6.6	12.4	7.6	4.1
5	10.0	5.5	11.3	6.7	2.7
6	12.4	4.6	10.7	6.1	2.0
7	13.5	3.9	9.9	5.7	1.6
8	14.3	3.3	9.3	5.2	1.3
9	14.8	2.7	8.9	4.6	1.1
10	15.2	2.1	8.4	4.2	1.0
11	15.5	1.5	8.1	3.7	1.6
12	15.8	.4	7.3	2.9	2.0
13	15.9	.8	7.0	3.1	
14	16.1	4.0	6.7	5.5	
15	16.3	6.3	6.4	7.3	3.4
16	16.6	8.1	6.1	8.7	
17	16.8	9.6	5.9	9.9	
18	17.1	10.7	5.9	10.7	
19	17.3	11.6	7.6	11.7	
20	17.6	12.3	9.4	12.5	
21(departure)	17.6	12.5	9.4	12.7	

TABLE VIII

COMPARISON OF THE THEORETICAL AVERAGED TEMPERATURE AT THE CENTER RESISTOR WITH AN EXPERIMENTAL TEMPERATURE-TIME CURVE AT THE CENTER RESISTOR FOR TOLUENE

t	T_o	T_1	T_2	$\bar{T}$	Texp 14-6-21-3
0	30.8	24.8	13.1	23.8	26.0
1	25.4	17.8	13.2	18.0	11.2
2	26.0	9.6	12.6	11.5	12.1
3	26.7	13.1	12.1	14.3	
4	27.2	15.6	11.6	16.2	17.4
5	27.7	17.6	11.0	18.5	
6	28.2	19.1	10.3	19.0	22.0
7	28.4	20.2	9.4	19.6	
8	28.8	21.2	8.3	20.3	
9	29.0	22.0	6.7	20.6	
10	29.2	22.6	4.8	20.8	
11	29.4	23.2	6.6	21.6	
12(departure)	29.6	23.6	9.3	22.4	
14	29.3	24.1	14.3	23.4	
16	29.0	24.2	15.3	23.5	

The area of the zero grid space is $\pi(\Delta R)^2/4$, the area of the first is $2\pi(\Delta R)^2$, and the area used for the second grid space is $2\pi(1.55)(.1)(\Delta R)^2$ (this being the area between 1.5 and 1.6 grid spaces). Tables VIIand VIII compare the values of T_o, T_1, T_2, and $\bar{T}$ with the experimental curves for ethyl alcohol and toluene respectively. Because of the large value of A_1, the value of T_1 is a good approximation to the average temperature. A finer grid size would show the averaging of the temperature sensor discussed in the experimental results section. There is good agreement between $\bar{T}$ and T_{exp}, when the assumptions which have been made are considered. For both cases shown in the tables the computer results are for the temperature traces resulting after several bubbles have nucleated from the surface. After this time there was almost no change from one bubble to the next.

6. Implications of the Film Theory

In addition to the comparison of temperature traces it is possible to compute the total volume of the microlayer evaporated. The thermal effects of bubble growth, nucleation and departure can also be discussed.

Starting with the initial uniform surface temperature, equal to the outer resistor temperature, it is possible to compute the total volume of the microlayer evaporated for successive bubbles. In addition, the dry spot area, and the waiting time, t_w, between bubble departure and the next nucleation, can be calculated. These results for ethyl alcohol and toluene are shown in Tables VIII and IX.

TABLE IX

BOILING OF ETHYL ALCOHOL P=500 mm of Hg, q=1.2 cal/cm^2-sec

Bubble #	Nucleation Temperature ΔT_n °C	Departure Temperature ΔT_d °C	Dry Spot Radius $R/R_{b\ max}$	Center $\bar{\Delta}_e$ $x10^6$cm	Center t_e msec	Evaporated Volume $x10^6 cm^3$	t_w msec
1	30°C	25.5	.23	590	7	20.4	0
2	26.5	21.8	.14	590	10	16.3	0
3	21.8	18.5	.14	590	15	15.2	23.0
4	20.0	17.6	.15	590	11	16.4	27.6
5	20.0	17.8	.15	590	11	16.4	30.7
6	20.0	17.8	.15	590	13.6	16.4	30.7
7	20.0	17.8	.15	590	14	16.4	31.2

TABLE X

BOILING OF TOLUENE P=500 mm of Hg, q=.75 cal/cm^2-sec

Bubble #	Nucleation Temperature ΔT_n °C	Departure Temperature ΔT_d °C	Dry Spot Radius $R/R_{b\ max}$	Center $\bar{\Delta}_e$ $x10^6$cm	Center te msec	Evaporated Volume $x10^6 cm^3$	tw msec
1	37.5	38	.76	450	1.00	23.2	0
2	38	36.4	.40	450	1.05	18.7	0
3	36.4	31.5	.40	450	1.45	17.8	0
4	31.5	30.7	.40	450	1.51	17.1	0
5	30.7	29.6	.30	450	2	16.3	70
6	30.0	--	--	450	1.6	--	--

For the first few bubbles, the temperature recovery of the surface is very rapid and at departure the surface temperature at the point of nucleation has almost completely recovered to its initial value. After several bubbles the recovery is much slower and a finite waiting time between bubbles is observed. This is exactly what has been experimentally observed in this study.

Based on the total volume of liquid evaporated in the microlayer, it is possible to estimate the total contribution of microlayer vaporization to the volume of vapor in a departing bubble. For toluene, at departure, the bubble volumes are close to spheres and have a radius approximately equal to .165 cm. The total volume of vapor in the bubble is therefore 19 x $10^{-3} cm^3$. Since the density at 500 mm of Hg at saturation is .0020 gm/cm^3 and the latent heat of vaporization is 89 cal/gm, the total heat content in a departing bubble is 3.36 x 10^{-3}cal. Based on the computer analysis the volume of liquid evaporated in the microlayer is: 16.3 x $10^{-6} cm^3$. The mean density of the liquid is .784 gm/cm^3, thus, the heat content from the microlayer is: 1.14 x 10^{-3}cal. This says that for toluene, about 34% of the heat within the bubble comes from microlayer. The most uncertain variable in the entire calculation is the experimental departure volume.

The same calculation can be made for ethyl alcohol. For ethyl alcohol the departure radius is about .25 cm at 500 mm of Hg. The volume at departure is 36 x $10^{-3} cm^3$. The density and latent heat at saturation are: .0010 gm/cm^3 and 208 cal/gm respectively. The heat content of a departing bubble is therefore 7.5 x 10^{-3}cal. Based on the computer analysis, the volume of liquid evaporated in the microlayer is 16.4×10^{-6} cm^3/gm. The mean density of ethyl alcohol is .739 gm/cm^3. Therefore the total heat content in a departing bubble arising from microlayer vaporization is 2.5×10^{-3} cal. This means that for ethyl alcohol, boiling off glass, the total percentage of heat in a bubble resulting from microlayer vaporization is 33%.

The computer analysis also shows that the maximum extent of the dry spot area for these two cases is: toluene .40 of $R_{b\ max}$ and ethyl alcohol .15 of $R_{b\ max}$. This means that for these two cases very little of the total microlayer actually evaporates. Even so, it can be seen that the contribution of the microlayer to vapor formation is considerable. It is easy to see that if the whole microlayer vaporized, a very efficient boiling process would be the result.

The nucleation theories, based on the thermal layer recovery, usually assume a constant surface temperature. In addition it is assumed that a bubble will nucleate when the temperature at some point in the fluid exceeds a specified temperature level. The theories are inadequate to explain the nucleation characteristics observed in this investigation because of the large surface temperature fluctuations which were present. At the present time, the assumption that nucleation occurs when a given surface temperature level is reached seems to be the only justifiable nucleation criterion.

One of the assumptions in this theory is a constant heat transfer coefficient outside $R_b(t)$. The break in the temperature time curve can be explained in two ways. If the surface is completely insulated, a temperature fluctuation of a sensitive surface element could be caused simply by the change in heat transfer rates between the presence of vapor and then liquid on the surface. It appears that since the fluctuations are larger than those observed in the computer solution at departure (see Table VIII, column under T_o) there must be an increase in the heat transfer coefficient at departure. It is very difficult to analyze because the ΔT driving force is unknown. Since the glass has such a large radial thermal gradient it is quite possible that cool and then hot fluid moves across the surface at departure. This flow and temperature pattern is not understood at present. This makes it difficult to estimate the heat transfer induced by departure under a bubble.

The calculation for other surfaces was not attempted mainly because the microlayer formation is very dependent on bubble dynamics. The dynamics of other fluids on other surfaces could be quite different and such data is not presently available in the literature, in sufficient detail.

VIII. DISCUSSION OF RESULTS

1. Experimental Techniques

Three new concepts have been used in this investigation of boiling from a glass surface. First, the study utilized a single-site heater. This permitted an excellent view of the bubble base. The heater design was feasible because the low thermal conductivity of the glass plate which allowed negligible radial heat flow. Since one site was used, the heat flux setting was adjusted until one site predominated in activity. At high heat fluxes, even if all the bubbles emanated from a single site, it was impossible to discern individual bubbles.

The second feature, which was successful only in the last series of runs, was the use of both a top and side view. The side view permitted the observation of the important bubble parameters. The top view served to scale and position the bubble relative to the resistor pattern. Although this view was frequently obscured by departed bubbles, there were a sufficient number of pictures to locate the nucleation center at a point within the boundaries of the central temperature sensor.

Finally, the temperature traces have been used successfully to determine when nucleation occurred. An estimate of the response time can be obtained by assuming that when the bubble completely covers the temperature sensor, the sensor will indicate the bubble's presence. The response time can be found from $R = \eta\sqrt{t}$. With the outer limit of the sensor at $R = .031$ cm, and η set equal to 2.34 (the value for ethyl alcohol), the response time is found to be

.17 msec. This is equivalent to using a motion picture camera filming the process at a rate of almost 8000 frames/sec. Thus the error in the use of the temperature trace for determining the nucleation time is very small.

2. Bubble Growth Rates During Boiling on a Glass Surface

For both toluene and ethyl alcohol, the bubble growth rate radically increased as the pressure decreased. The decrease in pressure also resulted in a slight (about 3%) decrease in heat flux which was not significant. As yet, no published bubble growth theory predicts such an effect. These bubble growth theories proceed along the following lines. Consider a vapor bubble in the shape of a hemisphere on a surface which is completely surrounded by a uniformly superheated liquid. If the base is insulated and the effect of the wall drag can be neglected, this bubble will grow at the same rate as a sphere in a uniformly superheated liquid. This sphere problem has been solved for the case where heat transfer from the liquid controls growth. The solution predicts bubble growth rates which are too high when compared to actual data obtained on a metal surface. In order to bring the theory into better agreement with the experimental results, a correction for the thermal gradient existing above the boiling surface has been considered. This results in the necessary six-tenths reduction in the spherical solution. Thus the theories require a rather arbitrary coefficient to agree with the data.

Such a line of reasoning cannot explain the growth rates which are observed in this investigation. The thermal gradient certainly exists and yet the results of the calculations show the bubble growing in some cases at a faster rate than the spherical bubble growth theory would predict. The only logical explanation is that the base of the hemisphere, which is assumed to be insulated so the spherical solution can be used, is, in fact, not insulated. A microlayer has been observed under a bubble but its contribution to bubble growth has not previously been estimated.

The analysis developed in this investigation, based on impulsive microlayer formation, has been shown to agree with the experimental temperature fluctuations under a bubble; and further the microlayer contribution to the rate of bubble growth has been shown to be significant. This analysis thus explains experimental growth rates which are higher than predicted by the spherical solutions.

3. Nature of Boiling from a Glass Surface

As many theories predict, it is very difficult to initiate boiling from a glass surface. The boiling of toluene was observed to start only at a small region covered by a flaky coating of Teflon*-like material. Ethyl alcohol, boiling on the same surface, exhibited nucleation both from the Teflon-like material and other naturally occurring sites.

Once boiling began, toluene and ethyl alcohol exhibited completely different boiling characteristics. Toluene nucleated many bubbles in quick succession and then the site deactivated. The secondary bubbles in such processes were smaller than the first one.

*DuPont Tradename

Ethyl alcohol, on the other hand, showed a form of periodic boiling which existed for long periods of time. It was observed in this investigation that by lowering the pressure this regular boiling changed to the type of boiling toluene exhibited.

From the microlayer theory, developed in this investigation, it is possible to theoretically explain the boiling phenomena which were observed for both toluene and ethyl alcohol. Microlayer vaporization is the controlling factor. For toluene the microlayer vaporizes rapidly and the surface is dry and essentially insulated for long periods of time before departure. After the bubble departs, the surface is above the required nucleation temperature and secondary nucleation follows immediately. Thus a rapid string of bubbles followed by a long recovery time is the result. For ethyl alcohol, again based on the microlayer theory, the microlayer extracts a great deal of energy from the area around the point of nucleation and at departure the surface temperature is below the required nucleation temperature. A waiting time before the next nucleation allows both the surface and the superheated liquid layer a chance to recover. The decrease in pressure causes the regular boiling of ethyl alcohol to become irregular and the bubbles grow much more rapidly. The theory explains this phenomenon as due to the thinner microlayer which, as with toluene, gives the surface a chance to recover almost fully from the initial fluctuation before departure. Since the surface cannot sustain the required nucleation temperature for rapidly nucleating bubbles, the site deactivates after several bubbles. In this way microlayer vaporization controls nucleation.

In the theoretical solution, the contribution of microlayer vaporization for the regular boiling of ethyl alcohol is about 30% of the energy within a departing bubble. The other 70% comes from the superheated liquid surrounding the bubble. However, considering the entire heat transfer process in boiling, roughly 90% of the heat transfer occurs through the agitated boundary layer outside the region contacted by the bubble base. This figure of 90% can be arrived at in several ways. One of the easiest is to consider the ratio of the heater area to the area contacted by the bubble base. That area ratio is 11:1 in favor of the liquid agitation mechanism in the case of ethyl alcohol. To make the point clear, two processes are occurring. The first is heat transfer to an agitated boundary layer. The second is latent heat transport by means of the bubble (about 10% of the total). In the latent heat transport process, 30% is transferred by microlayer vaporization and 70% from the superheated liquid. Thus even though only 3% of the total heat transfer comes from the microlayer, it is the microlayer which controls the nucleation characteristics.

In summary, the microlayer thickness is an important variable which controls the boiling characteristics on a glass surface; the microlayer theory, which is based on experimentally determined bubble growth rate and the kinematic viscosity of the liquid explains the boiling characteristics of both ethyl alcohol and toluene on a glass plate.

IX. CONCLUSIONS

1. A theory of microlayer vaporization was developed during the course of this investigation which successfully explains the phenomena associated with the boiling of ethyl alcohol and toluene from a glass surface. The theory predicts the surface temperature fluctuations and the nucleation characteristics, which agree reasonably well with those experimentally observed. Furthermore, the theory explains why the bubble growth rates observed in this investigation exceed those expected from previously published growth theories.

2. The technique of utilizing a single nucleating site on a surface, coupled with thin film instrumentation is an excellent method for the study of the boiling process. For instance, the base contact radius of the growing bubble, which has been previously neglected and yet was found to be an important parameter, is easily observed.

3. The use of the microlayer theory in conjunction with experimentally observed base contact radii permits the calculation of the contribution of microlayer vaporization to bubble growth. This calculation has not previously been possible.

4. The processes occurring during microlayer vaporization has been found to be of prime importance in predicting the stability of nucleation from an active site on a glass surface.

5. Only about 10% of the total heat transfer during nucleate boiling at low heat fluxes occurs via latent heat transport, with the remainder

being due to bubble induced agitation of the boundary layer. Thirty percent of this latent heat transport, i.e. 3% of the total heat transfer, is due to microlayer vaporization. The remaining 70% of the latent heat transport is due to superheated liquid surrounding the bubble. However, small as the microlayer contribution to boiling heat transfer may be, it is the controlling mechanism for nucleation. In addition, since the boundary layer agitation is caused by nucleation, growth, and departure of bubbles, it can be stated that at least under the conditions used in this investigation, microlayer vaporization processes govern boiling heat transfer.

RECOMMENDATIONS

Future investigations in the study of boiling heat transfer should be directed toward:

1. Including microlayer vaporization in a bubble growth theory.
2. Theoretically analyzing the variation of the base contact radius as a function of time and the experimental conditions.
3. Determining the contribution of microlayer vaporization to boiling heat transfer on various surfaces as a function of heat flux, pressure, and degree of bulk liquid subcooling.

REFERENCES

1. Bankoff , S.G. "The Prediction of Surface Temperatures at Incipient Boiling," Chem. Engr. Progr. Symposium Series No. 29, Vol. 55, p. 87 (1959).

2. Birkhoff, G., Margulies, R.S. and Horning, W.A. "Spherical Bubble Growth," Phys. Fluids, Vol. 1, pp. 201-204 (1958).

3. Bonnet, C., Macke, E. and Morin, R. "Visualization of the Boiling Bubbles in Water at Atmospheric Pressure and the Simultaneous Measurement of Surface Temperature Variations," EUR 1622 . f, (1964). (fr.)

4. Carnahan, B., Luther, H.A. and Wilkes, J.O. Applied Numerical Methods I and II, John Wiley and Sons, Inc., New York (1964).

5. Chang, L.P. and Snyder, N.W. "Heat Transfer in Saturated Boiling," Chem. Eng. Progr. Symposium Series No. 56, Vol. 30, pp. 25-38 (1960).

6. Clark, H.B., Strenge, P.S. and Westwater, J.W. "Active Sites for Nucleate Boiling," Chem. Eng. Progr. Symposium Series No. 29, Vol. 55, p. 103 (1959).

7. Cole, R. and Shulman, H.L. "Bubble Departure Diameters at Subatmospheric Pressures," Chem. Eng. Progr. Symposium Series No. 64, Vol. 62 (1966).

8. Cooper, M.G. and Lloyd, A.J.P. "Transient Local Heat Flux in Nucleate Boiling," Third Int. Heat Transfer Conference, Chicago (1966).

9. Corty, C. and Faust, A.S. "Surface Variables in Nucleate Boiling," Chem. Eng. Progr. Symposium Series No. 17, Vol. 51, pp. 1-12 (1956).

10. Douglas, J., Jr. "On the Numerical Integration of $\partial^2 u/\partial x^2 + \partial^2 u/\partial y^2 = \partial u/\partial t$ by Implicit Methods," J. Soc. Indust. Appl. Math., Vol. 3, pp. 42-65 (1955).

11. Douglas, J. Jr. and Rachford, H.H., Jr. "On the Numerical Solution of Heat Conduction Problems in Two and Three Space Variables," Trans. Amer. Math. Soc., Vol. 82, pp. 421-439 (1956).

12. Forster, H.K. and Zuber, N. "Growth of a Vapor Bubble in a Superheated Fluid," J. Appl. Phys., Vol. 25, pp. 474-488 (1954).

13. Fritz, W. "Maximum Volume of Vapor Bubbles," Phys. Zeits., Vol. 36, pp. 379-384 (1935).

14. Gaertner,R.F., U.S. Patent No. 3,301,314 (1967).

15. Gaertner,R.F. "Photographic Study of Nucleate Pool Boiling on a Horizontal Surface," ASME Paper No.63-WA-76 (1963).

16. Gaertner,R.F. and Westwater, J.W. "Population of Active Sites in Nucleate Boiling Heat Transfer," Chem. Eng. Progr. Symposium Series No. 30, Vol. 46, p. 39 (1960).

17. Golovin, V.S. et al "Measurement of the Rate of Growth of Vapor Bubbles During the Boiling of Different Liquids," Teplofizika Vysokikh Temperatur, Vol. 4, pp. 147-148 (1966).

18. Griffith ,P. "Bubble Growth Rates in Boiling," Trans. ASME, Vol. 80, pp. 721-727 (1958).

19. Griffith, P. and Wallis, J.D. "The Role of Surface Conditions in Nucleate Boiling," Chem. Engr. Progr. Symposium Series No. 30, Vol. 56, p. 49 (1960).

20. Han, C.H. and Griffith, P. Tech. Rept. 19, Div. of Sponsored Research, Mass. Inst. of Tech., Cambridge (1962).

21. Han, C.H. and Griffith, P. "The Mechanism of Heat Transfer in Nucleate Pool Boiling--Part I, Bubble Initiation, Growth and Departure," Int. J. of Heat and Mass Transfer, Vol. 8, pp. 887-904 (1965).

22. Han, C.H. and Griffith, P. "The Mechanism of Heat Transfer in Nucleate Pool Boiling--Part II, The Heat Flux-Temperature Difference Relation," Int. J. of Heat and Mass Transfer, Vol. 8, pp. 905-914 (1965).

23. Harmathy, T. "Velocity of Large Drops and Bubbles in Media of Infinite or Restricted Extent," Amer. Inst. Chem. Engr. J., Vol. 6, p. 281 (1961).

24. Hendricks, R.C. and Sharp, R.R. "Initiation of Cooling Due to Bubble Growth on a Heating Surface," NASA-TN-D-2290 (1964).

25. Hospeti, N.B. and Mesler, R.B. "Deposits Formed Beneath Bubbles During Nucleate Boiling of Calcium Sulphate Solutions," Chem. Eng. Progr. Symposium Series No. 64, Vol. 62, pp. 72-76 (1966).

26. Hsu, S.T. and Schmidt, F.W. "Measured Variations in Local Surface Temperatures in Pool Boiling of Water," Trans. ASME, Series C, Vol. 83, p. 254 (1961).

27. Hsu, Y.Y. and Graham, R.W. "An Analytical and Experimental Study of the Thermal Boundary Layer and Ebullition Cycle in Nucleate Boiling," NASA-TN-D-594 (1961).

28. Hsu, Y.Y. "On the Size Range of Active Nucleation Cavities on a Heating Surface," J. of Heat Transfer, Vol. 84, Series C No. 3, pp. 207-214 (1962).

29. Jakob, M. Heat Transfer, John Wiley and Sons, Inc., New York (1949).

30. Malkus, W.R. "The Heat Transport and Spectrum of Thermal Turbulence," Proc. Royal Soc., Series A255, p. 196 (1964).

31. Marcus, B.W. and Dropkin, D. "Measured Temperature Profiles Within the Superheated Boundary Layer Above a Horizontal Surface in Saturated Nucleated Pool Boiling of Water," Trans. ASME, Series C, Vol. 87, p. 333 (1965).

32. Marto, P.J. and Rohsenow, W.M. "Nucleate Boiling Instability of Alkali Metals," J. of Heat Transfer, Vol. 88, Series C, pp. 183-195 (1966).

33. Metals Handbook, 8th Edition, American Society of Metals, Novelty, Ohio (1961).

34. Moore, F.D. and Mesler, R.B. "The Measurement of Rapid Surface Temperature Fluctuations During Nucleate Boiling of Water," J. AIChE, Vol. 7, p. 620 (1961).

35. Peaceman, D.W. and Rachford, H.H., Jr. "The Numerical Solution of Parabolic and Elliptic Partial Differential Equations," J. Soc. Indust. Appl. Math., Vol. 3, pp. 28-41 (1955).

36. Peebles, F.N. and Garber, H.J. "Studies on the Motion of Gas Bubbles in Liquids," Chem. Eng. Progr., Vol. 49, p. 88 (1953).

37. Plesset, M.S. and Zwick, J.A. "The Growth of Vapor Bubbles in Superheated Liquids," J. Appl. Phys., Vol. 25, pp. 493-500 (1954).

38. Rallis, C.J. & Jawurek, H.H. "Intent Heat Transport in Saturated Nucleate Boiling," Int. J. of Heat and Mass Transfer, Vol. 7, p. 1051 (1964).

39. Roberts, G.E. and Kaufman, H. Table of Laplace Transforms, Saunders, Philadelphia (1966).

40. Rogers, T.F. and Mesler, R.B. "An Experimental Study of Surface Cooling by Bubbles During Nucleate Boiling of Water," J. AIChE, Vol. 10, p. 656 (1964).

41. Rohsenow, W.M. and Clark, J.A., "A Study of the Mechanism of Boiling Heat Transfer, Trans. ASME, Vol. 73, p. 609 (1951).

42. Semaria, R.L. "An Experimental Study of the Characteristics of Vapor Bubbles," Symposium on Two Phase Fluid Flow, IME, London (1962).

43. Schlichting, H. Boundary Layer Theory, 4th Edition, McGraw-Hill, New York 1955.

44. Scriven, L.E. "On the Dynamics of Phase Growth," Chem. Eng. Sci., Vol. 10, pp. 1-13 (1959).

45. Sharp, R.R. "The Nature of Liquid Film Evaporation During Nucleate Boiling," NASA-TN-D-1997 (1964).

46. Thomas, D.B. and Townsend, A.A. "Turbulent Convection Over a Heated Horizontal Surface," J. Fluid Mech., Vol. 2, p. 473 (1957).

47. Torikai, K., et al "Boiling Heat Transfer and Burnout Mechanism in Boiling Water Cooled Reactors," Proc. of Third Int. Conf. of the Peaceful Uses of Atomic Energy, Vol. 8, p. 146 (1964).

48. Tong, L.S. Boiling Heat Transfer and Two Phase Flow, John Wiley and Sons, Inc., New York (1965).

49. Townsend, A.A. "Temperature Fluctuations Over a Horizontal Heated Surface," J. Fluid Mech., Vol. 5, p. 209 (1959).

50. Wilkes, J.O. The Finite Difference Computation of Natural Convection in an Enclosed Rectangular Cavity, Ph.D. Thesis, The University of Michigan (1963).

51. Young, R.K. and Hummel, R.L. "Improved Nucleate Boiling Heat Transfer," Chem. Eng. Progr. Symposium Series No. 59, Vol. 61, pp. 264-270 (1965).

52. Zuber, N. "Hydrodynamic Aspects of Nucleate Pool Boiling," Report No. RW-RL-164 (1960).

53. Zuber, N. "Nucleate Boiling the Region of Isolated Bubbles and the Similarity with Natural Convection," Int. J. of Heat and Mass Transfer, Vol. 6, pp. 53-78 (1963).

APPENDIX A

Calibration of Surface Resistors

1. Resistance Measurement

The room temperature resistance of the square, vapor deposited resistors varies from 6KΩ to 11KΩ. Since all the resistors on one substrate are deposited simultaneously, all have nominally the same value and the same temperature sensitivity.

A comparison technique is used to determine the resistance of the surface elements at any temperature. A constant current is applied to a surface element and then to a standard resistor. The voltage drop across each resistor is balanced against the output of a 10 turn potentiometer which provides a variable voltage. Ohm's law requires that:

$$Re = Rs \frac{\Delta Ve}{\Delta Vs} \qquad \text{(A-1)}$$

Equation (A-1) assumes the current through both the surface element and the standard resistor is constant. The current source has an internal resistance of .9 MegΩ. The change in current between the two resistors can be related by the following equation:

$$\Delta i \simeq \Delta R/.9M\Omega \qquad \text{(A-2)}$$

The standard resistors have a resistance of 9480.Ω and 9472.Ω. If the surface element has a resistance of 11,000Ω, then $\Delta i \simeq 2000/900{,}000 = 1/450$. The constant current assumption results in a .2% error.

If the potentiometers are linear and if the input resistance of the null detector is much greater than the total potentiometer resistance, then the potentiometer settings relate the element resistance to the standard by the equation

$$Re = Rs \left(\frac{Se}{Ss}\right) \qquad \text{(A-3)}$$

The first variable voltage sources used have a total potentiometer resistance of 100KΩ; the null detector, a Tektronix 502 oscilloscope, has an input resistance to ground of 1 MegΩ. It is necessary to correct for the current drain through the oscilloscope for this resistance ratio. Equation (A-3) corrected to account for this current drain, becomes:

$$Re = Rs \left(\frac{Rn/Rv + Ss}{Rn/Rv + Se}\right) \left(\frac{Se}{Ss}\right) \qquad \text{(A-4)}$$

The ratio of the null detector resistance (Rn) to the potentiometer resistance (Rv) is 10. Since the potentiometer setting (S) varies from 0 to 1, the correction to equation (A-3) is at most 10%. The potentiometer is linear to .25% so no correction for non-linearity is needed.

Throughout the course of this investigation, equations (A-1) and (A-4) are used. The assumptions behind the use of each equation have to be realized. When this is done, the results and the accuracy are the same.

2. The Temperature Coefficient of Resistivity

Theoretically, the change in resistance with temperature can be expressed by the equation:

$$\frac{\Delta Re}{\Delta T} = Re\,\beta t \qquad \text{(A-5)}$$

This equation can be rearranged to obtain:

$$Re = Re_o\,[1 + \beta t\,(Te - Te_o)] \qquad \text{(A-6)}$$

Equation (A-5) can also be integrated exactly, which results in the following expression:

$$Re = Re_o\,\exp[\beta t\,(Te - Te_o)] \qquad \text{(A-7)}$$

If the exponential factor in equation (A-7) is expanded into an infinite series, the neglect of every term after the first order term simplifies the expression to equation (A-6). Both equations (A-6) and (A-7) have been used to correlate the resistance of the elements as a function of temperature. In every surface resistor the value of βt is very close to $8.6 \times 10^{-4} (C°)^{-1}$. With this value of βt, the deviation from linearity of equation (A-7) between 30 and 100°C is almost undetectable. Equation (A-6) is used to correlate the total element resistance as a function of temperature.

The standardization process involves determining the resistance of the surface elements at various temperatures with the surface covered with liquid and with it dry. Figures (36) and (37) show the calibration of two of the resistors on surface #14. When the liquid is toluene, no difference between the wet and dry resistance determinations can be noted. Ethyl alcohol does show a lower resistance of the elements at every temperature. This is explained by the electrical conductivity of the liquid. Since the surface resistors are insulated from the fluid by silicon monoxide, any current leakage through the parallel liquid circuit must exist at the lead wires. All but the ends of the lead wires, i.e. the region where the leads are soldered to the surface, are covered with teflon tubing. Since the magnitude of the current drain is a function of the liquid temperature, the correction for current flow is corrected using the resistance of the liquid at the bulk liquid temperature. By rearranging the parallel resistance formula, the liquid resistance at Tb is:

$$R_1 \text{ (Tb)} = \frac{\text{Re (Tb) Rw (Tb)}}{\text{Re (Tb)} - \text{Rw (Tb)}} \qquad \text{(A-8)}$$

The temperature of the surface during boiling is desired. The resistance observed is Rw (T), where T is not known. The resistance of the surface

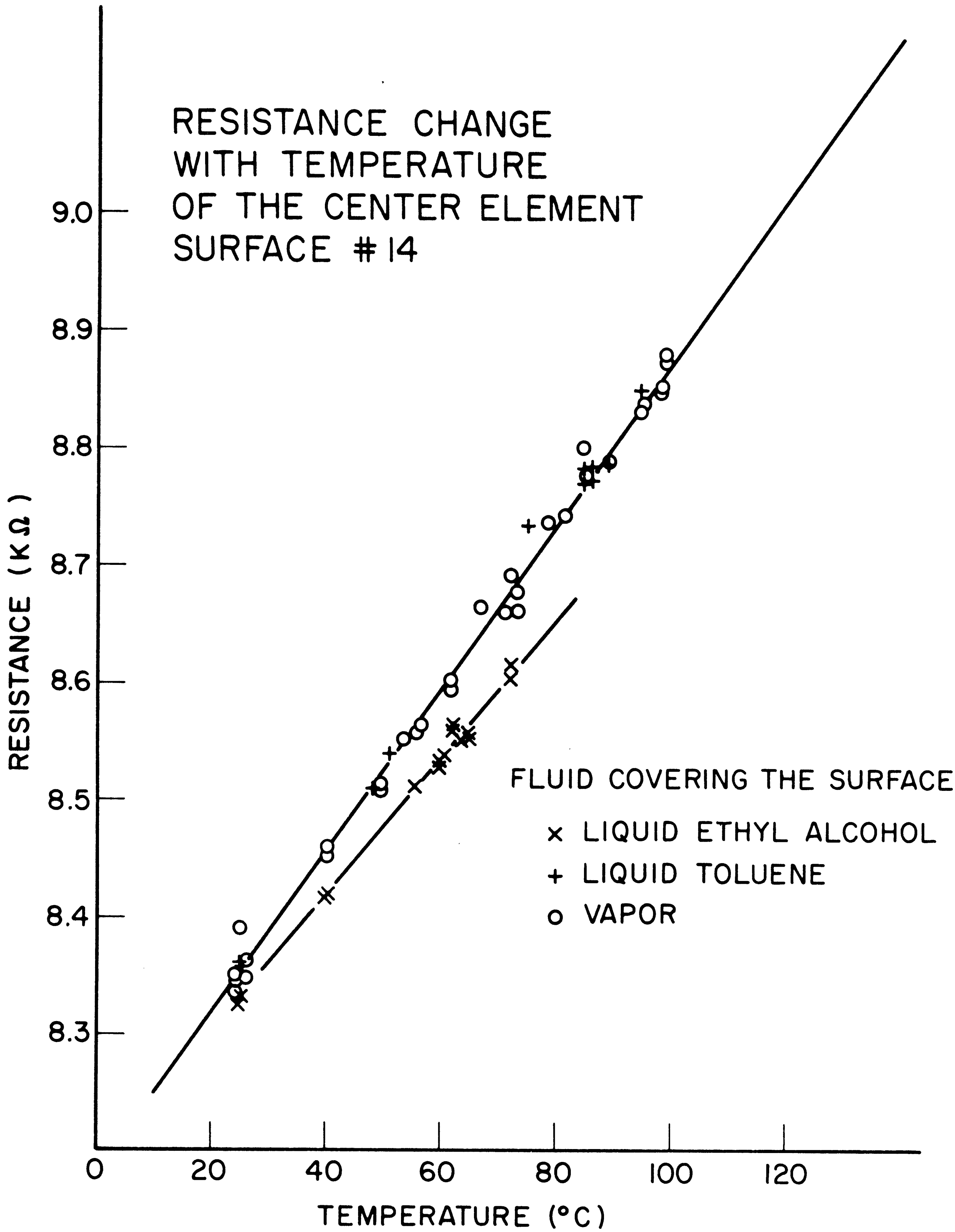

Figure 37 Calibration of Center Surface Resistor on Heater #14

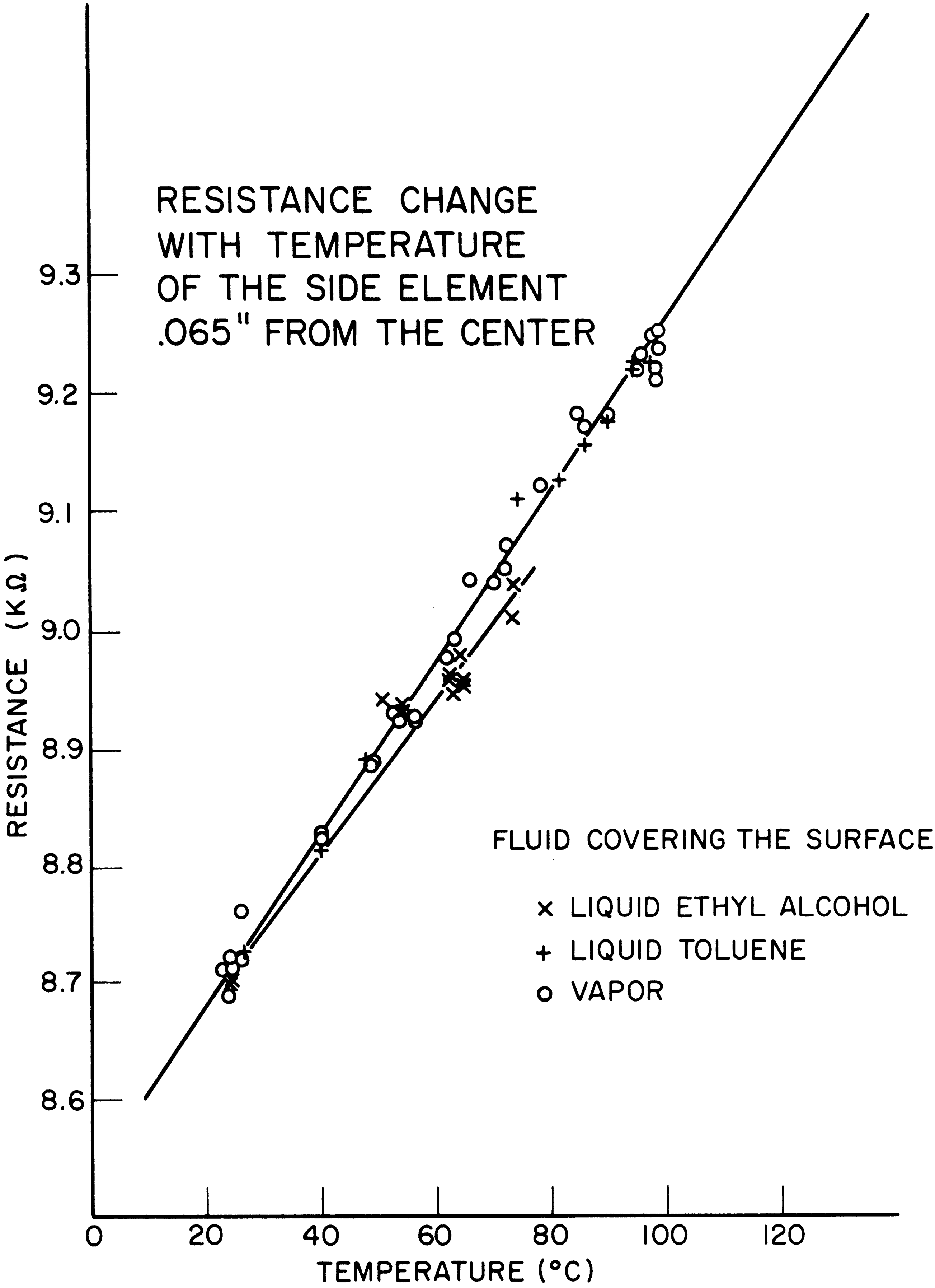

Figure 38 Calibration of Side Resistor (.165 cm away from center) on Heater #14

element, which takes into account liquid conductivity is:

$$Re(T) = \frac{Rw\ (T)}{1 - \frac{Rw(T)}{Rw(Tb)} \quad \frac{Re(Tb) - Rw(Tb)}{Rw(Tb)}} \qquad \text{(A-9)}$$

Since Rw (T) is quite close to Rw (Tb), this equation simplifies to:

$$Re(T) = \frac{Rw\ (T)}{1 - \frac{Re(Tb) - Rw(Tb)}{Re(Tb)}} \qquad \text{(A-10)}$$

Equation (A-10) is used to obtain T from a known resistance of the surface element and the fluid acting together.

APPENDIX B

Conversion of Voltage Levels Displayed on the Oscilloscope Screen to Temperatures

Figure (40) shows a typical photograph of the oscilloscope screen during boiling. The center resistor is always displayed on the top channel and one of the other temperature sensors is displayed on the bottom channel. The balance point, on the top channel between the voltage across the resistor and the voltage bucking it, is the top subdivided horizontal grid line. The bottom subdivided grid line is the balance point between the other surface resistor and its bucking voltage. The vertical oscilloscope amplification on each channel is one centimeter of deflection for each millivolt of imbalance. The oscilloscope sweep rate across the screen is 1 cm/5 msec.

The conversion of the null point to a reference temperature closely follows the standardization procedure described in Appendix A. The null voltage is converted to a resistance which is not corrected for any effects of liquid conduction. Before and after each run, the voltage drop across the element at the liquid bulk temperature is also recorded. This reading is also not corrected for liquid conduction. The temperature difference (T_w-T_b) at the null point is determined from the slope of the resistance calibration curves, i.e.:

$$(T_w - T_b)_{null} = \frac{(Rnull - Rb)}{(\beta t \; Rnull)} \qquad (B\text{-}1)$$

The temperature difference (T_n-T_{sat}) is obtained from knowledge of the difference between the liquid bulk temperature and the saturation temperature.

Any imbalance away from the null point, measured on the oscilloscope as a voltage, can be related to a temperature by the temperature coefficient of resistivity through the following equation

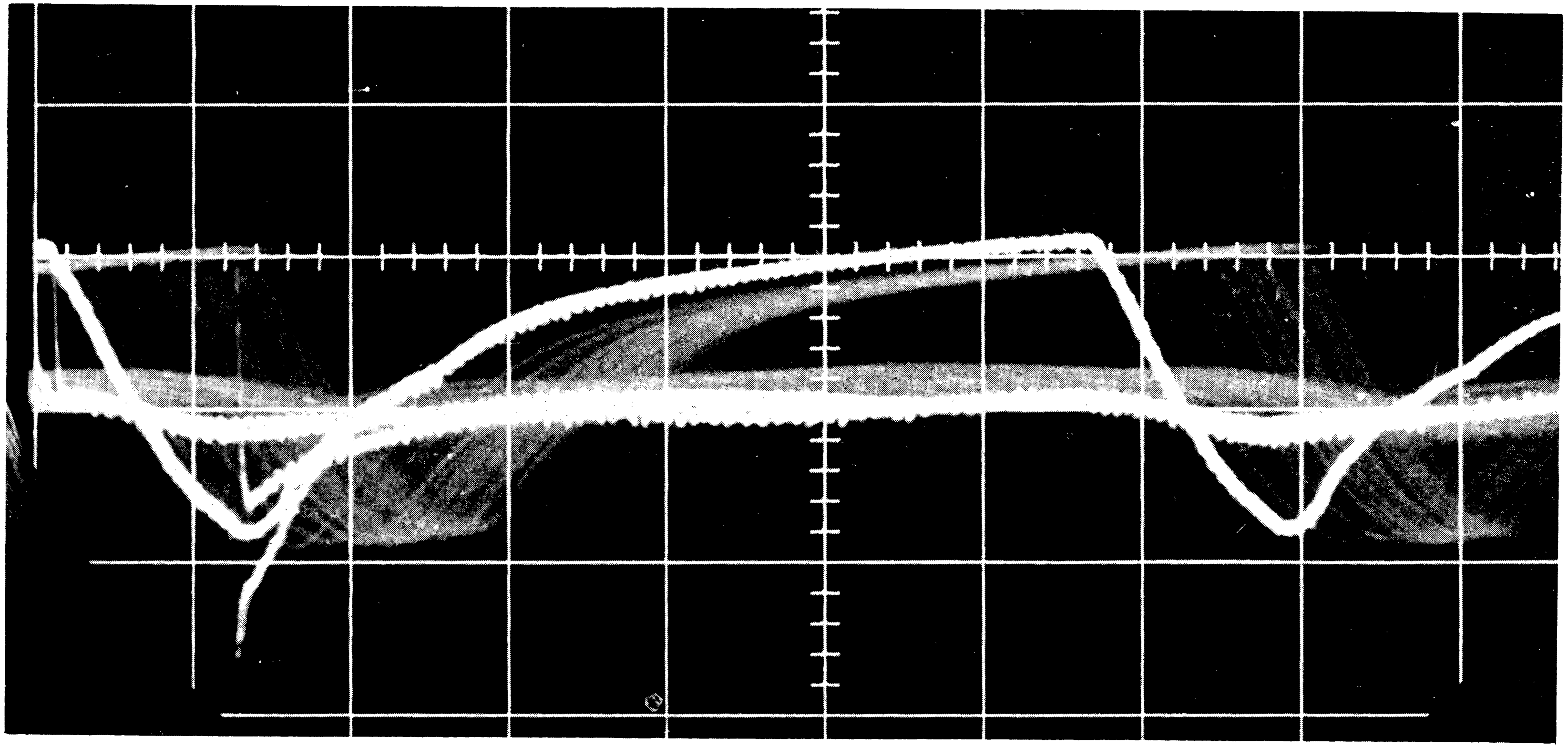

Figure 39 Photograph of an Oscilloscope Temperature Trace for Ethyl Alcohol

$$\frac{\Delta T}{\Delta V} = \frac{\Delta T}{ie\Delta R} = \frac{1}{ie\,(\beta t)\ Rnull} \qquad \text{(B-2)}$$

In this equation ie is determined from the measured voltage drop across the standard resistor. If the units on $\Delta T/\Delta V$ are °C/mV, the temperature level is linearly related to the deflection.

In picture #3, heater #14, run #7, the voltage setting at the null point is 82.60 mV. The voltage drop across the standard 9480.Ω resistor is 86.06 mV. This means the null resistance by equation (A-1) is 9110.6 Ω. The resistance of the central resistor at a bulk liquid temperature 73°C, based on figure (36), is 9020 Ω. From the slope of the temperature-resistance curve shown in figure (36); βtR_1 = 7Ω/°C. The null temperature is 12.8°C above the bulk liquid temperature. Therefore $(T_w - T_{sat})$ = 13.8°C for this picture. Based on a current flow through the standard resistor of 9.02μA, the value of $\Delta T/\Delta V$ in equation (B-2) is 15.9°C/mV. Thus 1 cm of deflection on the oscilloscope corresponds to a change in temperature of 15.9°C.

In heater #9, the same analysis gives a sensitivity of 11°C/mV. In this case the room temperature resistance of the element is 3KΩ higher. This gives rise to the greater sensitivity.

APPENDIX C

Heat Loss Calculations

The single site heater has been designed to minimize radial heat flow. Heat conduction down the lead wires cannot be eliminated. This loss is determined by applying power to the heater with only the base submerged in liquid and the wires from the surface resistors disconnected. Natural convection from the top surface is minimized by lowering the pressure in the chamber to the vapor pressure of the liquid. Essentially all the heat is lost down the lead wires.

Except for heater #9, a thermocouple has been placed in the copper core of the heater. The difference in temperature between the copper core and the liquid could be used to correlate heat losses. The temperature of the platinum wire, indicated by its resistance could be used. Which temperature difference is the correct one to use?

A Leeds and Northrup Portable Wheatstone Bridge gives a resistance of 4.13Ω at 30°C for heater #14. Figure (38) is a theoretical plot of the platinum resistance as a function of temperature for this heater. The equation for the curve, which the Metals Handbook (33) gives, is

$$Re = Ro\,(1 + .0039788\ Te - 5.88 \times 10^{-7}\ Te^2). \qquad \text{(C-1)}$$

In this equation Te is in °C and Ro is the resistance of the element at 0°C. Figure (39) summarizes a heat loss experiment by plotting both ($T_{cu} - T_b$) and ($Te - T_b$) on the abscissa. The ordinate is the amount of heat dissipated.

This figure shows the two temperature differences are not equivalent. Above a ΔTe of 100°C the copper rivet is lower in temperature. This indicates the beginning of convective losses within the heater. This gives rise to heat flow in the rivet and thus the difference

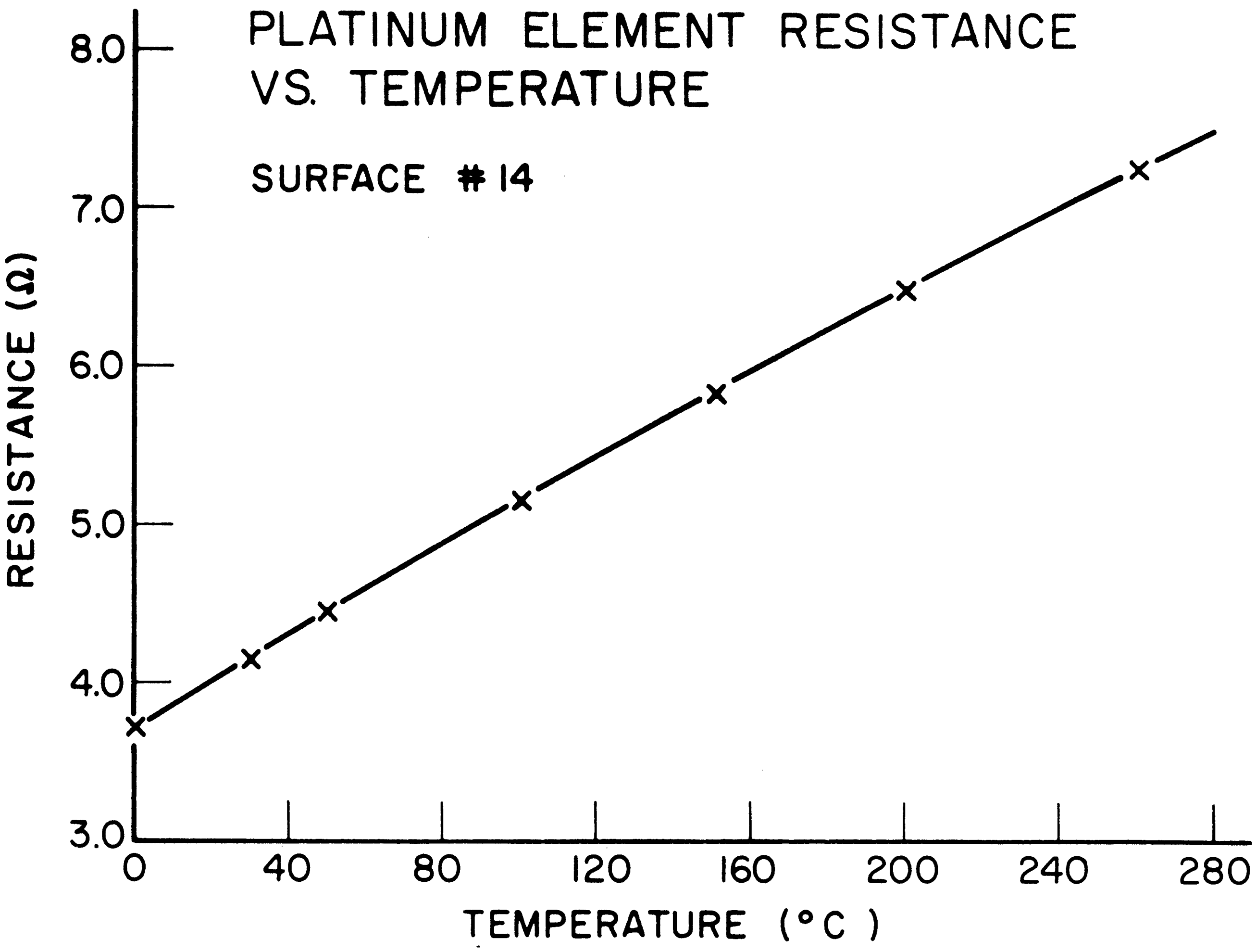

Figure 40 Change in the Resistance of Platinum Wire vs. Temperature

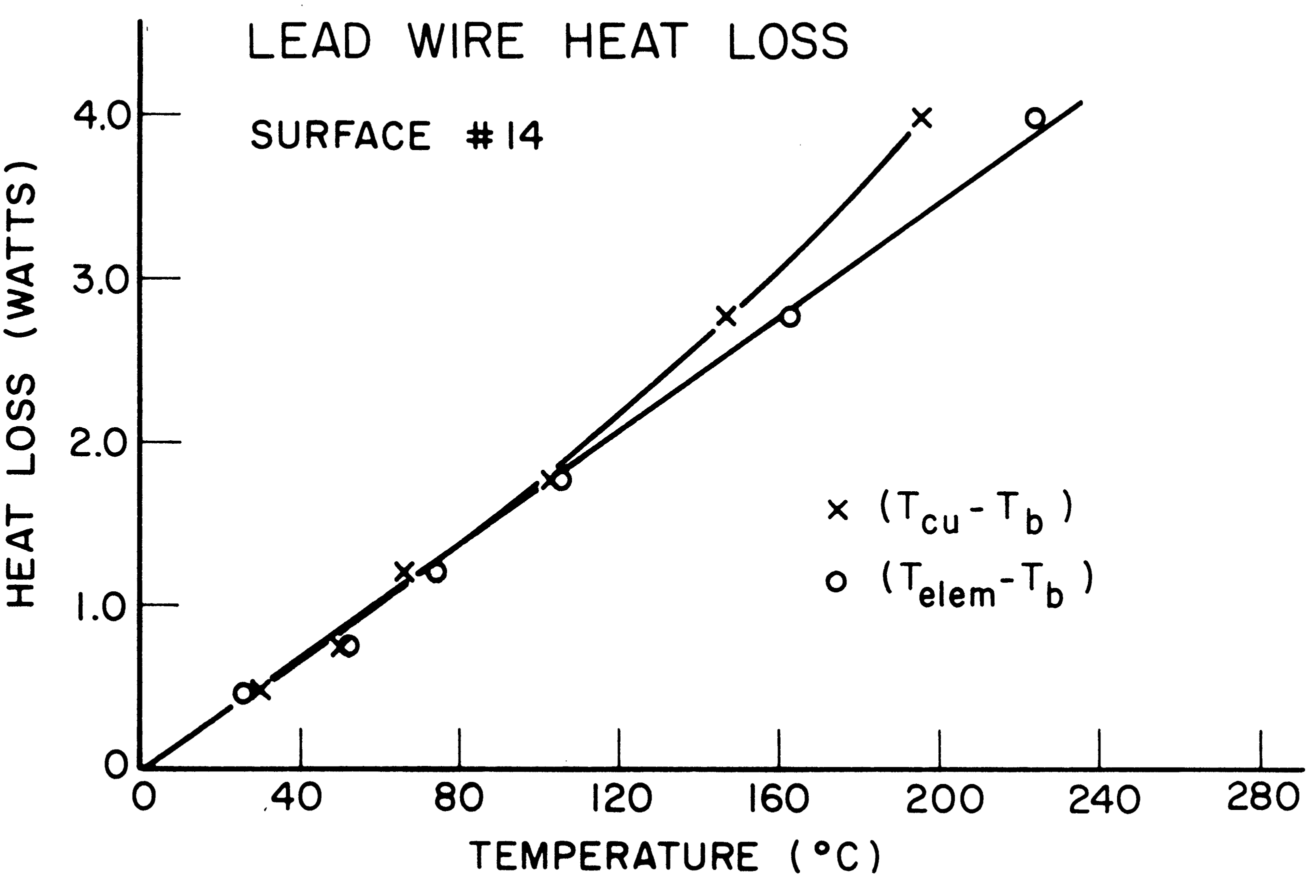

Figure 41 Calibration of Heater #14 for Lead Wire Heat Loss

in temperature between the wire and the copper core. When a fluid is being boiled on the surface this difference would be greater. Heat flow down the lead wires is not affected by any upward flow of heat. For these reasons the platinum element resistance is used to determine lead wire losses.

Table (C-I) is a summary of all the heat loss calculations. The notation appearing in this table refers to the series of pictures taken at a particular power setting. As an example, take the last entry in the table. In pictures #27 through 36 in run #9 on heater #14, the average heat flux through the surface is 1.23 cal/cm^2-sec.

Since the thermal resistance of the glass and the glue which binds the copper to the glass is constant, there is a check on the assumptions used to obtain Table (C-I).

A measure of the thermal resistance is:

$$\frac{\Delta x}{k_s} = \frac{\Delta T}{q} = \frac{123}{1.23} = 100 \qquad \text{(C-2)}$$

In other pictures, the resistance is between 111 and 86. Since the actual average surface temperature is not known, this calculation shows the uncertainty in the heat flux calculation. Of the three materials used, Conductalute * was the most successful. Unfortunately it was also quite difficult to use. Heater #9 used Conductalute* and it can be seen from Table C-1 that it gave a lower resistance of the glass and glue by a factor of almost four. Mercury worked extremely well for a while until it had all transferred to cooler areas leaving a gap between the heater and the glass plate.

---

*Sauereisen Tradename.

TABLE C-I

The Determination of the Average Boiling Heat Flux Transferred through the Glass Plate

Notation	Amps	Volts	Power Watts	Tcu °C	Power Less Watts	Power Up Watts	Flux cal/cm^2-sec
9-1-1 to 9-3-30	1.31	3.06	4.00	146*	.96	3.04	1.17
14-3-0 to 14-3-36	.89	6.90	6.15	233	3.55	2.60	1.00
14-4-0 to 14-4-20	.895	6.55	5.52	240	3.28	2.24	.82
14-4-21 to 14-4-39	.818	6.30	5.15	233	3.18	1.98	.77
14-5-1 to 14-5-14	.808	6.00	4.85	201.2	3.02	1.83	.71
14-5-15 to 14-5-30	.795	5.95	4.73	212.2	3.07	1.66	.64
14-6-4 to 14-6-12	.84	6.6	5.55	243.5	3.30	2.25	.87
14-6-13 to 14-6-20	.84	6.6	5.55	239.5	3.32	2.23	.86
14-6-21	.82	6.14	5.03	221.8	3.04	1.99	.77
14-6-22 to 14-6-35	.82	6.19	5.06	227.5	3.17	1.95	.75
14-7-1 to 14-7-26	.92	6.90	6.40	223.0	3.48	2.92	1.13
14-7-26 to 14-7-34	.94	7.31	6.90	227.8	4.03	2.87	1.11
14-8-1 to 14-8-10	.96	7.51	7.23	228.8	3.84	3.39	1.31
14-8-11 to 14-8-17	1.01	8.31	8.40	247.5	4.65	3.75	1.45
14-8-27 to 14-8-36	.93	7.11	6.60	220.0	3.71	2.89	1.11
14-9-1 to 14-9-10	.93	7.05	6.60	222.8	3.56	3.04	1.17
14-9-11 to 14-9-26	.98	7.76	7.65	232.5	3.78	2.83	1.09
14-9-27 to 14-9-36	.94	7.11	6.68	220.8	3.52	3.16	1.23

*Heater element temperature

APPENDIX D

The Solution of the Heat Conduction Equation in Cylindrical Coordinates by Finite Difference Techniques

1. Basic Equations

The heat conduction equation in cylindrical coordinates is:

$$\frac{\partial T}{\partial t} = \alpha_s \left(\frac{\partial^2 T}{\partial R^2} + \frac{1}{R}\frac{\partial T}{\partial R} + \frac{\partial^2 T}{\partial Z^2} \right) . \qquad \text{(D-1)}$$

The finite difference expression for the distance derivatives can be obtained by the use of Taylor series expansions for $T(x+\Delta x)$ and $T(x-\Delta x)$ based on the temperature and the derivatives at $T(x)$. The Taylor series expansion for $T(x+\Delta x)$ is:

$$T(x+\Delta x) = T(x) + \Delta x \left(\frac{\partial T}{\partial x}\right)_x + \frac{\Delta x^2}{2}\left(\frac{\partial^2 T}{\partial x^2}\right)_x + 0(\Delta x^3). \qquad \text{(D-2)}$$

For $T(x-\Delta x)$ the expansion is:

$$T(x-\Delta x) = T(x) - \Delta x \left(\frac{\partial T}{\partial x}\right)_x + \frac{\Delta x^2}{2}\left(\frac{\partial^2 T}{\partial x^2}\right)_x + 0(\Delta x^3). \qquad \text{(D-3)}$$

The addition of equations (D-2) and (D-3) results in an finite difference expression for $(\partial^2 T/\partial x^2)_x$:

$$\left(\frac{\partial^2 T}{\partial x^2}\right)_x = \frac{T(x+\Delta x) - 2T(x) + T(x-\Delta x)}{\Delta x^2} . \qquad \text{(D-4)}$$

The substraction of equation (D-3) from (D-2) gives an equation which can be solved for $(\partial T/\partial x)_x$:

$$\frac{\partial T}{\partial x} = \frac{T(x+\Delta x) - T(x-\Delta x)}{2\Delta x} . \qquad \text{(D-5)}$$

These equations are used to approximate both the derivatives in the R and Z direction shown in equation (D-1). The time derivative has been approximated as a forward difference, i.e.:

$$\frac{\partial T}{\partial t} = \frac{T(t+\Delta t) - T(t)}{\Delta t} \quad . \qquad \text{(D-6)}$$

It is quite easy to substitute equations (D-4), (D-5) and (D-6) into equation (D-1). There are, however, many techniques for solving the finite difference equivalent of equation (D-1). The solution techniques can be divided into implicit and explicit methods. The explicit methods solve the heat conduction equation at one point and then move to the next. With implicit methods, the temperature at a whole row of points is obtained at the same time. This temperature field solves the heat conduction equation exactly at each point in the row. An implicit method, called the implicit alternating direction (I.A.D.) method, has been used to solve the heat conduction equation with two distance coordinates. A method, which is a simplification of the I.A.D. method, is used for the one distance coordinate equation.

2. The Implicit Alternating Direction Method

The I.A.D. method has been discussed by Peaceman and Rachford (35), Douglas (10), Douglas and Rachford (11), and Wilkes (50). This method divides the time step between T(t) and T(t+Δt) into two half steps. An array T*(r,z) is an intermediate solution at the half time step between T(t+Δt) and T(t). At the half time step, the derivatives of either R or Z are evaluated based on the old temperature field. The coefficients of the difference derivatives in the other direction then form an array. When this array is solved for the whole perpendicular row of points, the temperature T* at these points is the new solution. After successive rows have been solved, the T* field is complete. The procedure switches to the other coordinate direction to obtain T(t+Δt) from T*.

The mathematical model divides the Z coordinate direction into N + 1 grid points from 0 to N; "J" is the general point. The R direction is divided into L + 1 points from 0 to L; "I" is defined as a general point in the R direction. At the point (I,J), the difference approximation to equation (-1) is:

$$\frac{T^*(I,J) - T(I,J)}{\Delta t/2} = \frac{\alpha_s}{\Delta R^2}\left\{\left[\left(1 + \frac{1}{2I}\right) T(I+1,J) - 2T(I,J) + T(I-1,J)\left(1 - \frac{1}{2I}\right)\right]\right.$$

$$\left. + \left(\frac{\Delta R}{\Delta Z}\right)^2 \left[T^*(I,J-1) - 2T^*(I,J) + T^*(I,J+1)\right]\right\}. \qquad \text{(D-7)}$$

As the starred quantities indicate, the derivatives in the R direction are specified but the Z derivatives will be based on the new T* temperature field at (t+Δt/2). When the unknown temperatures, the T*'s, are taken to the left hand side of the equation, and the known temperature, the T's placed on the right, an equation containing the three unknowns. T*(J-1,I) T*(J,I), and T*(J+1,I) is obtained. It can be written as:

$$AC(J)T^*(J-1,I) + (BC(J)+1)T^*(J,I) + CC(J)T^*(J+1,I) = DC(J), \qquad \text{(D-8)}$$

where $Cr = \alpha_s \Delta T/2\Delta R^2$ and $Cz = \left(\Delta R/\Delta Z\right)^2 C_r$

$$DC(J) = - AR(I)T(I-1,J) + [1-BR(I)]T(I,J) - CR(I)T(I+1,J), \qquad \text{(D-9)}$$

the coefficients are defined as: AC(J) = - Cz, BC(J) = 2Cz, CC(J) = - Cz, AR(I) =-(1-1/2I) Cr, BR(I) = 2Cr, and CR(I) =-(1+1/2I)Cr. The same procedure at all the points between 0 and N produces a set of N - 1 equations and N + 1 unknowns. The inclusion of the boundary conditions at the end points provides the two additional equations. The array can be expressed in the following form after the boundary conditions are included.

$$\begin{bmatrix} [B(0)+1] & C(0) & 0 & \cdots & \cdots & \cdots \\ A(1) & [B(1)+1] & C(1) & \cdots & \cdots & \cdots \\ \cdots & \cdots & \cdots & \cdots & \cdots & \cdots \\ \cdots & 0 & A(J) & [1+B(J)] & C(J) & 0 \\ \cdots & \cdots & \cdots & \cdots & \cdots & \cdots \\ \cdots & \cdots & \cdots & \cdots & \cdots & \cdots \\ \cdots & \cdots & 0 & A(N-1) & [1+B(N-1)] & C(N-1) \\ \cdots & \cdots & \cdots & \cdots & \cdots & \cdots \\ \cdots & \cdots & \cdots & 0 & A(N) & [1+B(N)] \end{bmatrix} \begin{bmatrix} T^*(I,0) \\ \cdots \\ \cdots \\ T^*(I,J) \\ \cdots \\ \cdots \\ \cdots \\ \cdots \\ T^*(I,N) \end{bmatrix} = \begin{bmatrix} D(0) \\ \cdots \\ \cdots \\ D(J) \\ \cdots \\ \cdots \\ \cdots \\ \cdots \\ D(N) \end{bmatrix} \tag{D-10}$$

The coefficient matrix is called tri-diagonal and can be solved by an elimination procedure described in section 5 of this Appendix. The process is similar for the second time step except this time the T* array is known and the T array at the $t+\Delta t$ is obtained by going across rows of constant J. The general equation is:

$$AR(I)T(I-1,J) + [1+BR(I)]T(I,J) + CR(I)T(I+1J] = DR(I), \tag{D-11}$$

where

$$DR(I) = -AC(J)T^*(I,J-1) + [1-BC(J)]T^*(I,J) - CC(J)T^*(I,J+1). \tag{D-12}$$

The definitions of the coefficients of both the T's and T*'s is the same as shown in equation (D-8). Once again the conditions at 0 and L provide the necessary number of equations to solve for the temperature along each successive row.

3. Boundary Conditions

a. Constant temperature: reduce the order of the matrix one unit
b. Constant heat flux or heat transfer coefficient

$$\left(\frac{\partial^2 T}{\partial x^2}\right)_o = 2\left[\frac{T(I,1) - T(I,0)}{\Delta x^2}\right] - \frac{2}{\Delta x}\left(\frac{\partial T}{\partial x}\right)_o \tag{D-13}$$

The heat flux specifies the gradient. The BC(0) coefficient remains the same. However CC(0) becomes $-2Cz$ and DC(0) becomes:

$$DC(0) = -T(I-1,0)AR(I) + [1-BR(I)]T(I,0) - CR(I)T(I+1,0) + 2Cz(q/k)\Delta Z \,. \quad \text{(D-14)}$$

The condition of a constant heat flux transfer coefficient adjusts BC(0) by inclusion of an additional term:

$$BC(0) = 2Cz(1-h\Delta Z/k). \quad \text{(D-15)}$$

If the heat transfer coefficient cannot be expressed as:

$$\left(\frac{\partial T}{\partial Z}\right)_o = \frac{h}{k}\,T(I,0) \quad \text{(D-16)}$$

Then an additional term is also added to the other side, in the D(0) term. This defines all the boundary conditions except for R=0 in cylindrical coordinates. As the R approaches 0 the $1/R(\partial T/\partial R)$ term is evaluated by L'Hospital's rule to obtain:

$$\frac{\partial^2 T}{\partial R^2} + \frac{1}{R}\frac{\partial T}{\partial R} = 2\,\frac{\partial^2 T}{\partial R^2} \quad \text{(D-17)}$$

The condition that $\partial T/\partial R = 0$ is a simplification of the constant flux case where Q = 0. At the center BR (0) = 4Cr = - CR(0).

4. Solution of the One Dimensional Equation

The one dimensional problem uses all the methods which are used to approximate the boundary conditions at the end points. The use of a T* matrix is unnecessary. The D(J) array becomes equal to the last temperature at T(J) for a general point.

5. Solution of the Tri-Diagonal Matrix

The matrix shown in equation (D-10) can be solved by the following scheme.

$$\beta_o = 1 + BC(0) \tag{D-18}$$

$$\gamma_o = DC(0)/(1+BC(0) \tag{D-19}$$

At intermediate points advancing up the column successively

$$\beta_J = AC(J)\ CC(J)/\beta_{J-1} + 1 + BC(J) \tag{D-20}$$

and

$$\gamma_J = [DC(J) - AC(J)\gamma_{J-1}]/\beta_J\ . \tag{D-21}$$

At the last point N

$$T^*(I,N) = \gamma_N \tag{D-22}$$

Then going successively from N down to 0

$$T^*(I,J) = \gamma_J - CC(J)T(N,J+1)/\beta_J. \tag{D-23}$$

The solution for T*(I,J) is then complete.

APPENDIX E

Computer Program for Determining the Amount of Liquid Evaporated from Temperature Traces

```
          THE ANALYSIS OF THE EXPERIMENTAL TEMPERATURE FLUCTUATIONS
          DURING BOILING

          THE LIQUID BASED CONTRIBUTION, CALCULATED BY INTEGRATING
          THE SURFACE TEMPERATURE FLUCTUATIONS, IS CALLED LDELT
          THE SOLID BASED CONTRIBUTICN,CALCJTATED FROM THE TEMPER-
          URE GRADIENT IN THE SOLID, IS CALLED EDELT
          FAC IS A SCALING FACTOR WHICH DETERMINES HOW MUCH OF THE
          SOLID IS ALLOWED TO CHANGE, FAC=1 CALCULATES THE CHANGE
          IN TEMPERATURE DOWN TO A DEPTH OF 2* NUC TEMP. THIS IS THE
          TEMPERATURE AT N=0.
          A IS A VARIABLE WHICH SPECIFIES HOW MUCH OF THE SOLID
          FROM C TO N IS INCLUDED IN THE TEMPERATURE SOLUTION

          P IS THE NUMBER CF POINTS CF THE TEMPERATURE TIME CURVE
          THEY MUST BE AT EQUAL INCREMENTS APART
          RATIO IS THE VARIABLE SPECIFYING THE NUMBER CF POINTS
          BETWEEN THE GIVEN POINTS TO BE SPECIFIED BY LINEAR
          INTERPOLATION
          S  IS THE TOTAL NUMBER CF TEMPERATURE POINTS USED, THIS
          DOES NOT INCLUDE THE FIRST POINT AT ZERO TIME
          EVAPTM IS THE TIME INTEVRAL BETWEEN NUCLEATION AND THE
          OCURRENCE OF THE MINIMUM TEMPERATURE

          THE TEMPERATURE GRADIENT IN THE SOLID,MEASURED BY THE FLUX
          Q,IS ITERATED UNTIL THE TEMPERATURE OF THE SURFACE
          IS LESS THAN MIN AWAY FROM TEMPF AT TOTALT
          BETWEEN EVAPTM AND TOTALT (TIME) THE SURFACE IS INSULATED

         FTRAP.
         REFERENCES ON
         PROGRAN COMMON AC,BC,CC,DDC,T,X,L,M,N
         DIMENSION T(6000),X(200),AC(80),BC(80),CC(80),DDC(80)
         INTEGER X,L,M,N
         DIMENSION TIME(200),IF(200),FLUX(200),B(10),Y(200)
         INTEGER P,S,RATIO,TAU,I,J,K,INC,INCMX,MAX,INCR,INCRM,INCRMX,
       1 FL,A,INCRL
         INTEGER HEATN,ROLLN,DATAPT,SPECD,FLUID(2)
         FORMAT VARIABLE FL
         VECTOR VALUES HEADTN=$1H ,H* THE TEMPERATURE DISTRIBUTION IS**$
         VECTOR VALUES HEADD=$1H ,H* THE FLUX THROUGH THE SURFACE IS**$
         VECTOR VALUES HEADT=$1H ,H* AT THESE TIMES**$
         VECTOR VALUES HEAD1=$S3,I2,S7,I2,I2,I3,I2,S6,3C6*$
         VECTOR VALUES HEAD2=$S3,I2,S7,I2,I2,I3,I2,S6,3C6,2F12.8*$
         VECTOR VALUES HEADM=$1H+,S36,H* DATA POINT NUMBER*S3,I2,I2,I3,I2*$
         VECTOR VALUES HEADN=$1H1,H*BOILING OF *3C6*$
         VECTOR VALUES SIPUNH=$S1,I2,(5E15.7)*$
         VECTOR VALUES HEAD=$1H2*$
         VECTOR VALUES SPRT=$1H ,S5,'FL'F10.6*$
         BOOLEAN POLY,CHECK
         SCALE=1000.
         POLY=0B
         CHECK=0B
         A=1
         FAC=1.
         IF(0)=0.
         X=2
         TSAT=0.
         TLIQ=1.
 TART    READ FCRMAT HEAD1,P,HEATN,ROLLN,DATAPT,SPECD,FLUID(0)...FLUID(2)
         READ AND PRINT DATA
         INC=0
         S=RATIO*(P-1)
         DT=EVAPTM/S
 IL      THROUGH CAL,FOR K=S,1,DT*K.G.TOTALT
         L=K
         THROUGH SET, FOR K=1,1,K.G.200
         X(K)=(L+1)*K+2
 SET     IF(K)=IF(K-1)+1.
         FL=INCRMX+1
         ZERO.(T(0)...T(6000),FLUX(0)...FLUX(200))
         WHENEVER POLY

            FILL IN TEMP BY LINEAR REGRESSION COEFFICIENTS

         READ  FORMAT SIPUNH,MAX,B(0)...B(MAX)
         TSURF=B
         THROUGH SETP, FOR K=0,1,K.G.S
         T(X(N)+K)=B
         THROUGH SETP, FOR J=1,1,J.G.MAX
 SETP    T(X(N)+K)=T(X(N)+K)+B(J)*(IF(K)*DT*SCALE).P.J
         OTHERWISE

            FILL IN TEMP BY LINEAR INTERPOLATION

         T(X(N))=Y(1)
         TSURF=Y(1)
         THROUGH SETT, FOR K=1,1,K.E.P
         T(X(N)+RATIO*K)=Y(K+1)
         THROUGH SETT, FOR J=1,1,J.E.RATIO
 SETT    T(X(N)+RATIO*K-J)=Y(K+1)-(Y(K+1)-Y(K))*IF(J)/IF(RATIO)
         END OF CONDITIONAL

          SPECIFICATION TO THE INITIAL TEMPERATURE GRADIENT IN THE
          SOLID

         DX=1./IF(N)
         THROUGH SETA, FOR I=0,1,I.G.N
 SETA    T(X(N-I))=TSURF*(1.+IF(I)*DX*FAC)
         THROUGH SETC, FOR K=1,1,K.G.L
 SETC    T(X(A-1)+K)=T(X(A-1))

 LOOP    FB=DT/DX/DX/KS/ROS/CPS*(Q/TSURF/FAC).P.2
         TAU=0
         INC=INC+1
         FLUX=Q
```

```
             CALCULATION OF THE MATRIX COEFICIENTS FOR THE TRI-DIAGIONAL
             MATRIX SOLUTION

            THROUGH SET1, FOR I=1,1,I.E.N
            AC(I)=-FB
            BC(I)=2.*FB
SET1        CC(I)=-FB
            AC(N)=-2.*FB
            BC(N)=2.*FB
            CC(N)=0.

             CALCULATION OF THE TEMPERATURE GRADIENTS IN THE SOLID FOR
             THE NEXT TIME INTERVAL BASED ON THE SPECIFIED SURFACE
             TEMPERATURE AT THAT TIME

CYCLE       TAU=TAU+1
            TIME(TAU)=DT*IF(TAU)
            WHENEVER TAU.G.S
            M=N
            OTHERWISE
            M=N-1
            END OF CONDITIONAL
            THROUGH SET2, FOR I=A,1,I.G.M
SET2        DDC(I)=T(X(I)+TAU-1)
            DDC(A)=DDC(A)-AC(A)*T(X(A-1)+TAU)
            DDC(M)=DDC(M)-CC(M)*T(X(M+1)+TAU)
            COLS.(A,M,X+TAU,T)

              CALCULATION OF THE RATE OF HEAT TRANSFER FOR THE TIME
             INTERVAL DT

            WHENEVER TAU.G.S
            FLUX(TAU)=0.
            OTHERWISE
            FLUX(TAU)=FLUX*(T(X(N-1)+TAU)-T(X(N)+TAU))/T(X(N))/FAC/DX
            END OF CONDITIONAL
            WHENEVER TAU.L.L,TRANSFER TO CYCLE

              CALCULATION OF THE TOTAL AMOUNT OF HEAT TRANSFERED FROM
             THE SOLID DURING A TEMPERATURE FLUCTUATION

            TFLUX=0.
            THROUGH FIN, FOR K=0,1,K.G.TAU
FIN         TFLUX=TFLUX+FLUX(K) *DT
            EDELT=TFLUX         /LL/ROL
            PRINT RESULTS INC,Q,TFLUX,EDELT,T(X(N)+TAU),TEMPF
            WHENEVER INC.G.1
            CONTINUE
            OTHERWISE
            WHENEVER T(X(N)+TAU).G.TEMPF
            F1=1.
            OTHERWISE
            F1=-1.
            F=-F
            END OF CONDITIONAL
            END OF CONDITIONAL
            WHENEVER INC.G.INCMX, TRANSFER TO OUT
            WHENEVER .ABS.(T(X(N)+L)-TEMPF).G.MIN
            WHENEVER (T(X(N)+TAU)-TEMPF)*F1.G.0.
            Q=Q-F
            OTHERWISE
            TRANSFER TO LOOP
            OTHERWISE
            TRANSFER TO OUT
            END OF CONDITIONAL
OUT         PRINT FORMAT HEADN,FLUID(0)...FLUID(2)
            PRINT FORMAT HEADM,HEATN,ROLLN,DATAPT,SPECD
            PRINT RESULTS INC,Q,TFLUX,EDELT,T(X(N)+TAU),TEMPF

             CALCULATION OF LDELT

            INTGRT=0.
            THROUGH CALT, FOR J=0,1,J.G.S
CALT        INTGRT=INTGRT+T(X(N)+J)*DT
            LDELT=SQRT.(2.*KL*INTGRT/ROL/LL)
            PRINT RESULTS EDELT,LDELT
            INCRL=0
            INCRM=INCRMX
            THROUGH SET3, FOR K=0,1,K.G.TAU
            WHENEVER K.E.TAU,INCRM=K
            WHENEVER K.E.INCRM
            PRINT FORMAT HEADT
            PRINT FORMAT SPRT,TIME(INCRL)...TIME(K)
            PRINT FORMAT HEADD
            PRINT FORMAT SPRT,FLUX(INCRL)...FLUX(K)
            PRINT FORMAT HEADTN
            THROUGH SET4, FOR I=N,-1,I.E.A
SET4        PRINT FORMAT SPRT,T(X(I)+INCRL)...T(X(I)+K)
            PRINT FORMAT HEAD
            INCRL=INCRM+1
            INCRM=INCRM+INCRMX+1
            OTHERWISE
SET3        END OF CONDITIONAL
            PUNCH FORMAT HEAD2,P,HEATN,ROLLN,DATAPT,SPECD,FLUID(0)...FLUI
          1 D(2),EDELT,LDELT
            WHENEVER CHECK
            ERROR.
            OTHERWISE
            TRANSFER TO START
            END OF CONDITIONAL
            END OF PROGRAM
```

SOLUTION OF THE TRI-DIAGICNAL MATRIX

```
          EXTERNAL FUNCTION(B,P,XZ,Q)
          PROGRAN COMMON AC,BC,CC,DCC,T,X,L,M,N
          DIMENSION T(6000),X(200),AC(80),BC(80),CC(80),DDC(80)
          INTEGER X,L,M,N
          INTEGER K,F,R,I,P,B,XZ
          DIMENSION BETA(80),GAMMA(80),VAR(80)
          ENTRY TO COLS.
          F=B
          R=P
          K=XZ
          BETA(F)=1.+BC(F)
          GAMMA(F)=DDC(F)/BETA(F)
          THROUGH FIVE,FOR I=F+1,1,I.G.R
          BETA(I)=1.+BC(I)-AC(I)*CC(I-1)/BETA(I-1)
FIVE      GAMMA(I)=(DDC(I)-AC(I)*GAMMA(I-1))/BETA(I)
          VAR(R)=GAMMA(R)
          THROUGH SIX,FOR I=R-1,-1,I.L.F
SIX       VAR(I)=GAMMA(I)-CC(I)*VAR(I+1)/BETA(I)
          THROUGH SEVEN,FOR I=F,1,I.G.R
SEVEN     Q(I*(L+1)+K)=VAR(I)
          FUNCTION RETURN
          END OF FUNCTION
```

APPENDIX F

Computer Program for Determining the Total Contribution of the Microlayer During Boiling

```
 PROGRAM FOR CALCULATION THE AMOUNT OF LIQUID EVAPORATED
 FROM UNDERNEATH A BOILING BUBBLE


 DELT IS THE FILM THICKNESS ALLOWING FOR VAPORIZATION
 NDELT IS THE FILM THICKNESS BASED ON NO VAPORIZATION
 EDELT IS THE TOTAL AMOUNT OF VAPORIZATION
 TDELTN IS THE TOTAL AMOUNT OF THINNING OF THE VAPORIZING
FILM
 DDELT IS THE AMOUNT OF VAPORIZATION PER TIME INCREMENT
 DELTN IS THE AMOUNT OF THINNING PER TIME INCREMENT

 RBMAX IS THE MAXIMUM EXTENT OF THE BUBBLE ON THE SURFACE
 DELZER IS THE THICKNESS OF THE LIQUID FILM AT RBMAX
 ZB IS THE THICKNESS OF THE SOLID
 TIMEZ IS THE TIME INTERVAL FROM NUCLEATION TO THE TIME
 WHEN THE BUBBLE REACHES RBMAX
  TAURM IS THE INTEGER VALUE OF TAU WHEN THE TIME=TIMEZ
 TAURD IS THE INTEGER VALUE OF TAU AT DEPARTURE
  IF THINNING OF THE MICRO LAYER IS ASSUMED,THIN=1B
 IF THE PHYSICAL PROPERTIES OF THE SOLID AND LIQUID ARE USED
 CAL MUST BE SET EQUAL TO 1B
  ALF IS THE VARIABLE RELATING THE MAXIMUM BUBBLE RADIUS
 TO THE SQUARE ROOT OF TIME

  FTRAP.
  REFERENCES ON
  PROGRAM COMMON T,TSTAR,IF,JF,KF,X,AR,BR,CR,AC,BC,CC,DDR,DDC,Y
1 ,BUB,DELT,DDELT,TAURM,IMAX,N,L,TAURD,TTMAX,TAUFIN,TAU,EDELT
2 ,NDELT,DELTIN,TDELTN
  INTEGER TAURM,IMAX,N,X,L,Y,TAURD,TTMAX,TAUFIN,TAU
  DIMENSION T(1071),TSTAR(1071),IF(40),JF(40),KF(40),X(40),AR(4
1 0),BR(40),CR(40),AC(40),BC(40),CC(40),DDR(40),DDC(40),Y(800),
2 BUB(800),DELT(9900),DDELT(40),EDELT(40),NDELT(40),DELTIN(40),
3 TDELTN(40)
  DIMENSION LDELT(40)
  INTEGER INCR,RDAT,A,COUNT,K,I,J,XJ,P,PERIOD,INCRMX ,TLMAX
  INTEGER IMA,TTMA,TLMAX1
  BOOLEAN CHECK,CAL,STOP,READAT,UNKN ,THIN
  DIMENSION AREA(40)
  CHECK=0B
  CAL=1B
  THIN=1B
  STOP=0B
  READAT=0B
  UNKN=0B
  INCR=0
  TIME=0.
  TAU=0
  RDAT=-10
  TTMAX=0
  TINIT=1.
  TZERO=0.
  A=1
  COUNT=0
  ERC=1.
  ERAF=1.
  ZERO.(T(0)...T(1071),TSTAR(0)...TSTAR(1071),DELT(0)...DELT(60
1 00),DDELT(0)...DDELT(40))
  ZERO.(EDELT(0)...EDELT(40),NDELT(0)...NDELT(40),DELTIN(0)...D
1 ELTIN(40),TDELTN(0)...TDELTN(40))
  READ AND PRINT DATA
  WHENEVER CAL

   CALCULATION OF DIMENSIONLESS GROUPS

  NUT=VISC/ROT

  PRANDT=NUT*ROT*CPT/KT
  SUPH=CPT*TEMPZ/HFG
  RATO=TOUT/TEMPZ
  JA=ROT*CPT*TEMPZ/VAPORD/HFG
  WHENEVER UNKN
  ALF=ERAF*1.77245*JA*SQRT.(KT/ROT/CPT)
  END OF CONDITIONAL
  WHENEVER THIN
  DELZER=ERC*2./9.*(SQRT.(3.14159*NUT*TIMEZ))
  OTHERWISE
  DELZER=ERC*1./3.*(SQRT.(3.14159*NUT*TIMEZ))
  END OF CONDITIONAL
  NUB=4.*ALF*ALF/9.
  PRANDB=NUB*CPB*ROB/KB
  ROZ2=RBMAX/ZB*RBMAX/ZB
  SUPT=SUPH/PRANDT
  NU=FLUX*DELZER/KT/TEMPZ
  NUS=FLUX*ZB/KB/TEMPZ
  OTHERWISE
  CONTINUE
  END OF CONDITIONAL

  PRINT COMMENT $1$
  PRINT RESULTS ALF,DELZER
  PRINT COMMENT$0 THE DIMENSIONLESS GROUPS ARE$
  PRINT RESULTS PRANDT,HOK,        NUB,PRANDB,ROZ2,SUPT,NU,NUS,JA,RATO
  DT=1./TAURM
  DR=1./IMAX
  DZB=1./N
  FF=DT/2./DZB/DZB/PRANDB*ROZ2
  CF=DT/2./DR/DR/PRANDB
  WHENEVER THIN
  EVAP=SUPT/3.14159/ERC/ERC*81./4.
  OTHERWISE
  EVAP=SUPT/3.14159/ERC/ERC*9.
  END OF CONDITIONAL
  COEF=DT/DZB*ROZ2/PRANDB*HOK
  COEFIN=DT/DZB*ROZ2/PRANDB/NU *NUS
  PRINT COMMENT$0 THE FACTORS CONTROLLING VAPORIZATION ARE $
  PRINT RESULTS FF,CF,EVAP,COEF,COEFIN
  X(0)=0
  IF(0)=0.
  THROUGH SET2,FOR K=1,1,K.G.40
  IF(K)=IF(K-1)+1.
  JF(K)=1.+1./2./IF(K)
  KF(K)=1.-1./2./IF(K)
SET2      X(K)=X(K-1)+L+1
```

```
              CALCULATION OF MATRIX COEFICIENTS

             THROUGH SET3,FOR I=1,1,I.E.L
             AR(I)=-CF*KF(I)
             BR(I)=2.*CF
SET3         CR(I)=-CF*JF(I)
             THROUGH SET4,FOR J=1,1,J.E.N
             AC(J)=-FF
             BC(J)=2.*FF
SET4         CC(J)=-FF
             AC(N)=-2.*FF
             BC(N)=2.*FF
             CC(N)=0.
             BC(0)=2.*FF
             CC(0)=-2.*FF
             AC(0)=0.
             AR(L)=-2.*CF
             BR(L)=2.*CF
             CR(L)=0.
             AR(0)=0.
             BR(0)=4.*CF
             CR(0)=-4.*CF


             AREA=3.1416/4.*DR*DR
             THROUGH SETAF,FOR I=1,1,I.G.IMAX
SETAF        AREA(I)=IF(I)*2.*3.1416*DR*DR

              SPECIFICATION OF THE INITIAL TEMPERATURE DISTRIBUTION IN
              THE SOLID

             THROUGH SETT, FOR J=0,1,J.G.N
             XJ=X(J)
             THROUGH SETT,FOR I=0,1,I.G.L
             T(XJ+I)=TBASE-(TBASE-RATO)*DZB*IF(J)
SETT         TSTAR(XJ+I)=T(XJ+I)

             Y(0)=0
             THROUGH SETY,FOR K=1,1,K.G.PERIOD
SETY         Y(K)=Y(K-1)+IMAX+1
             THROUGH SETB,FOR P=0,1,P.G.PERIOD
             WHENEVER P.L.TAURD

              BUB(P) IS THE DIMENSIONLESS BUBBLE CONTACT RADIUS VS TIME

             BUB(P)=3./2.*SQRT.(DT*P)*(1.-1./3.*DT*P)
             OTHERWISE
             BUB(P)=0.
SETB         END OF CONDITIONAL
             WHENEVER L.L.IMAX
             IMA=L
             OTHERWISE
             IMA=IMAX
             END OF CONDITIONAL
             PRINT COMMENT $0 THE MATRIX COEFICIENTS ARE$
             PRINT RESULTS AR(0)...AR(L),BR(0)...BR(L),CR(0)...CR(L)
             PRINT RESULTS AC(0)...AC(N),BC(0)...BC(N),CC(0)...CC(N)
LOOP         CONTINUE
             WHENEVER THIN
             ZERO.(DELT(Y(0       ))...DELT(Y(TAURD+1)),EDELT(0)...EDELT(IM
           1 AX),TDELTN(0)...TDELTN(IMAX),NDELT(0)...NDELT(IMAX))
             OTHERWISE
             ZERO.(EDELT(0)...EDELT(IMAX))
             THROUGH SETF, FOR P=0,1,P.G.TAURD
             DELT(Y(P   ))=DR/3.
             THROUGH SETF, FOR I=1,1,I.G.IMA
SETF         DELT(Y(P   )+I)=IF(I)*DR*(1.+1./IF(I)/IF(I)/12.)
             END OF CONDITIONAL
             TTMAX=0
BCYCLE       READ AND PRINT DATA

              WHENEVER READAT  PUNCHED DATA IS READ IN FOR T,DELT,ETC

             PRNT.(TIME,VOLUME,STOP,READAT)
             TZERO=TIME-DT*TAU
             READAT=0B
             WHENEVER TAU.L.TAURD
SETE         THROUGH SETE,FOR K=0,1,IF(K).G.BUB(TAU)/DR-.5
             TLMAX=K
             TTMAX=K
             END OF CONDITIONAL
CYCLE        TAU=TAU+1
             INCR=INCR+1
             TIME=TZERO+DT*TAU
             COUNT=COUNT+1
             WHENEVER TAU.G.TAURD
             TTMAX=-1
             OTHERWISE
             BUBB=BUB(TAU)/DR
             TLMAX=TTMAX
SETA         THROUGH SETA,FOR K=C,1,IF(K).G.BUBB-.5
             TTMAX=K
             AREAB=BUBB*BUBB-(IF(K-1)+.5)*(IF(K-1)+.5)
             AREAF=AREAB/2./IF(TTMAX)
             END OF CONDITIONAL
             WHENEVER TAU.LE.TAURM
             WHENEVER TTMAX.G.L
             TTMA=L
             OTHERWISE
             TTMA=TTMAX
             END OF CONDITIONAL
             WHENEVER THIN
             LDELT=NDELT
             NDELT=DR*DR/8./SQRT.(DT*TAU)
             THROUGH SETM, FOR I=1,1,I.G.TTMA
             LDELT(I)=NDELT(I)
SETM         NDELT(I)=IF(I)*IF(I)*DR*DR/SQRT.(DT*TAU)*(1.+1./16./IF(I)/IF(
           1 I))
             THROUGH SETP, FOR I=TLMAX,1,I.G.TTMA
             LDELT(I)=NDELT(I)
             DELT(Y+I)=NDELT(I)
SETP         DELT(Y(TAU)+I)=NDELT(I)
             THROUGH SETN, FOR I=0,1,I.G.TTMA
             DELTIN(I)=DELT(Y(TAU)+I)*(1.-NDELT(I)/LDELT(I))
             TDELTN(I)=TDELTN(I)+DELTIN(I)
SETN         DELT(Y(TAU)+I)=DELT(Y(TAU)+I)-DELTIN(I)
             OTHERWISE
             END OF CONDITIONAL
             OTHERWISE
             END OF CONDITIONAL
```

```
         SOLUTION FOR TEMPERATURE BY THE ALTERNATING DIRECTION
         METHOD

         THROUGH SIX, FOR I=0,1,I.G.L
         THROUGH SEVEN, FOR J=A,1,J.G.N
         XJ=X(J)
SEVEN    DDC(J)=-AR(I)*T(XJ+I-1)+(1.-BR(I))*T(XJ+I)-CR(I)*T(XJ+I+1)
         DDC(A)=DDC(A)-AC(A)*TSTAR(X(A-1)+I)
         WHENEVER I.G.TTMAX
         BC(N)=2.*FF+COEF
         OTHERWISE
         DELTTI=DELT(Y(TAU)+I)
         WHENEVER DELTTI.L.MIN
         BC(N)=2.*FF
         OTHERWISE
         WHENEVER I.L.TTMAX
         BC(N)=2.*FF+COEFIN/DELTTI
         OTHERWISE
         BC(N)=2.*FF+COEFIN/DELTTI*AREAF+COEF*(1.-AREAF)
         END OF CONDITIONAL
         END OF CONDITIONAL
         END OF CONDITIONAL
SIX      COLS.(A,N,X+I,TSTAR)
         BC(N)=2.*FF
         THROUGH FIVE,FOR J=A,1,J.G.N
         XJ=X(J)
         THROUGH FOUR,FORI=0,1,I.G.L
         DDR(I)=-AC(J)*TSTAR(X(J-1)+I)+(1.-BC(J))*TSTAR(XJ+I)-CC(J)*TS
       1 TAR(X(J+1)+I)
         WHENEVER J.L.N
         CONTINUE
         OTHERWISE
         WHENEVER I.G.TTMAX
         DDR(I)=DDR(I)-COEF*TSTAR(XJ+I)
         OTHERWISE
         DELTTI=DELT(Y(TAU)+I)
         WHENEVER DELTTI.L.MIN
         CONTINUE
         OTHERWISE
         WHENEVER I.L.TTMAX
         DDR(I)=DDR(I)-COEFIN*TSTAR(XJ+I)/DELTTI
         OTHERWISE
         DDR(I)=DDR(I)-COEFIN*TSTAR(XJ+I)/DELTTI*AREAF-COEF*TSTAR(XJ+I
       1 )*(1.-AREAF)
         END OF CONDITIONAL
         END OF CONDITIONAL
         END OF CONDITIONAL
FOUR     END OF CONDITIONAL
         ROWS.(0,L,X(J),T)
FIVE     CONTINUE

         DETERMINATION OF THE AMOUNT OF VAPORIZATION

         WHENEVER TAU.G.TAURD
         CONTINUE
         OTHERWISE
         THROUGH EIGHT,FOR I=0,1,I.G.IMA
         DELTTI=DELT(Y(TAU)+I)
         WHENEVER I.G.TTMAX
         DDELT(I)=0.
         OTHERWISE
         WHENEVER DELTTI.G.MIN
         DDELT(I)=EVAP*DT*T(X(N)+I)/DELTTI
         OTHERWISE
         DDELT(I)=0.
         END OF CONDITIONAL
EIGHT    END OF CONDITIONAL
         DDELT(TTMAX)=DDELT(TTMAX)*AREAF
         THROUGH NINE, FOR I=0,1,I.G.TTMA
         DELTTI=DELT(Y(TAU)+I)
         WHENEVER DELTTI-DDELT(I).L.MIN
         EDELT(I)=          DELTTI +EDELT(I)
         DELT(Y(TAU+1)+I)=0.
         OTHERWISE
         EDELT(I)=EDELT(I)+DDELT(I)
         DELT(Y(TAU+1)+I)=DELTTI-DDELT(I)
NINE     END OF CONDITIONAL
         END OF CONDITIONAL
         WHENEVER TAU.E.TAURD
         INCR=INCRMX

         CALCULATION OF THE AMOUNT OF LIQUID EVAPORATED

         ACTUAL VOLUME MUST BE OBTAINED BY MULTIPLYING BY RBMAX
         SQUARED TIMES DELZER

         WHENEVER L.L.IMAX,PRINT COMMENT $0 ONLY PART OF THE BUBBLE FILM IS
       1 IS BEING CALCULATED $

         VOLUME=0.
         THROUGH SETV,FOR I=0,1,I.G.IMAX
SETV     VOLUME=VOLUME+AREA(I)*EDELT(I)
         OTHERWISE
         END OF CONDITIONAL
         WHENEVER INCR.E.INCRMX
         INCR=0
         PRNT.(TIME,VOLUME,0B,0B)
         OTHERWISE
         CONTINUE
         END OF CONDITIONAL
         WHENEVER COUNT.L.TAUFIN
         WHENEVER TAU.E.RDAT,TRANSFER TO BCYCLE
         WHENEVER TAU.G.TAURD
         WHENEVER T(X(N)).G.TINIT
         PERIOD=TAU
         PRINT RESULTS PERIOD
         TZERO=TZERO+DT*TAU
         TAU=0
         TRANSFER TO LOOP
         OTHERWISE
         END OF CONDITIONAL
         OTHERWISE
         END OF CONDITIONAL
         TRANSFER TO CYCLE
         OTHERWISE
         PRNT.(TIME,VOLUME,1B,0B)
         END OF CONDITIONAL
         WHENEVER CHECK,ERROR.
         END OF PROGRAM
```

PRINT SUBROUTINE

```
  EXTERNAL FUNCTION (TIME1,VOL1,STOP1,REDA1)
  PROGRAM COMMON T,TSTAR,IF,JF,KF,X,AR,BR,CR,AC,BC,CC,DDR,DDC,Y
1 ,BUB,DELT,DDELT,TAURM,IMAX,N,L,TAURD,TTMAX,TAUFIN,TAU,EDELT
2 ,NDELT,DELTIN,TDELTN
  DIMENSION T(1071),TSTAR(1071),IF(40),JF(40),KF(40),X(40),AR(4
1 0),BR(40),CR(40),AC(40),BC(40),CC(40),DDR(40),DDC(40),Y(800),
2 BUB(800),DELT(9900),DDELT(40),EDELT(40),NDELT(40),DELTIN(40),
3 TDELTN(40)
  INTEGER TAURM,IMAX,N,X,L,Y,TAURD,TTMAX,TAUFIN,TAU
  INTEGER J,L1,TSMAX,M ,IMA
  INTEGER JXI,JXL
  FORMAT VARIABLE L1
  BOOLEAN STOP,STOP1,REDA1,READAT
  VECTOR VALUES HEADNN=$1H0,H*THE LIQUID THICKNESS ASSUMING NO EVAPORATIO
1 N WOULD BE**$
  VECTOR VALUES HEADTM=$1H0,H* THE AMOUNT OF MICROLAYER THINNING DUE TO B
1 UBBLE GROWTH DURING THE LAST TIME INCREMENT IS**$
  VECTOR VALUES HEADTT=$1H0, ,H* THE TOTAL THICKNESS OF THE MICROLAYER NO
1 T EVAPORATED BUT MOVED BECAUSE OF THINNING IS**$
  VECTOR VALUES  INITAT=$94H1THE ASSUMED BUBBLE INITIATION TEMPERATURE HA
1 S BEEN EXCEEDED AND THE BUBBLE WILL START TO GROW*$
  VECTOR VALUES HEADV=$73H0THE TOTAL DIMENSIONLESS VOLUME OF LIQUID EVAPO
1 RATED DURING THIS CYCLE ISF10.8*$
  VECTOR VALUES DEPART=$29H1THE BUBBLE HAS JUST DEPARTED*$
  VECTOR VALUES HEADS=$58H0 THE TOTAL DEPTH  OF LIQUID EVAPORAT
1 ED UP TO THIS TIME IS*$
  VECTOR VALUES HEADE=$66H0DURING THE LAST TIME INCREMENT THE A
1 MOUNT OF LIQUID EVAPORATED IS*$
  VECTOR VALUES NATCV=$55H1 THE TOP SURFACE IS UNDERGOING NATUR
1 AL CONVECTION ONLY*$
  VECTOR VALUES HEADD=$38H1THE BUBBLE COVERS THE SURFACE OUT TO
1  F8.5*$
  VECTOR VALUES HEAD=$1H0,H* THE DIMENSIONLESS FILM THICKNESS UNDER THE B
1 UBBLE AT RADIAL DISTANCES FROM THE POINT OF NUCLEATION IS**$
  VECTOR VALUES HEADG=$4H   J=I3*$
  VECTOR VALUES SIPUNH=$S1,6F13.5/(S1,6F13.5)*$
  VECTOR VALUES SIPRT=$1H ,'L1'F 9.6*$
  VECTOR VALUES HEADT=$10H0 AT TIME=F12.6*$
  VECTOR VALUES HEADT1=$1H+,S25,H* THE TEMPERATURE DISTRIBUTION IN THE SO
1 LID IS**$
  VECTOR VALUES HEADJ=$S10,F10.6,S10,I4*$
  ENTRY TO PRNT.
  M=N
  TIME=TIME1
  STOP=STOP1
  READAT=REDA1
  WHENEVER READAT
  READ  FORMAT HEADJ,TIME,TAU
  THROUGH THREE,FOR J=0,1,J.G.M
  JXI=X(J)
  JXL=X(J+1)-1
THREE  READ  FORMAT SIPUNH,T(JXI)...T(JXL)
  READ   FORMAT SIPUNH,DELT(Y(TAU+1))...DELT(Y(TAU+1)+IMAX)
  READ  FORMAT SIPUNH,EDELT(0)...EDELT(IMAX)
  READ  FORMAT SIPUNH,NDELT(0)...NDELT(IMAX)
  READ  FORMAT SIPUNH,TDELTN(0)...TDELTN(IMAX)
  TIME1=TIME
  OTHERWISE
  END OF CONDITIONAL
  WHENEVER STOP
  PUNCH FORMAT HEADJ,TIME,TAU
  THROUGH TWO,FOR J=0,1,J.G.M
  JXI=X(J)
  JXL=X(J+1)-1
TWO  PUNCH FORMAT SIPUNH,T(JXI)...T(JXL)
  PUNCH  FORMAT SIPUNH,DELT(Y(TAU+1))...DELT(Y(TAU+1)+IMAX)
  PUNCH FORMAT SIPUNH,EDELT(0)...EDELT(IMAX)
  PUNCH FORMAT SIPUNH,NDELT(0)...NDELT(IMAX)
  PUNCH FORMAT SIPUNH,TDELTN(0)...TDELTN(IMAX)
  OTHERWISE
  END OF CONDITIONAL
  WHENEVER TAU.G.TAURD
  PRINT FORMAT NATCV
  OTHERWISE
  WHENEVER TAU.G.0
  WHENEVER TAU.L.TAURD
  WHENEVER TTMAX.G.L
  L1=L+1
  TSMAX=L
  OTHERWISE
  L1=TTMAX+1
  TSMAX=TTMAX
  END OF CONDITIONAL
  BUBT=BUB(TAU)*IF(IMAX)
  PRINT FORMAT HEADD,BUBT
  PRINT FORMAT HEAD
  PRINT FORMAT SIPRT,DELT(Y(TAU+1))...DELT(Y(TAU+1)+TSMAX)
  PRINT FORMAT HEADE
  PRINT FORMAT SIPRT,DDELT(0)...DDELT(TSMAX)
  WHENEVER TAU.G.TAURM
  CONTINUE
  OTHERWISE
  PRINT FORMAT HEADNN
  PRINT FORMAT SIPRT,NDELT(0)...NDELT(TSMAX)
  PRINT FORMAT HEADTM
  PRINT FORMAT SIPRT,DELTIN(0)...DELTIN(TSMAX)
  END OF CONDITIONAL
  OTHERWISE
  PRINT FORMAT DEPART
  VOLUME=VOL1
  PRINT FORMAT HEADV,VOLUME
  END OF CONDITIONAL
  OTHERWISE
  PRINT FORMAT INITAT
  END OF CONDITIONAL
  END OF CONDITIONAL
  WHENEVER TAU.LE.TAURD
  PRINT FORMAT HEADS
  WHENEVER L.G.IMAX
  IMA=IMAX
```

```
          L1=IMAX+1
          OTHERWISE
          IMA=L
          L1=L+1
          END OF CONDITIONAL
          PRINT FORMAT SIPRT,EDELT(0)...EDELT(IMA )
          PRINT FORMAT HEADTT
          PRINT FORMAT SIPRT,TDELTN(0)...TDELTN( IMA )
          OTHERWISE
          END OF CONDITIONAL
          PRINT FORMAT HEADT ,TIME
          PRINT FORMAT HEADT1
          L1=L+1
          THROUGH EPS5,FOR J=M,-1,J.L.0
          JXI=X(J)
          JXL=X(J)+L
          PRINT FORMAT HEADG,J
EPS5      PRINT FORMAT SIPRT,T(JXI)...T(JXL)
          FUNCTION RETURN
          END OF FUNCTION
```

SOLUTION OF THE TRI-DIAGONAL MATRIX

```
          EXTERNAL FUNCTION(B,P,XZ,Q)
          PROGRAM COMMON T,TSTAR,IF,JF,KF,X,AR,BR,CR,AC,BC,CC,DDR,DDC,Y
        1 ,BUB,DELT,DDELT,TAURM,IMAX,N,L,TAURC,TTMAX,TAUFIN,TAU,EDELT
        2 ,NDELT,DELTIN,TDELTN
          DIMENSION T(1071),TSTAR(1071),IF(40),JF(40),KF(40),X(40),AR(4
        1 0),BR(40),CR(40),AC(40),BC(40),CC(40),DDR(40),DDC(40),Y(800),
        2 BUB(800),DELT(9900),DDELT(40),EDELT(40),NDELT(40),DELTIN(40),
        3 TDELTN(40)
          DIMENSION BETA(40),GAMMA(40),VAR(40)
          INTEGER K,F,R,P,B,XZ,W,I
          INTEGER TAURM,IMAX,N,X,L,Y,TAURC,TTMAX,TAUFIN,TAU
          BOOLEAN DEC
          ENTRY TO ROWS.
          DEC=1B
          F=B
          R=P
          K=XZ
          TRANSFER TO ONE
          ENTRY TO COLS.
          DEC=0B
          F=B
          R=P
          K=XZ
ONE       WHENEVER DEC
          BETA(F)=1.+BR(F)
          GAMMA(F)=DDR(F)/BETA(F)
          THROUGH TWO,FOR I=F+1,1,I.G.R
          BETA(I)=1.+BR(I)-AR(I)*CR(I-1)/BETA(I-1)
TWO       GAMMA(I)=(DDR(I)-AR(I)*GAMMA(I-1))/BETA(I)
          VAR(R)=GAMMA(R)
          THROUGH THREE,FOR I=R-1,-1,I.L.F
THREE     VAR(I)=GAMMA(I)-CR(I)*VAR(I+1)/BETA(I)
          THROUGH FOUR,FOR I=F,1,I.G.R
FOUR      Q(K+I)=VAR(I)
          OTHERWISE
          BETA(F)=1.+BC(F)
          GAMMA(F)=DDC(F)/BETA(F)
          THROUGH FIVE,FOR I=F+1,1,I.G.R
          BETA(I)=1.+BC(I)-AC(I)*CC(I-1)/BETA(I-1)
FIVE      GAMMA(I)=(DDC(I)-AC(I)*GAMMA(I-1))/BETA(I)
          VAR(R)=GAMMA(R)
          THROUGH SIX,FOR I=R-1,-1,I.L.F
SIX       VAR(I)=GAMMA(I)-CC(I)*VAR(I+1)/BETA(I)
          THROUGH SEVEN,FOR I=F,1,I.G.R
SEVEN     Q(I*(L+1)+K)=VAR(I)
          END OF CONDITIONAL
          FUNCTION RETURN
          END OF FUNCTION
```

APPENDIX G

Analysis of Temperature Trace 9-1-13 for Δl and Δs

```
BOILING OF ETHYL ALCOHOL             DATA POINT NUMBER    9 1 13 1

          INC =            3,            Q =        .085000,          TFLUX =       .018108,          EDELT =  1.171684E-04

   T(4713) =       3.410573,        TEMPF =       3.400000

      EDELT =  1.171684E-04,         LDELT =  5.146253E-04
 AT THESE TIMES
      .000000   .000099   .000199   .000298   .000398   .000497   .000597   .000696   .000796   .000895
 THE FLUX THROUGH THE SURFACE IS
      .085000   .180805   .273331   .362653   .448850   .531995   .612163   .689427   .763859   .835531
 THE TEMPERATURE DISTRIBUTION IS
     18.663330 17.960996 17.281569 16.624523 15.989340 15.375507 14.782519 14.209874 13.657079 13.123647
     19.285441 19.284301 19.282063 19.278766 19.274449 19.269151 19.262907 19.255754 19.247728 19.238862
     19.907552 19.907550 19.907544 19.907534 19.907516 19.907490 19.907454 19.907406 19.907345 19.907270
     20.529663 20.529663 20.529663 20.529663 20.529664 20.529664 20.529664 20.529664 20.529664 20.529664
     21.151773 21.151773 21.151773 21.151773 21.151773 21.151773 21.151773 21.151773 21.151773 21.151773
     21.773885 21.773885 21.773885 21.773885 21.773885 21.773886 21.773886 21.773886 21.773886 21.773887
     22.395995 22.395995 22.395995 22.395995 22.395995 22.395995 22.395995 22.395995 22.395995 22.395995
     23.018106 23.018106 23.018106 23.018106 23.018106 23.018106 23.018106 23.018106 23.018106 23.018106
     23.640218 23.640218 23.640218 23.640218 23.640218 23.640219 23.640219 23.640219 23.640219 23.640220
     24.262329 24.262329 24.262329 24.262329 24.262330 24.262330 24.262330 24.262330 24.262331 24.262331

 AT THESE TIMES
      .000995   .001094   .001194   .001293   .001393   .001492   .001592   .001691   .001791   .001890
 THE FLUX THROUGH THE SURFACE IS
      .904514   .970876  1.034687  1.096013  1.154922  1.211479  1.265748  1.317794  1.367680  1.415466
 THE TEMPERATURE DISTRIBUTION IS
     12.609094 12.112945 11.634731 11.173967 10.730256 10.303087  9.892033  9.496656  9.116523  8.751205
     19.229190 19.218744 19.207556 19.195657 19.183075 19.169842 19.155984 19.141530 19.126505 19.110935
     19.907180 19.907073 19.906948 19.906804 19.906641 19.906456 19.906250 19.906020 19.905768 19.905490
     20.529663 20.529663 20.529662 20.529661 20.529660 20.529658 20.529656 20.529654 20.529651 20.529648
     21.151773 21.151773 21.151773 21.151773 21.151773 21.151773 21.151773 21.151773 21.151773 21.151773
     21.773887 21.773887 21.773887 21.773888 21.773888 21.773888 21.773888 21.773889 21.773889 21.773889
     22.395995 22.395995 22.395995 22.395995 22.395995 22.395995 22.395995 22.395995 22.395996 22.395996
     23.018106 23.018106 23.018106 23.018106 23.018106 23.018106 23.018106 23.018106 23.018106 23.018106
     23.640220 23.640220 23.640220 23.640221 23.640221 23.640221 23.640221 23.640222 23.640222 23.640222
     24.262331 24.262331 24.262331 24.262332 24.262332 24.262332 24.262332 24.262333 24.262333 24.262333

 AT THESE TIMES
      .001990   .002089   .002189   .002288   .002388   .002487   .002587   .002686   .002786   .002885
 THE FLUX THROUGH THE SURFACE IS
      1.461215  1.504986  1.546839  1.586831  1.625020  1.661461  1.696212  1.729325  1.760855  1.790854
 THE TEMPERATURE DISTRIBUTION IS
      8.400283  8.063340  7.739968  7.429764  7.132332  6.847280  6.574224  6.312785  6.062591  5.823275
     19.094846 19.078263 19.061208 19.043704 19.025774 19.007438 18.988719 18.969635 18.950206 18.930452
     19.905188 19.904860 19.904504 19.904122 19.903712 19.903273 19.902806 19.902308 19.901782 19.901224
     20.529645 20.529641 20.529636 20.529631 20.529625 20.529618 20.529611 20.529603 20.529594 20.529584
     21.151773 21.151773 21.151773 21.151773 21.151773 21.151773 21.151773 21.151773 21.151773 21.151773
     21.773889 21.773890 21.773890 21.773890 21.773890 21.773890 21.773891 21.773891 21.773891 21.773891
     22.395996 22.395996 22.395997 22.395997 22.395997 22.395997 22.395998 22.395998 22.395998 22.395998
     23.018106 23.018106 23.018106 23.018106 23.018106 23.018106 23.018106 23.018106 23.018106 23.018106
     23.640222 23.640223 23.640223 23.640223 23.640223 23.640224 23.640224 23.640224 23.640224 23.640224
     24.262333 24.262334 24.262334 24.262334 24.262334 24.262335 24.262335 24.262335 24.262335 24.262336

 AT THESE TIMES
      .002985   .003084   .003184   .003283   .003383   .003482   .003582   .003681   .003781   .003880
 THE FLUX THROUGH THE SURFACE IS
      1.819374  1.846465  1.872178  1.896561  1.919663  1.941530  1.962209  1.981746  2.000183  2.017566
 THE TEMPERATURE DISTRIBUTION IS
      5.594477  5.375843  5.167025  4.967680  4.777473  4.596073  4.423157  4.258407  4.101512  3.952165
     18.910389 18.890035 18.869408 18.848523 18.827396 18.806043 18.784476 18.762711 18.740761 18.718638
     19.900636 19.900017 19.899367 19.898685 19.897970 19.897223 19.896443 19.895631 19.894786 19.893907
     20.529573 20.529562 20.529549 20.529535 20.529520 20.529504 20.529487 20.529468 20.529448 20.529427
     21.151773 21.151773 21.151773 21.151773 21.151773 21.151773 21.151773 21.151772 21.151772 21.151772
     21.773892 21.773892 21.773892 21.773892 21.773893 21.773893 21.773893 21.773893 21.773894 21.773894
     22.395998 22.395999 22.395999 22.395999 22.395999 22.396000 22.396000 22.396000 22.396000 22.396001
     23.018106 23.018106 23.018106 23.018106 23.018106 23.018106 23.018106 23.018106 23.018106 23.018106
     23.640225 23.640225 23.640225 23.640225 23.640226 23.640226 23.640226 23.640226 23.640226 23.640226
     24.262336 24.262336 24.262336 24.262336 24.262337 24.262337 24.262337 24.262337 24.262338 24.262338

 AT THESE TIMES
      .003980   .004079   .004179   .004278   .004378   .004477   .004577   .004676   .004776   .004875
 THE FLUX THROUGH THE SURFACE IS
      2.033937  2.049336  2.063806  2.077386  2.090115  2.102031  2.113172  2.123573  2.133270  2.142298
 THE TEMPERATURE DISTRIBUTION IS
      3.810068  3.674926  3.546453  3.424367  3.308393  3.198261  3.093710  2.994482  2.900325  2.810996
     18.696355 18.673923 18.651355 18.628659 18.605848 18.582930 18.559915 18.536812 18.513629 18.490375
     19.892996 19.892051 19.891071 19.890059 19.889013 19.887933 19.886818 19.885670 19.884488 19.883272
     20.529404 20.529380 20.529354 20.529327 20.529298 20.529268 20.529236 20.529202 20.529166 20.529129
     21.151772 21.151772 21.151771 21.151771 21.151770 21.151770 21.151769 21.151768 21.151768 21.151767
     21.773894 21.773894 21.773895 21.773895 21.773895 21.773895 21.773896 21.773896 21.773896 21.773896
     22.396001 22.396001 22.396001 22.396002 22.396002 22.396002 22.396002 22.396003 22.396003 22.396003
     23.018106 23.018106 23.018106 23.018106 23.018106 23.018106 23.018106 23.018106 23.018106 23.018106
     23.640226 23.640226 23.640226 23.640226 23.640226 23.640226 23.640226 23.640226 23.640226 23.640226
     24.262338 24.262338 24.262339 24.262339 24.262339 24.262339 24.262340 24.262340 24.262340 24.262340

 AT THESE TIMES
      .004974   .005074   .005173   .005273   .005372   .005472   .005571   .005671   .005770   .005870
 THE FLUX THROUGH THE SURFACE IS
      2.150690  2.158480  2.165698  2.172376  2.178544  2.184232  2.189467  2.194278  2.198690  2.202730
 THE TEMPERATURE DISTRIBUTION IS
      2.726255  2.645870  2.569614  2.497268  2.428615  2.363450  2.301568  2.242774  2.186878  2.133695
     18.467056 18.443681 18.420255 18.396786 18.373280 18.349741 18.326177 18.302591 18.278988 18.255374
     19.882023 19.880739 19.879421 19.878069 19.876684 19.875265 19.873812 19.872326 19.870806 19.869252
     20.529089 20.529047 20.529004 20.528959 20.528911 20.528861 20.528809 20.528755 20.528698 20.528639
     21.151766 21.151765 21.151764 21.151763 21.151762 21.151761 21.151760 21.151758 21.151757 21.151755
     21.773896 21.773897 21.773897 21.773897 21.773897 21.773898 21.773898 21.773898 21.773898 21.773899
     22.396003 22.396003 22.396004 22.396004 22.396004 22.396004 22.396005 22.396005 22.396005 22.396005
     23.018106 23.018106 23.018106 23.018106 23.018106 23.018106 23.018106 23.018106 23.018106 23.018106
     23.640226 23.640226 23.640226 23.640226 23.640226 23.640226 23.640226 23.640226 23.640226 23.640226
     24.262341 24.262341 24.262341 24.262341 24.262341 24.262342 24.262342 24.262342 24.262342 24.262343

 AT THESE TIMES
      .005969   .006069   .006168   .006268   .006367   .006467   .006566   .006666   .006765   .006865
 THE FLUX THROUGH THE SURFACE IS
      2.206422  2.209791  2.212859  2.215649  2.218183  2.220480  2.222560  2.224442  2.226145  2.227685
 THE TEMPERATURE DISTRIBUTION IS
      2.083048  2.034766  1.988681  1.944636  1.902475  1.862053  1.823226  1.785860  1.749826  1.715001
     18.231751 18.208124 18.184496 18.160870 18.137250 18.113638 18.090037 18.066449 18.042876 18.019320
     19.867665 19.866045 19.864392 19.862705 19.860986 19.859234 19.857449 19.855631 19.853781 19.851899
     20.528578 20.528515 20.528448 20.528380 20.528308 20.528234 20.528158 20.528079 20.527997 20.527912
     21.151754 21.151752 21.151750 21.151748 21.151746 21.151744 21.151742 21.151739 21.151736 21.151734
     21.773899 21.773899 21.773899 21.773900 21.773900 21.773900 21.773900 21.773901 21.773901 21.773901
     22.396006 22.396006 22.396006 22.396006 22.396007 22.396007 22.396007 22.396007 22.396008 22.396008
     23.018106 23.018106 23.018106 23.018106 23.018106 23.018106 23.018106 23.018106 23.018106 23.018106
     23.640226 23.640226 23.640226 23.640226 23.640226 23.640226 23.640226 23.640226 23.640226 23.640226
     24.262343 24.262343 24.262343 24.262344 24.262344 24.262344 24.262344 24.262345 24.262345 24.262345
```

```
AT THESE TIMES
   .006964   .007064   .007163   .007263   .007362   .007462   .007561   .007661   .007760   .007860
THE FLUX THROUGH THE SURFACE IS
   2.229078  2.230340  2.231485  2.232527  2.233479  2.234353  2.235160  2.235909  2.236612  2.237275
THE TEMPERATURE DISTRIBUTION IS
   1.681267  1.648513  1.616635  1.585533  1.555115  1.525294  1.495990  1.467128  1.438639  1.410462
  17.995783 17.972265 17.948769 17.925295 17.901845 17.878420 17.855019 17.831644 17.808295 17.784973
  19.849984 19.848037 19.846058 19.844048 19.842006 19.839932 19.837827 19.835690 19.833523 19.831324
  20.527824 20.527734 20.527640 20.527543 20.527444 20.527341 20.527236 20.527127 20.527015 20.526900
  21.151731 21.151729 21.151726 21.151723 21.151719 21.151716 21.151712 21.151709 21.151705 21.151700
  21.773901 21.773901 21.773902 21.773902 21.773902 21.773902 21.773903 21.773903 21.773903 21.773903
  22.396008 22.396008 22.396008 22.396009 22.396009 22.396009 22.396009 22.396010 22.396010 22.396010
  23.018106 23.018106 23.018106 23.018106 23.018106 23.018106 23.018106 23.018106 23.018106 23.018106
  23.640226 23.640226 23.640226 23.640226 23.640226 23.640226 23.640226 23.640226 23.640226 23.640226
  24.262345 24.262346 24.262346 24.262346 24.262346 24.262347 24.262347 24.262347 24.262347 24.262347

AT THESE TIMES
   .007959   .008059   .008158   .008258   .008357   .008457   .008556   .008656   .008755   .008855
THE FLUX THROUGH THE SURFACE IS
   2.237907  2.238515  2.239105  2.239681  2.240249  2.240812  2.241372  2.241932  2.242492  2.243053
THE TEMPERATURE DISTRIBUTION IS
   1.382539  1.354821  1.327265  1.299830  1.272486  1.245208  1.217974  1.190771  1.163593  1.136436
  17.761677 17.738408 17.715167 17.691952 17.668765 17.645605 17.622472 17.599366 17.576287 17.553234
  19.829094 19.826834 19.824544 19.822223 19.819871 19.817489 19.815078 19.812636 19.810165 19.807664
  20.526781 20.526659 20.526535 20.526406 20.526274 20.526139 20.526000 20.525858 20.525713 20.525563
  21.151696 21.151692 21.151687 21.151682 21.151677 21.151671 21.151666 21.151660 21.151654 21.151648
  21.773903 21.773903 21.773903 21.773903 21.773903 21.773903 21.773903 21.773903 21.773903 21.773903
  22.396010 22.396011 22.396011 22.396011 22.396011 22.396012 22.396012 22.396012 22.396012 22.396013
  23.018106 23.018106 23.018106 23.018106 23.018106 23.018106 23.018106 23.018106 23.018106 23.018106
  23.640226 23.640226 23.640226 23.640226 23.640226 23.640226 23.640226 23.640226 23.640226 23.640226
  24.262348 24.262348 24.262348 24.262348 24.262349 24.262349 24.262349 24.262349 24.262349 24.262349

AT THESE TIMES
   .008954   .009054   .009153   .009253   .009352   .009452   .009551   .009651   .009750   .009849
THE FLUX THROUGH THE SURFACE IS
   2.243614  2.244173  2.244729  2.245277  2.245815  2.246338  2.246839  2.247313  2.247752   .000000
THE TEMPERATURE DISTRIBUTION IS
   1.109304  1.082212  1.055173  1.028211  1.001355   .974638   .948103   .921796   .895772   .949081
  17.530208 17.507209 17.484236 17.461290 17.438370 17.415478 17.392612 17.369772 17.346961 17.324306
  19.805133 19.802573 19.799984 19.797366 19.794719 19.792043 19.789338 19.786605 19.783844 19.781054
  20.525411 20.525254 20.525094 20.524930 20.524762 20.524590 20.524415 20.524236 20.524053 20.523865
  21.151642 21.151635 21.151628 21.151621 21.151614 21.151606 21.151598 21.151590 21.151582 21.151573
  21.773903 21.773903 21.773903 21.773903 21.773903 21.773903 21.773903 21.773903 21.773903 21.773903
  22.396013 22.396013 22.396013 22.396013 22.396014 22.396014 22.396014 22.396014 22.396015 22.396015
  23.018106 23.018106 23.018106 23.018106 23.018106 23.018106 23.018106 23.018106 23.018106 23.018106
  23.640226 23.640226 23.640226 23.640226 23.640226 23.640226 23.640226 23.640226 23.640226 23.640226
  24.262349 24.262349 24.262349 24.262349 24.262349 24.262349 24.262349 24.262349 24.262349 24.262349

AT THESE TIMES
   .009949   .010048   .010148   .010247   .010347   .010446   .010546   .010645   .010745   .010844
THE FLUX THROUGH THE SURFACE IS
   .000000   .000000   .000000   .000000   .000000   .000000   .000000   .000000   .000000   .000000
THE TEMPERATURE DISTRIBUTION IS
   1.002144  1.054962  1.107537  1.159870  1.211962  1.263814  1.315428  1.366805  1.417947  1.468853
  17.301805 17.279459 17.257266 17.235225 17.213335 17.191595 17.170005 17.148564 17.127270 17.106123
  19.778236 19.775392 19.772520 19.769621 19.766696 19.763745 19.760767 19.757765 19.754737 19.751684
  20.523674 20.523479 20.523279 20.523076 20.522868 20.522657 20.522441 20.522221 20.521997 20.521769
  21.151564 21.151555 21.151546 21.151536 21.151525 21.151515 21.151504 21.151493 21.151482 21.151470
  21.773903 21.773903 21.773902 21.773902 21.773902 21.773902 21.773901 21.773901 21.773901 21.773901
  22.396015 22.396015 22.396016 22.396016 22.396016 22.396016 22.396017 22.396017 22.396017 22.396017
  23.018106 23.018106 23.018106 23.018106 23.018106 23.018106 23.018106 23.018106 23.018106 23.018106
  23.640226 23.640226 23.640226 23.640226 23.640226 23.640226 23.640226 23.640226 23.640226 23.640226
  24.262349 24.262349 24.262349 24.262349 24.262349 24.262349 24.262349 24.262349 24.262349 24.262349

AT THESE TIMES
   .010944   .011043   .011143   .011242   .011342   .011441   .011541   .011640   .011740   .011839
THE FLUX THROUGH THE SURFACE IS
   .000000   .000000   .000000   .000000   .000000   .000000   .000000   .000000   .000000   .000000
THE TEMPERATURE DISTRIBUTION IS
   1.519527  1.569968  1.620178  1.670159  1.719911  1.769436  1.818735  1.867809  1.916659  1.965287
  17.085122 17.064266 17.043554 17.022985 17.002558 16.982273 16.962128 16.942123 16.922257 16.902529
  19.748607 19.745506 19.742380 19.739231 19.736059 19.732863 19.729645 19.726404 19.723142 19.719857
  20.521536 20.521299 20.521058 20.520812 20.520562 20.520308 20.520049 20.519785 20.519518 20.519246
  21.151458 21.151446 21.151433 21.151420 21.151406 21.151392 21.151378 21.151363 21.151348 21.151333
  21.773901 21.773900 21.773900 21.773900 21.773899 21.773899 21.773898 21.773898 21.773897 21.773897
  22.396018 22.396018 22.396018 22.396018 22.396019 22.396019 22.396019 22.396019 22.396019 22.396020
  23.018106 23.018106 23.018106 23.018106 23.018106 23.018106 23.018106 23.018106 23.018106 23.018106
  23.640226 23.640226 23.640226 23.640226 23.640226 23.640226 23.640226 23.640226 23.640226 23.640226
  24.262349 24.262349 24.262349 24.262349 24.262349 24.262349 24.262349 24.262349 24.262349 24.262349

AT THESE TIMES
   .011939   .012038   .012138   .012237   .012337   .012436   .012536   .012635   .012735   .012834
THE FLUX THROUGH THE SURFACE IS
   .000000   .000000   .000000   .000000   .000000   .000000   .000000   .000000   .000000   .000000
THE TEMPERATURE DISTRIBUTION IS
   2.013693  2.061879  2.109847  2.157596  2.205128  2.252445  2.299548  2.346437  2.393113  2.439579
  16.882939 16.863484 16.844165 16.824981 16.805931 16.787014 16.768229 16.749575 16.731052 16.712659
  19.716551 19.713223 19.709875 19.706506 19.703116 19.699707 19.696277 19.692828 19.689359 19.685871
  20.518969 20.518688 20.518402 20.518112 20.517817 20.517518 20.517213 20.516905 20.516591 20.516273
  21.151317 21.151301 21.151284 21.151268 21.151250 21.151232 21.151214 21.151195 21.151176 21.151156
  21.773896 21.773896 21.773896 21.773895 21.773894 21.773894 21.773893 21.773892 21.773891 21.773891
  22.396020 22.396020 22.396020 22.396021 22.396021 22.396021 22.396021 22.396022 22.396022 22.396022
  23.018106 23.018106 23.018106 23.018106 23.018106 23.018106 23.018106 23.018106 23.018106 23.018106
  23.640226 23.640226 23.640226 23.640226 23.640226 23.640226 23.640226 23.640226 23.640226 23.640226
  24.262349 24.262349 24.262349 24.262349 24.262349 24.262349 24.262349 24.262349 24.262349 24.262349

AT THESE TIMES
   .012934   .013033   .013133   .013232   .013332   .013431   .013531   .013630   .013730   .013829
THE FLUX THROUGH THE SURFACE IS
   .000000   .000000   .000000   .000000   .000000   .000000   .000000   .000000   .000000   .000000
THE TEMPERATURE DISTRIBUTION IS
   2.485834  2.531881  2.577720  2.623352  2.668778  2.714000  2.759018  2.803834  2.848448  2.892862
  16.694395 16.676259 16.658251 16.640369 16.622613 16.604983 16.587476 16.570094 16.552834 16.535697
  19.682364 19.678839 19.675296 19.671734 19.668155 19.664558 19.660944 19.657312 19.653664 19.650000
  20.515950 20.515623 20.515290 20.514953 20.514612 20.514265 20.513914 20.513558 20.513197 20.512831
  21.151136 21.151115 21.151094 21.151073 21.151051 21.151028 21.151005 21.150982 21.150958 21.150933
  21.773890 21.773889 21.773888 21.773887 21.773886 21.773885 21.773884 21.773883 21.773882 21.773881
  22.396022 22.396023 22.396023 22.396023 22.396023 22.396023 22.396023 22.396023 22.396023 22.396023
  23.018106 23.018106 23.018106 23.018106 23.018106 23.018106 23.018106 23.018106 23.018106 23.018106
  23.640226 23.640226 23.640226 23.640226 23.640226 23.640226 23.640226 23.640226 23.640226 23.640226
  24.262349 24.262349 24.262349 24.262349 24.262349 24.262349 24.262349 24.262349 24.262349 24.262349

AT THESE TIMES
   .013929   .014028   .014128   .014227   .014327   .014426   .014526   .014625   .014724   .014824   .014923   .015023
THE FLUX THROUGH THE SURFACE IS
   .000000   .000000   .000000   .000000   .000000   .000000   .000000   .000000   .000000   .000000   .000000   .000000
THE TEMPERATURE DISTRIBUTION IS
   2.937076  2.981092  3.024911  3.068534  3.111962  3.155195  3.198235  3.241083  3.283740  3.326206  3.368484  3.410573
  16.518681 16.501785 16.485009 16.468353 16.451815 16.435394 16.419091 16.402904 16.386832 16.370876 16.355033 16.339304
  19.646319 19.642622 19.638909 19.635180 19.631436 19.627677 19.623903 19.620115 19.616312 19.612494 19.608663 19.604818
  20.512461 20.512086 20.511706 20.511321 20.510931 20.510536 20.510136 20.509732 20.509322 20.508908 20.508488 20.508064
  21.150908 21.150882 21.150856 21.150829 21.150802 21.150774 21.150746 21.150717 21.150688 21.150658 21.150627 21.150596
  21.773880 21.773879 21.773877 21.773876 21.773875 21.773873 21.773872 21.773870 21.773869 21.773867 21.773866 21.773864
  22.396023 22.396023 22.396023 22.396023 22.396023 22.396023 22.396023 22.396023 22.396023 22.396023 22.396023 22.396023
  23.018106 23.018106 23.018106 23.018106 23.018106 23.018106 23.018106 23.018106 23.018106 23.018106 23.018106 23.018106
  23.640226 23.640226 23.640226 23.640226 23.640226 23.640226 23.640226 23.640226 23.640226 23.640226 23.640226 23.640226
  24.262349 24.262349 24.262349 24.262349 24.262349 24.262349 24.262349 24.262349 24.262349 24.262349 24.262349 24.262349
```

APPENDIX H

Analysis of 9-1-13 Based on the Film Theory

```
ALF =        2.340000,          DELZER =  3.770635E-03
THE DIMENSIONLESS GROUPS ARE
     PRANCT =      7.785371,          HUK =       1.000000,          NUB =     2.433600,       PRANDB =    573.721161
     ROZ2 =        6.024793,          SUPT =  9.324687E-03,          NU =       .542537,       NUS =        1.500000
     JA =         49.674590,          RATO =      1.500000
THE FACTORS CONTROLLING VAPORIZATION ARE
     FF =  7.500898E-03,              CF =  6.100524E-04,            EVAP =     .026713,      COEF =  1.500180E-03
     COEFIN =  4.147676E-03
THE MATRIX COEFICIENTS ARE

              AR(0)...AR(10)

  .000000E+00  -3.050262E-04  -4.575393E-04  -5.083770E-04  -5.337959E-04  -5.490472E-04  -5.592147E-04  -5.664773E-04
-5.719242E-04  -5.761606E-04  -1.220105E-03

              BR(0)...BR(10)

 2.440210E-03   1.220105E-03   1.220105E-03   1.220105E-03   1.220105E-03   1.220105E-03   1.220105E-03   1.220105E-03
 1.220105E-03   1.220105E-03   1.220105E-03

              CR(0)...CR(10)

-2.440210E-03  -9.150787E-04  -7.625655E-04  -7.117278E-04  -6.863090E-04  -6.710577E-04  -6.608901E-04  -6.536276E-04
-6.481807E-04  -6.439442E-04    .000000E+00

              AC(0)...AC(10)

  .000000E+00  -7.500898E-03  -7.500898E-03  -7.500898E-03  -7.500898E-03  -7.500898E-03  -7.500898E-03  -7.500898E-03
-7.500898E-03  -7.500898E-03  -1.500180E-02

              BC(0)...BC(10)

 1.500180E-02   1.500180E-02   1.500180E-02   1.500180E-02   1.500180E-02   1.500180E-02   1.500180E-02   1.500180E-02
 1.500180E-02   1.500180E-02   1.500180E-02

              CC(0)...CC(10)

-1.500180E-02  -7.500898E-03  -7.500898E-03  -7.500898E-03  -7.500898E-03  -7.500898E-03  -7.500898E-03  -7.500898E-03
-7.500898E-03  -7.500898E-03    .000000E+00

   INCRMX=10      *


THE ASSUMED BUBBLE INITIATION TEMPERATURE HAS BEEN EXCEEDED AND THE BUBBLE WILL START TO GROW

 THE TOTAL DEPTH  OF LIQUID EVAPORATED UP TO THIS TIME IS
  .000000  .000000  .000000  .000000  .000000  .000000  .000000  .000000

 THE TOTAL THICKNESS OF THE MICROLAYER NOT EVAPORATED BUT MOVED BECAUSE OF THINNING IS
  .000000  .000000  .000000  .000000  .000000  .000000  .000000  .000000

 AT TIME=   33.899999     THE TEMPERATURE DISTRIBUTION IN THE SOLID IS
 J= 10
 1.000144  .991365 1.022563 1.106088 1.199216 1.287232 1.366658 1.431593 1.469987 1.486688 1.490982
 J=  9
 1.117441 1.108710 1.142503 1.231120 1.329947 1.423472 1.507903 1.576928 1.617829 1.635685 1.640287
 J=  8
 1.269865 1.262898 1.298041 1.385222 1.482518 1.574932 1.658454 1.726723 1.767425 1.785373 1.790034
 J=  7
 1.452600 1.448430 1.483387 1.563761 1.653588 1.739378 1.817029 1.880464 1.918639 1.935731 1.940217
 J=  6
 1.657543 1.656315 1.689366 1.759358 1.837768 1.913156 1.981489 2.037254 2.071205 2.086692 2.090810
 J=  5
 1.875985 1.877104 1.906607 1.964449 2.029468 2.092429 2.149559 2.196108 2.224811 2.238169 2.241770
 J=  4
 2.100717 2.103203 2.127849 2.173142 2.224273 2.274122 2.319380 2.356182 2.379158 2.390063 2.393041
 J=  3
 2.327012 2.329844 2.348774 2.381897 2.419459 2.456293 2.489739 2.516877 2.534007 2.542277 2.544561
 J=  2
 2.552534 2.554880 2.567640 2.589235 2.613826 2.638046 2.660035 2.677841 2.689179 2.694724 2.696268
 J=  1
 2.776712 2.778020 2.784425 2.795063 2.807211 2.819209 2.830099 2.838906 2.844544 2.847324 2.848102
 J= -0
 3.000000 3.000000 3.000000 3.000000 3.000000 3.000000 3.000000 3.000000 3.000000 3.000000 3.000000

 THE BUBBLE COVERS THE SURFACE OUT TO  2.14265

 THE DIMENSIONLESS FILM THICKNESS UNDER THE BUBBLE AT RADIAL DISTANCES FROM THE POINT OF NUCLEATION IS
  .028045  .148728  .290617

 DURING THE LAST TIME INCREMENT THE AMOUNT OF LIQUID EVAPORATED IS
  .006260  .002205  .000770

 THE TOTAL DEPTH  OF LIQUID EVAPORATED UP TO THIS TIME IS
  .019574  .006034  .001050  .000000  .000000  .000000  .000000  .000000

 THE TOTAL THICKNESS OF THE MICROLAYER NOT EVAPORATED BUT MOVED BECAUSE OF THINNING IS
  .000000  .000000  .000000  .000000  .000000  .000000  .000000  .000000

 AT TIME=   33.942855     THE TEMPERATURE DISTRIBUTION IN THE SOLID IS
 J= 10
  .562783  .872012 1.004301 1.107507 1.200249 1.287936 1.367059 1.431718 1.469996 1.486677 1.490969
 J=  9
 1.109100 1.108081 1.144180 1.232574 1.330995 1.424186 1.508311 1.577055 1.617837 1.635672 1.640273
 J=  8
 1.270974 1.264473 1.299678 1.386468 1.483417 1.575546 1.658805 1.726828 1.767428 1.785359 1.790019
 J=  7
 1.453538 1.449634 1.484586 1.564666 1.654243 1.739828 1.817284 1.880535 1.918635 1.935716 1.940203
 J=  6
 1.658135 1.657081 1.690104 1.759908 1.838167 1.913431 1.981644 2.037290 2.071195 2.086677 2.090796
 J=  5
 1.876287 1.877505 1.906973 1.964715 2.029660 2.092561 2.149631 2.196118 2.224797 2.238155 2.241757
 J=  4
 2.100826 2.103360 2.127977 2.173227 2.224333 2.274162 2.319399 2.356175 2.379144 2.390051 2.393030
 J=  3
 2.327020 2.329872 2.348782 2.381893 2.419454 2.456288 2.489732 2.516864 2.533995 2.542267 2.544552
 J=  2
 2.552508 2.554861 2.567610 2.589207 2.613803 2.638029 2.660021 2.677830 2.689170 2.694717 2.696262
 J=  1
 2.775691 2.778000 2.784402 2.795042 2.807195 2.819197 2.830090 2.838899 2.844539 2.847320 2.848099
 J= -0
 3.000000 3.000000 3.000000 3.000000 3.000000 3.000000 3.000000 3.000000 3.000000 3.000000 3.000000
```

```
THE BUBBLE COVERS THE SURFACE OUT TO  5.35953

 THE DIMENSIONLESS FILM THICKNESS UNDER THE BUBBLE AT RADIAL DISTANCES FROM THE POINT OF NUCLEATION IS
  .000000  .115131  .268335  .417305  .565388  .713977

DURING THE LAST TIME INCREMENT THE AMOUNT OF LIQUID EVAPORATED IS
  .000000  .001366  .000990  .000821  .000726  .000567

 THE TOTAL DEPTH  OF LIQUID EVAPORATED UP TO THIS TIME IS
  .047619  .039631  .023332  .015235  .009017  .002690  .000000  .000000

 THE TOTAL THICKNESS OF THE MICROLAYER NOT EVAPORATED BUT MOVED BECAUSE OF THINNING IS
  .000000  .000000  .000000  .000000  .000000  .000000  .000000  .000000

 AT TIME=   34.228570     THE TEMPERATURE DISTRIBUTION IN THE SOLID IS
 J= 10
  .266632  .416852  .698630  .899225 1.077118 1.252318 1.369532 1.432539 1.470060 1.486601 1.490884
 J=  9
  .931268 1.024370 1.106856 1.215259 1.326383 1.427064 1.510948 1.577883 1.617894 1.635588 1.640182
 J=  8
 1.252346 1.263977 1.305303 1.392351 1.488598 1.579507 1.661097 1.727525 1.767453 1.785268 1.789923
 J=  7
 1.457293 1.456671 1.492127 1.570531 1.658559 1.742809 1.818979 1.881018 1.918617 1.935621 1.940107
 J=  6
 1.662019 1.662189 1.695074 1.763640 1.840876 1.915295 1.982693 2.037548 2.071137 2.086581 2.090704
 J=  5
 1.878434 1.880300 1.909551 1.966598 2.031023 2.093498 2.150142 2.196195 2.224714 2.238065 2.241674
 J=  4
 2.101674 2.104531 2.128958 2.173896 2.224808 2.274483 2.319553 2.356141 2.379055 2.389972 2.392958
 J=  3
 2.327158 2.330149 2.348932 2.381944 2.419476 2.456292 2.489705 2.516786 2.533915 2.542204 2.544496
 J=  2
 2.552386 2.554788 2.567468 2.589056 2.613679 2.637931 2.659943 2.677756 2.689112 2.694673 2.696223
 J=  1
 2.776572 2.777895 2.784268 2.794920 2.807097 2.819122 2.830035 2.838857 2.844508 2.847298 2.848079
 J= -0
 3.000000 3.000000 3.000000 3.000000 3.000000 3.000000 3.000000 3.000000 3.000000 3.000000 3.000000

THE BUBBLE COVERS THE SURFACE OUT TO  6.54443

 THE DIMENSIONLESS FILM THICKNESS UNDER THE BUBBLE AT RADIAL DISTANCES FROM THE POINT OF NUCLEATION IS
  .000000  .090697  .250026  .401860  .551624  .701341  .852589 1.001675

DURING THE LAST TIME INCREMENT THE AMOUNT OF LIQUID EVAPORATED IS
  .000000  .001138  .000865  .000738  .000661  .000609  .000577  .000023

 THE TOTAL DEPTH  OF LIQUID EVAPORATED UP TO THIS TIME IS
  .047619  .064065  .041641  .030680  .022781  .015326  .006537  .000026

 THE TOTAL THICKNESS OF THE MICROLAYER NOT EVAPORATED BUT MOVED BECAUSE OF THINNING IS
  .000000  .000000  .000000  .000000  .000000  .000000  .000000  .000000

 AT TIME=   34.514284     THE TEMPERATURE DISTRIBUTION IN THE SOLID IS
 J= 10
  .545733  .273748  .568751  .778994  .957266 1.120535 1.290474 1.432422 1.470127 1.486528 1.490801
 J=  9
  .893147  .921215 1.042181 1.167977 1.290769 1.404345 1.505761 1.578609 1.617958 1.635508 1.640091
 J=  8
 1.220847 1.241839 1.296736 1.388180 1.486979 1.580071 1.662750 1.728209 1.767487 1.785181 1.789829
 J=  7
 1.453731 1.458692 1.496823 1.574716 1.661971 1.745451 1.820621 1.881510 1.918610 1.935528 1.940013
 J=  6
 1.664681 1.666660 1.699778 1.767286 1.843576 1.917184 1.983767 2.037827 2.071090 2.086488 2.090614
 J=  5
 1.880629 1.883206 1.912301 1.968643 2.032507 2.094518 2.150703 2.196298 2.224640 2.237976 2.241591
 J=  4
 2.102709 2.105895 2.130151 2.174738 2.225408 2.274888 2.319757 2.356130 2.378971 2.389894 2.392887
 J=  3
 2.327444 2.330580 2.349241 2.382121 2.419590 2.456359 2.489717 2.516724 2.533840 2.542142 2.544440
 J=  2
 2.552350 2.554808 2.567419 2.588978 2.613608 2.637872 2.659887 2.677691 2.689055 2.694630 2.696184
 J=  1
 2.776491 2.777831 2.784175 2.794828 2.807023 2.819064 2.829989 2.838818 2.844479 2.847276 2.848059
 J= -0
 3.000000 3.000000 3.000000 3.000000 3.000000 3.000000 3.000000 3.000000 3.000000 3.000000 3.000000

THE BUBBLE COVERS THE SURFACE OUT TO  6.97282

 THE DIMENSIONLESS FILM THICKNESS UNDER THE BUBBLE AT RADIAL DISTANCES FROM THE POINT OF NUCLEATION IS
  .000000  .068773  .233386  .387564  .538774  .689502  .841431  .998412

DURING THE LAST TIME INCREMENT THE AMOUNT OF LIQUID EVAPORATED IS
  .000000  .001070  .000808  .000697  .000628  .000579  .000544  .000243

 THE TOTAL DEPTH  OF LIQUID EVAPORATED UP TO THIS TIME IS
  .047619  .085988  .058281  .044975  .035630  .027165  .017695  .003289

 THE TOTAL THICKNESS OF THE MICROLAYER NOT EVAPORATED BUT MOVED BECAUSE OF THINNING IS
  .000000  .000000  .000000  .000000  .000000  .000000  .000000  .000000

 AT TIME=   34.799998     THE TEMPERATURE DISTRIBUTION IN THE SOLID IS
 J= 10
  .675018  .195843  .495933  .709455  .888145 1.047322 1.200359 1.395777 1.469884 1.486455 1.490719
 J=  9
  .901985  .837255  .982200 1.119943 1.249990 1.369789 1.480093 1.574890 1.617971 1.635430 1.640002
 J=  8
 1.200511 1.208799 1.278260 1.375441 1.477638 1.573822 1.660031 1.728454 1.767523 1.785096 1.789736
 J=  7
 1.446666 1.454134 1.497025 1.575681 1.663043 1.746580 1.821653 1.881974 1.918611 1.935439 1.939920
 J=  6
 1.665425 1.669386 1.703467 1.770311 1.845897 1.918885 1.984798 2.038123 2.071052 2.086398 2.090524
 J=  5
 1.882501 1.885927 1.915036 1.970728 2.034041 2.095587 2.151300 2.196424 2.224574 2.237890 2.241509
 J=  4
 2.103845 2.107391 2.131511 2.175723 2.226118 2.275371 2.320007 2.356141 2.378895 2.389818 2.392817
 J=  3
 2.327863 2.331154 2.349700 2.382418 2.419792 2.456488 2.489764 2.516678 2.533768 2.542081 2.544384
 J=  2
 2.552402 2.554922 2.567465 2.588973 2.613593 2.637851 2.659855 2.677635 2.689002 2.694588 2.696146
 J=  1
 2.776451 2.777811 2.784125 2.794770 2.806973 2.819023 2.829955 2.838783 2.844450 2.847254 2.848039
 J= -0
 3.000000 3.000000 3.000000 3.000000 3.000000 3.000000 3.000000 3.000000 3.000000 3.000000 3.000000
```

THE BUBBLE COVERS THE SURFACE CUT TO 6.95525

THE DIMENSIONLESS FILM THICKNESS UNDER THE BUBBLE AT RADIAL DISTANCES FROM THE POINT OF NUCLEATION IS
.0C0000 .058162 .225406 .380667 .532553 .683766 .836049 .995889

DURING THE LAST TIME INCREMENT THE AMOUNT OF LIQUID EVAPORATED IS
.0C0000 .001055 .000790 .000684 .000617 .000569 .000534 .000251

THE TOTAL DEPTH OF LIQUID EVAPORATED UP TO THIS TIME IS
.047619 .C96600 .066261 .051872 .041851 .032900 .023078 .005811

THE TOTAL THICKNESS OF THE MICROLAYER NOT EVAPORATED BUT MOVED BECAUSE OF THINNING IS
.0C0000 .000000 .000000 .000000 .000000 .000000 .000000 .000000

AT TIME= 34.942855 THE TEMPERATURE DISTRIBUTION IN THE SOLID IS
J= 10
.713102 .163687 .468529 .683443 .862563 1.020971 1.170471 1.374328 1.469505 1.486417 1.490678
J= 9
.909824 .801676 .955550 1.C97870 1.230592 1.352402 1.464898 1.569571 1.617881 1.635391 1.639958
J= 8
1.194102 1.190838 1.267C33 1.367115 1.471003 1.568658 1.656585 1.727876 1.767525 1.785055 1.789691
J= 7
1.442949 1.449720 1.495454 1.574859 1.662518 1.746307 1.821622 1.882114 1.918613 1.935396 1.939874
J= 6
1.665188 1.669869 1.704730 1.771424 1.846774 1.919550 1.985228 2.038267 2.071037 2.086354 2.090480
J= 5
1.883234 1.887098 1.916312 1.971725 2.034784 2.096112 2.151601 2.196494 2.224545 2.237848 2.241469
J= 4
2.104413 2.108154 2.132230 2.176255 2.226503 2.275635 2.320147 2.356153 2.378859 2.389780 2.392782
J= 3
2.328113 2.331487 2.349981 2.3826C9 2.419925 2.456575 2.489801 2.516661 2.533735 2.542051 2.544357
J= 2
2.552461 2.555015 2.567523 2.588999 2.613605 2.637855 2.659847 2.677611 2.688976 2.694566 2.696127
J= 1
2.776447 2.777818 2.784117 2.794754 2.806957 2.819010 2.829942 2.838767 2.844437 2.847243 2.848030
J= -0
3.0C0000 3.000000 3.000000 3.000000 3.000000 3.000000 3.000000 3.000000 3.000000 3.000000 3.000000

THE BUBBLE COVERS THE SURFACE CUT TO 6.48568

THE DIMENSIONLESS FILM THICKNESS UNDER THE BUBBLE AT RADIAL DISTANCES FROM THE POINT OF NUCLEATION IS
.0C0000 .C26869 .202262 .360597 .514403 .667016 .820359

DURING THE LAST TIME INCREMENT THE AMOUNT OF LIQUID EVAPORATED IS
.0C0000 .001036 .000757 .000658 .000595 .000550 .000509

THE TOTAL DEPTH OF LIQUID EVAPORATED UP TO THIS TIME IS
.047619 .127893 .089404 .071943 .060002 .049650 .038767 .010294

THE TOTAL THICKNESS OF THE MICROLAYER NOT EVAPORATED BUT MOVED BECAUSE OF THINNING IS
.0C0000 .000000 .000000 .000000 .000000 .000000 .000000 .000000

AT TIME= 35.371427 THE TEMPERATURE DISTRIBUTION IN THE SOLID IS
J= 10
.775029 .075755 .402832 .622526 .803576 .961814 1.108256 1.365204 1.468175 1.486282 1.490558
J= 9
.928916 .711557 .887112 1.040012 1.178710 1.304651 1.421105 1.552590 1.617129 1.635262 1.639828
J= 8
1.182704 1.136713 1.230407 1.338582 1.447088 1.548514 1.640709 1.722850 1.767331 1.784931 1.789555
J= 7
1.432806 1.430536 1.485395 1.567920 1.657054 1.742059 1.818697 1.881534 1.918576 1.935268 1.939738
J= 6
1.662908 1.667618 1.705777 1.772717 1.847807 1.920331 1.985727 2.038519 2.070994 2.086226 2.090349
J= 5
1.884524 1.889370 1.919373 1.974214 2.036657 2.097452 2.152385 2.196703 2.224468 2.237725 2.241349
J= 4
2.105948 2.110275 2.134375 2.177886 2.227697 2.276462 2.320596 2.356217 2.378763 2.389671 2.392679
J= 3
2.328959 2.332602 2.350980 2.383318 2.420428 2.456910 2.489959 2.516632 2.533640 2.541962 2.544275
J= 2
2.552752 2.555416 2.567830 2.589184 2.613724 2.637924 2.659858 2.677554 2.688902 2.694504 2.696070
J= 1
2.776497 2.777906 2.784159 2.794758 2.806950 2.818998 2.829919 2.838727 2.844397 2.847211 2.848001
J= -0
3.000000 3.000000 3.000000 3.C00000 3.000000 3.000000 3.000000 3.000000 3.000000 3.000000 3.000000

THE BUBBLE COVERS THE SURFACE CUT TO 5.30686

THE DIMENSIONLESS FILM THICKNESS UNDER THE BUBBLE AT RADIAL DISTANCES FROM THE POINT OF NUCLEATION IS
.0C0000 .000000 .179851 .341124 .496759 .650991

DURING THE LAST TIME INCREMENT THE AMOUNT OF LIQUID EVAPORATED IS
.0C0000 .00C000 .000739 .000642 .000582 .000428

THE TOTAL DEPTH OF LIQUID EVAPORATED UP TO THIS TIME IS
.047619 .154762 .111815 .091416 .077646 .065675 .045485 .010294

THE TOTAL THICKNESS OF THE MICROLAYER NOT EVAPORATED BUT MOVED BECAUSE OF THINNING IS
.0C0000 .000000 .0C0000 .000000 .000000 .000000 .000000 .000000

AT TIME= 35.799998 THE TEMPERATURE DISTRIBUTION IN THE SOLID IS
J= 10
.795970 .039436 .349832 .575263 .758817 .923680 1.163975 1.389530 1.467674 1.486136 1.490438
J= 9
.935658 .636563 .831C86 .992151 1.135229 1.264389 1.396703 1.549736 1.616294 1.635112 1.639699
J= 8
1.174644 1.C85080 1.193411 1.308627 1.421031 1.525448 1.622375 1.717593 1.766848 1.784794 1.789422
J= 7
1.423847 1.406020 1.469850 1.556122 1.647145 1.733635 1.812085 1.879558 1.918403 1.935141 1.939605
J= 6
1.659173 1.660463 1.702803 1.770834 1.846213 1.918930 1.984568 2.038226 2.070921 2.086101 2.090221
J= 5
1.884533 1.889334 1.920791 1.975518 2.037616 2.098093 2.152705 2.196800 2.224398 2.237608 2.241231
J= 4
2.107039 2.111765 2.136191 2.179328 2.228759 2.277197 2.320994 2.356290 2.378679 2.389565 2.392577
J= 3
2.329823 2.333727 2.352089 2.384145 2.421024 2.457314 2.490162 2.516630 2.533556 2.541876 2.544194
J= 2
2.553169 2.555955 2.568301 2.5895C8 2.613948 2.638068 2.659915 2.677518 2.688836 2.694443 2.696014
J= 1
2.776631 2.778084 2.784296 2.794840 2.807002 2.819026 2.829921 2.838698 2.844360 2.847179 2.847972
J= -0
3.0C0000 3.000000 3.000000 3.000000 3.000000 3.000000 3.000000 3.000000 3.000000 3.000000 3.000000

```
THE BUBBLE COVERS THE SURFACE CUT TO  3.58602

 THE DIMENSIONLESS FILM THICKNESS UNDER THE BUBBLE AT RADIAL DISTANCES FROM THE POINT OF NUCLEATION IS
  .000000  .000000  .157711  .322008  .483625

DURING THE LAST TIME INCREMENT THE AMOUNT OF LIQUID EVAPORATED IS
  .000000  .000000  .000739  .000633  .000047

 THE TOTAL DEPTH  OF LIQUID EVAPORATED UP TO THIS TIME IS
  .047619  .154762  .133956  .110531  .090779  .068746  .045485  .010294

 THE TOTAL THICKNESS OF THE MICROLAYER NOT EVAPORATED BUT MOVED BECAUSE OF THINNING IS
  .000000  .000000  .000000  .000000  .000000  .000000  .000000  .000000

 AT TIME=   36.228570     THE TEMPERATURE DISTRIBUTION IN THE SOLID IS
 J= 10
  .828110  .406525  .306996  .535537  .787741 1.038663 1.232938 1.399998 1.467442 1.485990 1.490318
 J=  9
  .940296  .665247  .784356  .951212 1.103041 1.256203 1.406415 1.551760 1.615747 1.634954 1.639571
 J=  8
 1.166278 1.050339 1.158205 1.279428 1.395531 1.505602 1.612042 1.714835 1.766315 1.784646 1.789290
 J=  7
 1.414800 1.380549 1.451313 1.541470 1.634516 1.722890 1.804602 1.877380 1.918103 1.935007 1.939474
 J=  6
 1.654324 1.649743 1.696483 1.766166 1.842204 1.915433 1.981896 2.037432 2.070782 2.085978 2.090095
 J=  5
 1.883389 1.886900 1.920298 1.975345 2.037366 2.097744 2.152309 2.196673 2.224313 2.237493 2.241116
 J=  4
 2.107542 2.112266 2.137329 2.180293 2.229450 2.277640 2.321192 2.356315 2.378601 2.389464 2.392477
 J=  3
 2.330557 2.334634 2.353118 2.384946 2.421602 2.457701 2.490354 2.516640 2.533482 2.541793 2.544114
 J=  2
 2.553638 2.556537 2.568863 2.589920 2.614239 2.638260 2.660002 2.677500 2.688776 2.694384 2.695959
 J=  1
 2.776824 2.778325 2.784508 2.794986 2.807102 2.819089 2.829944 2.838680 2.844327 2.847149 2.847944
 J= -0
 3.000000 3.000000 3.000000 3.000000 3.000000 3.000000 3.000000 3.000000 3.000000 3.000000 3.000000


THE BUBBLE COVERS THE SURFACE CUT TO  1.41140

 THE DIMENSIONLESS FILM THICKNESS UNDER THE BUBBLE AT RADIAL DISTANCES FROM THE POINT OF NUCLEATION IS
  .000000  .000000

DURING THE LAST TIME INCREMENT THE AMOUNT OF LIQUID EVAPORATED IS
  .000000  .000000

 THE TOTAL DEPTH  OF LIQUID EVAPORATED UP TO THIS TIME IS
  .047619  .154762  .150080  .115539  .090791  .068746  .045485  .010294

 THE TOTAL THICKNESS OF THE MICROLAYER NOT EVAPORATED BUT MOVED BECAUSE OF THINNING IS
  .000000  .000000  .000000  .000000  .000000  .000000  .000000  .000000

 AT TIME=   36.657141     THE TEMPERATURE DISTRIBUTION IN THE SOLID IS
 J= 10
  .867394  .581685  .379420  .695543  .926976 1.110515 1.266966 1.405992 1.467282 1.485845 1.490200
 J=  9
  .956684  .738851  .753723  .945192 1.120509 1.278032 1.422080 1.554521 1.615397 1.634796 1.639443
 J=  8
 1.162784 1.047957 1.126677 1.255055 1.380087 1.498336 1.610123 1.713857 1.765855 1.784490 1.789159
 J=  7
 1.406488 1.362463 1.431629 1.525607 1.621687 1.713491 1.799155 1.875664 1.917750 1.934866 1.939344
 J=  6
 1.648620 1.638057 1.687697 1.759337 1.836408 1.910692 1.978691 2.036430 2.070581 2.085853 2.089972
 J=  5
 1.881182 1.882535 1.917948 1.973670 2.035862 2.096382 2.151256 2.196328 2.224199 2.237380 2.241003
 J=  4
 2.107373 2.111633 2.137574 2.180583 2.229591 2.277638 2.321085 2.356250 2.378520 2.389365 2.392380
 J=  3
 2.331035 2.335129 2.353885 2.385571 2.422041 2.457975 2.490467 2.516634 2.533413 2.541713 2.544037
 J=  2
 2.554078 2.557053 2.569423 2.590349 2.614544 2.638458 2.660092 2.677491 2.688723 2.694327 2.695905
 J=  1
 2.777043 2.778585 2.784761 2.795173 2.807233 2.819174 2.829980 2.838669 2.844298 2.847120 2.847916
 J= -0
 3.000000 3.000000 3.000000 3.000000 3.000000 3.000000 3.000000 3.000000 3.000000 3.000000 3.000000


THE BUBBLE HAS JUST DEPARTED

THE TOTAL DIMENSIONLESS VOLUME OF LIQUID EVAPORATED DURING THIS CYCLE IS .23842242

 THE TOTAL DEPTH  OF LIQUID EVAPORATED UP TO THIS TIME IS
  .047619  .154762  .150080  .115539  .090791  .068746  .045485  .010294

 THE TOTAL THICKNESS OF THE MICROLAYER NOT EVAPORATED BUT MOVED BECAUSE OF THINNING IS
  .000000  .000000  .000000  .000000  .000000  .000000  .000000  .000000

 AT TIME=   36.899998     THE TEMPERATURE DISTRIBUTION IN THE SOLID IS
 J= 10
  .888805  .641155  .521332  .770312  .970320 1.135622 1.279964 1.408472 1.467214 1.485764 1.490133
 J=  9
  .969294  .778939  .772575  .965757 1.138722 1.291560 1.430373 1.556045 1.615255 1.634707 1.639370
 J=  8
 1.163978 1.055345 1.115414 1.249059 1.378179 1.498628 1.611153 1.713784 1.765636 1.784401 1.789085
 J=  7
 1.402961 1.356758 1.421017 1.517572 1.615969 1.709791 1.797234 1.874955 1.917549 1.934784 1.939271
 J=  6
 1.645352 1.632167 1.682015 1.754896 1.832838 1.907985 1.977001 2.035865 2.070447 2.085780 2.089903
 J=  5
 1.879554 1.879556 1.915888 1.972117 2.034534 2.095275 2.150481 2.196064 2.224120 2.237316 2.240940
 J=  4
 2.106971 2.110512 2.137261 2.180407 2.229393 2.277419 2.320887 2.356168 2.378468 2.389310 2.392325
 J=  3
 2.331157 2.335162 2.354147 2.385799 2.422188 2.458048 2.490476 2.516616 2.533374 2.541668 2.543993
 J=  2
 2.554283 2.557275 2.569701 2.590570 2.614698 2.638555 2.660132 2.677485 2.688694 2.694296 2.695874
 J=  1
 2.777164 2.778724 2.784907 2.795284 2.807311 2.819224 2.830002 2.838665 2.844282 2.847103 2.847900
 J= -0
 3.000000 3.000000 3.000000 3.000000 3.000000 3.000000 3.000000 3.000000 3.000000 3.000000 3.000000
```